

ENHANCEMENT OF THE THERMAL PERFORMANCE
OF AN EVACUATED TUBE SOLAR COLLECTOR USING
NANOFLUIDS WITH GRAPHENE NANOPATELETS

SOUDEH IRANMANESH

FACULTY OF ENGINEERING
UNIVERSITY OF MALAYA
KUALA LUMPUR

2019

**ENHANCEMENT OF THE THERMAL
PERFORMANCE OF AN EVACUATED TUBE SOLAR
COLLECTOR USING NANOFLUIDS WITH
GRAPHENE NANOPATELETS**

SOUDEH IRANMANESH

**THESIS SUBMITTED IN FULFILMENT OF THE
REQUIREMENTS FOR THE DEGREE OF DOCTOR OF
PHILOSOPHY**

**FACULTY OF ENGINEERING
UNIVERSITY OF MALAYA
KUALA LUMPUR**

2019

UNIVERSITY OF MALAYA
ORIGINAL LITERARY WORK DECLARATION

Name of Candidate: SOUDEH IRANMANESH Matric No: KHA150035

Name of Degree: Doctor of Philosophy

Title of Project Paper/Research Report/Dissertation/Thesis (“this Work”): Enhancement of the Thermal Performance of an Evacuated Tube Solar Collector Using Nanofluids With Graphene Nanoplates.

Field of Study: Energy

I do solemnly and sincerely declare that:

- (1) I am the sole author/writer of this Work;
- (2) This Work is original;
- (3) Any use of any work in which copyright exists was done by way of fair dealing and for permitted purposes and any excerpt or extract from, or reference to or reproduction of any copyright work has been disclosed expressly and sufficiently and the title of the Work and its authorship have been acknowledged in this Work;
- (4) I do not have any actual knowledge, nor do I ought reasonably to know that the making of this work constitutes an infringement of any copyright work;
- (5) I hereby assign all and every right in the copyright to this Work to the University of Malaya (“UM”), who henceforth shall be owner of the copyright in this Work and that any reproduction or use in any form or by any means whatsoever is prohibited without the written consent of UM having been first had and obtained;
- (6) I am fully aware that if in the course of making this work, I have infringed any copyright whether intentionally or otherwise, I may be subject to legal action or any other action as may be determined by UM.

Candidate’s Signature

Date:

Subscribed and solemnly declared before,

Witness’s Signature

Date:

Name:

Designation:

UNIVERSITI MALAYA
PERAKUAN KEASLIAN PENULISAN

Nama: Soudeh Iranmanesh

No. Matrik: KHA150035

Nama Ijazah: Doktor Falsafah

Tajuk Kertas Projek/Laporan Penyelidikan/Disertasi/Tesis (“Hasil Kerja ini”):
PENINGKATAN PRESTASI TERHADAP PEMBEKAL SOLAR TUBE
EVACUATED MENGGUNAKAN NAPOLFLIPE DENGAN NANOPLATI
GRAPHENE

Bidang Penyelidikan:

Saya dengan sesungguhnya dan sebenarnya mengaku bahawa:

- (1) Saya adalah satu-satunya pengarang/penulis Hasil Kerja ini;
- (2) Hasil Kerja ini adalah asli;
- (3) Apa-apa penggunaan mana-mana hasil kerja yang mengandungi hakcipta telah dilakukan secara urusan yang wajar dan bagi maksud yang dibenarkan dan apa-apa petikan, ekstrak, rujukan atau pengeluaran semula daripada atau kepada mana-mana hasil kerja yang mengandungi hakcipta telah dinyatakan dengan sejelasnya dan secukupnya dan satu pengiktirafan tajuk hasil kerja tersebut dan pengarang/penulisnya telah dilakukan di dalam Hasil Kerja ini;
- (4) Saya tidak mempunyai apa-apa pengetahuan sebenar atau patut semunasabahnya tahu bahawa penghasilan Hasil Kerja ini melanggar suatu hakcipta hasil kerja yang lain;
- (5) Saya dengan ini menyerahkan kesemua dan tiap-tiap hak yang terkandung di dalam hakcipta Hasil Kerja ini kepada Universiti Malaya (“UM”) yang seterusnya mula dari sekarang adalah tuan punya kepada hakcipta di dalam Hasil Kerja ini dan apa-apa pengeluaran semula atau penggunaan dalam apa jua bentuk atau dengan apa juga cara sekalipun adalah dilarang tanpa terlebih dahulu mendapat kebenaran bertulis dari UM;
- (6) Saya sedar sepenuhnya sekiranya dalam masa penghasilan Hasil Kerja ini saya telah melanggar suatu hakcipta hasil kerja yang lain sama ada dengan niat atau sebaliknya, saya boleh dikenakan tindakan undang-undang atau apa-apa tindakan lain sebagaimana yang diputuskan oleh UM.

Tandatangan Calon

Tarikh:

Diperbuat dan sesungguhnya diakui di hadapan,

Tandatangan Saksi

Tarikh:

Nama:

Jawatan:

**ENHANCEMENT OF THE THERMAL PERFORMANCE OF AN
EVACUATED TUBE SOLAR COLLECTOR USING NANOFLUIDS WITH
GRAPHENE NANOPATELETS**

ABSTRACT

Solar thermal energy can be a good replacement for fossil fuel because it is clean and sustainable. However, the current solar technology is still not efficient. This research is carried out experimentally and analytically to investigate the thermal performance of evacuated tube solar collector (ETSC) using graphene nanoplatelets (GNP) nanofluid as working fluid. Therefore, in order to achieve the desired thermal conductivity and viscosity; experimental and statistical approaches were combined by selecting the best concentration, temperature, proper surface area and type of base fluid. In the first stage of this study, three influential parameters on the viscosity and thermal conductivity including concentration, temperature and specific surface area of GNP were investigated. A mathematical model was developed by response surface methodology (RSM) based on a central composite design (CCD). In addition, the significance of the models was tested using the analysis of variance (ANOVA). The optimum results of GNP nanofluid showed that the concentration has a direct effect on the relative viscosity and thermal conductivity. Furthermore, predicted responses proposed by the Design Expert software were compared with the experimental results. The statistical analysis of the predicted values was in satisfactory agreement with the empirical data.

In the second stage, the effect of GNP/distilled water nanofluid on the thermal performance of evacuated tube solar collector (ETSC) was investigated. The mass percentage of GNP considered was 0.025, 0.05, 0.075 and 0.1 wt%. The thermal efficiency tests on the solar collector were carried out for varying a volumetric flow rate of 0.5, 0.1, and 1.5 L/min following the ASHRAE standard 93E2003. The results

indicated that the solar collector thermal efficiency gave the enhancement up to 90.7% at a flow rate of 1.5 L/min when the GNP nanofluid 0.1 wt% was used as an absorption medium. The results indicated that by increasing the mass percentage of nanoparticles, thermal energy gain also increases, reaching a higher outlet temperature of the fluid when graphene nanoplatelets are used.

In addition, the thermodynamic performance of the cycle for the second law analysis also investigated. For this purpose, the experimental data on the performance of set-up is used to estimate the exergy efficiency and destruction, entropy generation, Bejan number and pumping power. The results showed that the exergy efficiency was enhanced with particle concentration and simultaneously decrease with mass flow rate. It also found that the entropy generation reduced with increasing the nanofluid concentration. The Bejan number surge up with increasing the concentration while this number decreases with enhancement the mass flow rate.

In the last stage, Numerical simulation was carried out using 3-dimensional computational fluid dynamic (CFD) to confirm the results for outlet temperature at 0.5 L/min. Comparison of the simulation results with the experimental data reveals that the model could predict the outlet nanofluid temperatures within a maximum relative error of 9.4% and mass flow rate were found in reasonable agreement with the available experimental outcome.

Keywords: graphene nanoplatelets, nanofluid, Thermal efficiency, thermo-physical properties, evacuated tube solar collector

**PENINGKATAN PRESTASI TERHADAP PEMBEKAL SOLAR TUBE
EVACUASI YANG MENGGUNAKAN NANOFLUIDS DENGAN NANOPLATI
GRAPHENE**

ABSTRAK

Tenaga terma suria boleh menjadi pengganti bahan api fosil yang baik kerana ia bersih dan mampan. Walau bagaimanapun, teknologi solar semasa masih tidak cekap. Penyelidikan ini dijalankan secara eksperimen dan analitikal untuk menyiasat prestasi haba pengumpul suria tiub yang dipindahkan (ETSC) apabila nanofluid graphene nanoplatelets (GNP) digunakan sebagai cecair kerja. Oleh itu, untuk mencapai kekonduksian haba yang dikehendaki dan kelikatan; pendekatan eksperimen dan statistik digabungkan dengan memilih kepekatan, suhu, kawasan permukaan dan jenis bendalir yang terbaik. Pada peringkat pertama kajian ini, tiga parameter berpengaruh terhadap kelikatan dan kekonduksian terma termasuk tumpuan, suhu dan kawasan permukaan spesifik GNP telah disiasat. Model matematik telah dibangunkan oleh metodologi permukaan respons (RSM) berdasarkan reka bentuk komposit pusat (CCD). Di samping itu, kepentingan model diuji menggunakan analisis varians (ANOVA). Hasil optimum nanofluid GNP menunjukkan bahawa kepekatannya mempunyai kesan langsung kepada kelikatan relatif dan kekonduksian terma. Tambahan pula, ramalan yang dijangkakan yang dicadangkan oleh perisian Pakar Reka Bentuk berbanding dengan keputusan percubaan. Analisis statistik nilai yang diramalkan adalah dalam persetujuan yang memuaskan dengan data empirikal.

Dalam peringkat kedua, kesan nanofluid GNP / air suling pada prestasi terma pengumpul suria tiub yang dipindahkan (ETSC) telah disiasat. Peratusan jisim bagi GNP adalah 0.025, 0.05, 0.075 dan 0.1 wt%. Ujian kecekapan terma pada pengumpul suria telah dilakukan untuk kadar aliran volumetrik yang berlainan sebanyak 0.5, 0.1, dan 1.5

L/min mengvkiti standard ASHRAE 93E2003 telah digunakan. Keputusan menunjukkan bahawa kecekapan haba pengumpul suria memberikan peningkatan sehingga 90.7% pada kadar aliran 1.5 L / min apabila GNP nanofluid 0.1% berat digunakan sebagai medium penyerapan. Keputusan menunjukkan bahawa dengan meningkatkan peratusan jisim nanopartikel, peningkatan tenaga haba juga meningkat, mencapai suhu keluar yang lebih tinggi daripada bendalir apabila graphene nanoplatelet digunakan.

Di samping itu, prestasi termodinamik kitaran untuk analisis undang-undang kedua juga disiasat. Untuk tujuan ini, data eksperimen mengenai prestasi set-up digunakan untuk menganggarkan kecekapan dan kemusnahan eksogen, penjanaan entropi, nombor Bejan dan kuasa pam. Keputusan menunjukkan bahawa kecekapan exergy dipertingkatkan dengan kepekatan zarah dan secara bersamaan menurun dengan kadar aliran jisim. Ia juga mendapati bahawa generasi entropi dikurangkan dengan meningkatkan kepekatan nanofluid. Nombor Bejan melonjak dengan meningkatkan kepekatan sementara jumlah ini menurun dengan peningkatan kadar aliran jisim.

Pada peringkat terakhir, simulasi berangka dilakukan dengan menggunakan dinamik cecair pengiraan 3 dimensi (CFD) untuk mengesahkan keputusan untuk suhu keluar pada 0.5 L / min. Perbandingan keputusan simulasi dengan data eksperimen mendedahkan bahawa model boleh meramalkan suhu nanofluid keluar dalam kesilapan relatif maksimum 9.4% dan kadar aliran jisim didapati dalam perjanjian yang berpatutan dengan hasil eksperimen yang tersedia.

Keywords: graphene nanoplatelets, nanofluid, Kecekapan terma, sifat terma-fizikal, pengumpul tiub solar yang dipindahkan

ACKNOWLEDGEMENTS

I would like to express my heartfelt thanks to my parents, A.nabizadeh and M.Iranmanesh. They gave me my name, they gave me my life, and everything else in between. I deeply appreciate all the efforts they have put into giving me the life I have now. Success is in my stride, because I have parents like them by my side. I wish for you to have long life in health and happiness.

I would like to thank to my supervisor, Associate Prof. Ir. Dr. Ang Bee Chin, for giving me the opportunity of working with her research team and creating a calm research environment. If I did not have her constant companion and great tolerance in the entire duration of the research period, without a doubt, I could not complete my PhD program. Apart from the scientific points, I learned from her that to be successful in other aspects of life, I should also have unremitting efforts while being patient.

I must also thank to my second supervisor, Dr. Ong Hwai Chyuan, for his unlimited supports. He always was supportive and attempted to push me forward to do higher quality of the works. His office door was always open for me. I never forget his kind helps when I faced problems.

If I say my best luck in these years was getting to know Dr. Mohammad Mehrali and Dr. Emad sadeghinezhad, it is nothing less than truth. They guided me in the right direction when I was facing the hardest time. Our deep and challenging discussions about the technical issues of the research work will always remain in my mind as one of the sweetest memories.

Also, heartfelt thanks are extended to my best colleague and friend Alireza Esmailzadeh, not only for his continues support and encourage but also for all valuable discussion, suggestions and help during my study.

Finally, I would like to thank the University of Malaya for financial support from the High Impact Research Grant (HIRG) scheme (UM.C/HIR/MOHE/ENG/40) and

postgraduate research funds (PG068-2015B) and (RP34C-15AET-UMRG) without these grants, I defiantly could not do my PhD.

Universiti Malaya

TABLE OF CONTENTS

Abstract	iii
ABSTRAK	v
Acknowledgements	vii
Table of Contents	ix
List of Figures	xiv
List of Tables	xvii
List of Symbols and Abbreviations.....	xviii
List of Appendices	xxi
CHAPTER 1: INTRODUCTION.....	1
1.1 Background.....	1
1.2 Significance of study	6
1.3 Objectives of present research.....	7
1.4 Scope of this study.....	8
1.5 Layout of thesis	8
CHAPTER 2: LITERATURE REVIEW.....	9
2.1 Background.....	9
2.2 Solar Energy	11
2.3 Solar Collectors	11
2.3.1 Evacuated tube solar collectors (ETSCs)	13
2.3.1.1 Single walled glass evacuated tube	14
2.3.1.2 Dewar tube	16
2.3.2 Flat-Plate Collectors	16
2.3.3 Linear Fresnel reflector (LFR)	17

2.3.3.1	Parabolic trough collector	18
2.3.3.2	Parabolic dish reflector (PDR)	19
2.3.3.3	Heliostat field collector (HFC).....	19
2.4	Heat transfer in evacuated tube solar collectors	20
2.5	Nanofluids	21
2.5.1	Base fluids	22
2.5.2	Carbon based nanoparticle	23
2.5.2.1	Graphene	24
2.5.2.2	Graphene nanoplatelets (GNP)	25
2.6	Thermal conduction of carbon-based materials.....	26
2.7	Preparation of nanofluids.....	28
2.7.1	The single-step preparation process	29
2.7.2	The two-step preparation process.....	29
2.8	Stability of nanofluid.....	30
2.9	Efficiency enhancement of solar collector when using nanofluid.....	31
2.10	Efficiency enhancement of ETSC when using nanofluid.....	34
2.11	Different modes of energy transports in nanofluids	36
2.12	Thermo-physical properties of nanofluid	38
2.13	Thermal conductivity enhancement in nanofluids.....	40
2.14	Convective heat transfer of nanofluids.....	43
2.15	Viscosity of nanofluids.....	45
2.16	Evaluation of thermal conductivity and viscosity of nanofluids by design of experiment (DOE)	47
2.17	Statistical software for optimization.....	49
2.17.1	Screening.....	50
2.17.2	Factorial.....	51

2.17.3	Response surface methodology (RSM).....	51
2.17.3.1	Central composite design (CCD)	52
2.17.3.2	Box-Behnken Design (BBD)	52
2.18	3-dimensional computational fluid dynamics (CFD).....	53
2.19	Summary.....	56
CHAPTER 3: METHODOLOGY.....		58
3.1	Introduction	58
3.2	Part I: Experimental design by DOE	59
3.3	Part II: Experimental	61
3.3.1	Material and nanoparticles dispersion in liquid	61
3.3.2	Thermo-physical properties measurements.....	62
3.3.3	Thermal conductivity measurement	62
3.3.4	Viscosity measurement	62
3.3.5	Stability analysis	63
3.3.6	Thermal analysis	63
3.4	Morphology study	64
3.5	Specification of the ETCS apparatus.....	64
3.6	ASHRAE standard.....	67
3.7	Uncertainty analysis	68
3.8	Part III: Analytical approach	69
3.8.1	Energy analysis (First law of thermodynamics).....	69
3.8.2	Exergy analysis (Second law of thermodynamics)	70
3.8.3	Pressure drop and pumping power	74
3.9	Part IV: CFD Solver	75
3.9.1	Problem definition.....	75
3.9.2	Physical properties and key parameters	76

3.9.3	Geometry Modeling	76
3.9.4	Mesh generation	77
3.9.5	Boundaries condition.....	77
3.9.6	Governing Equations.....	78
3.9.7	Solution procedure	80
 CHAPTER 4: RESULTS & DISCUSSION.....		81
4.1	Introduction	81
4.2	Design of Experiment.....	81
4.2.1	Statistical analysis of relative thermal conductivity.....	82
4.2.2	Statistical analysis of relative viscosity.....	84
4.2.3	Proposed Models	85
4.3	Nanofluid preparation without surfactant.....	90
4.4	Morphology of GNP dispersion	91
4.5	Solar radiation and ambient temperature measurement	92
4.6	Distilled water as working fluid	93
4.7	Thermal performance of the ETSC with GNP nanofluid as working fluid.....	94
4.8	Correlation development between thermal efficiency and thermal conductivity..	98
4.9	Energy and exergy efficiency	100
4.10	Pumping power.....	104
4.11	Exergy destruction, entropy generation and Bejan number	105
4.12	Model validation.....	108
4.12.1	Comparison of CFD predicted outlet nanofluid temperature with experimental data	112
 CHAPTER 5: CONCLUSION AND RECOMMENDATIONS.....		114
5.1	Conclusion.....	114

5.2 Challenges and future recommendations.....	116
References.....	119
List of Publications and Papers Presented	133
Appendix.....	134

Universiti Malaya

LIST OF FIGURES

Figure 1.1: Types of solar collectors.....	5
Figure 2.1: Representations of a water-in glass collector (a), of a U-type collector (b) and of a heat-pipe collector (c) (Evangelisti, Vollaro, & Asdrubali, 2019).....	13
Figure 2.2: Cross-section of (a) Model I, (b) Model II, (c) Model III and (d) Model IV(Kim & Seo, 2007)	15
Figure 2.3: Flat Plate Collectors (Kalogirou, 2009).....	17
Figure 2.4: Linear Fresnel reflectors (Larsen, Altamirano, & Hernández, 2012).....	18
Figure 2.5: Parabolic trough collectors (Reddy, Kaushik, & Tyagi, 2012).....	18
Figure 2.6: Parabolic dish reflectors (Z. Wang, 2010).....	19
Figure 2.7: Heliostat field collectors (Kalogirou, 2004)	20
Figure 2.8: Common base fluids, nanoparticles, and surfactants for synthesizing nanofluid	22
Figure 2.9: Modes of energy transport in nanofluids.....	37
Figure 2.10: Three-factor full factorial design with center point.....	51
Figure 2.11: Graphic representations of central composite, face-centered cube and Box–Behnken designs	53
Figure 3.1: Flowchart of experimental and analytical analysis	58
Figure 3.2: Schematic setup of KD2 thermal properties analyzer	62
Figure 3.3: A schematic of evacuated tube arrangement.....	65
Figure 3.4: Photograph of the experimental setup (front and back view).....	67
Figure 3.5: Schematic the manifold network of ETSC with 12 heat pipes.....	76
Figure 3.6: Geometry modeling of manifold network	76
Figure 3.7: Magnified meshed part of the computational domain.....	77
Figure 4.1: Correlation between experimental and predicted values for (a) viscosity (b) thermal conductivity	87

Figure 4.2: Relative thermal conductivity of GNP nanofluids versus temperatures, at three different concentration	88
Figure 4.3: Relative viscosity of GNP nanofluids versus temperatures in different concentration.....	88
Figure 4.4: Interaction effect of temperature and concentration on thermal conductivity ratio response: (a) 3-D surface; (b) contour plot and Interaction effect of temperature and concentration on viscosity response: (c) 3D surface; (d) contour plot.	89
Figure 4.5: Studentized residuals versus (a) predicted response (b) run number for viscosity and (c) predicted response (d) run number for thermal conductivity	90
Figure 4.6: Photograph image of prepared sample of GNP nanofluid after three months	91
Figure 4.7: TEM images of GNP	92
Figure 4.8: Variation of total energy gain of ETSC system as a function of different tilt angle.....	92
Figure 4.9: The average solar radiation versus time for the test period.....	93
Figure 4.10: Efficiency of ETSC and temperature difference for Distilled water.....	94
Figure 4.11: Thermal efficiency of ETSC versus time at different concentrations of GNP nanofluid (a) 0.025 wt%, (b) 0.05 wt%, (c) 0.075 wt% and (d) 0.1 wt%.....	95
Figure 4.12: Effect of concentration and mass flow rate on temperature difference.....	97
Figure 4.13: Thermal Efficiency with the enhancement of concentration.....	98
Figure 4.14: Experimental data versus predicted data of thermal efficiency.....	99
Figure 4.15: Impact of particle concentration and mass flow rate on energy efficiency (a) and exergy efficiency (b)	101
Figure 4.16: Effect of mass flow rate on pumping power and pressure drop at varying particle concentration.....	104
Figure 4.17: (a) Variation of exergy destruction with respect to mass flow and concentration and (b) effect of mass flow rate on entropy generation.....	106
Figure 4.18: (a) Effect of mass flow rate on Bejan number and (b) Effect of nanofluid concentration (wt%) on Bejan number	107
Figure 4.19:CFD result of outlet temperature for water and nanofluid.	108

Figure 4.20: Variation of a)water , b) nanofluid temperature along the manifold at 10 am.	109
Figure 4.21: Variation of a)water , b) nanofluid temperature along the manifold at 11 am.	110
Figure 4.22: Variation of a)water , b) nanofluid temperature along the manifold at 12 pm.	111
Figure 4.23: Variation of a)water , b) nanofluid temperature along the manifold at 1 pm.	112
Figure 4.24: Variation of predicted and experimental outlet nanofluid temperature vs time for $\dot{m} = 0.5$ L/min.....	113

Universiti Malaysia

LIST OF TABLES

Table 2.1: Solar radiation in Malaysia (average value throughout the year) (Mekhilef et al., 2012)	11
Table 2.2: Solar Energy Collectors (Kalogirou, 2004)	12
Table 2.3: Selected base fluid properties affecting nanofluid heat transfer at 20°C.....	23
Table 2.4: Selected study of different carbon-based nanofluids and some parameters effect on thermal conductivity enhancement	26
Table 2.5: Performance of evacuated tube collectors based on working fluids.....	34
Table 2.6: Properties of different nano fluids (Kamyar, Saidur, & Hasanuzzaman, 2012; Namburu, Kulkarni, Dandekar, & Das, 2007).....	39
Table 2.7 Summary of some researchers conducted 3D numerical modeling of solar collectors	55
Table 3.1: Variable factors and their specifications.....	59
Table 3.2: Experimental design and results.	60
Table 3.3: GNP specifications.	61
Table 3.4: Specifications and details of the ETSC experimental set up	66
Table 3.5: ASHRAE standard that used in this experimental test	68
Table 3.6: Uncertainty analysis for the ETSC collector	68
Table 4.1: Analysis of variance table for relative thermal conductivity	83
Table 4.2: Analysis of variance table for Relative Viscosity.....	85
Table 4.3: Confirmation experiments	87
Table 4.4: Comparison of results obtained for thermal efficiency from this study with other researches.....	103

LIST OF SYMBOLS AND ABBREVIATIONS

Symbol

A	:	Absorbance area, m ²
Be	:	Bejan number
c	:	Collector
C _p	:	Specific heat capacity, J/kg K
Ė _x	:	Exergy, W
h	:	Specific enthalpy, J/kg
i	:	inlet
K	:	Thermal conductivity, W/m K
ṁ	:	Mass flow rate, kg/s
o	:	outlet
Q	:	Energy, W
Ṡ	:	Entropy rate, W/K
S	:	Received solar radiation to plate, W/m ²
S _{gen}	:	Entropy, J/kg K
T	:	Temperature, °C
wt%	:	Weight percentage

Greeks

α	:	Thermal diffusivity, m ² /s
β	:	Slope of solar collector
ρ	:	Appropriate transmittance-absorptance
Φ	:	Latitude
η	:	Efficiency

Abbreviations

Al ₂ O ₃	:	Aluminum Oxide
CPC	:	Compound parabolic collector
CTC	:	Cylindrical trough collector
CuO	:	Copper Oxide
CNT	:	Carbon Nanotube
CCD	:	Central composite design
CFD	:	Computational fluid dynamic
C.V	:	Coefficient of variation
DOE	:	Design of Experiment
D	:	Diameter of the pipe
DASC	:	Direct absorption solar collector
DWCNT	:	Double-Walled Carbon Nanotubes
DW	:	Distilled water
DI	:	Deionized
ETSC	:	Evacuated tube solar collector

EG	:	Ethylene Glycol
FPC	:	Flat-plate collector
GNP	:	Graphene nanoplatelets
GO	:	Graphene Oxide
GA	:	Gum Arabic
HFC	:	Heliostat field collector
LFR	:	Linear Fresnel reflector
MWCNT	:	Multi-Walled Carbon Nanotubes
Nu	:	Nusselt number
NDG	:	Nitrogen-dropped graphene
PDR	:	Parabolic dish reflector
PTC	:	Parabolic trough collector
Re	:	Reynolds number
RSM	:	Response surface methodology
SWCNT	:	Single-wall carbon nanotube
SA	:	Surface area
TiO ₂	:	Titanium Oxide

LIST OF APPENDICES

Appendix A: IMAGES OF EXPERIMENTAL APPARATUS	139
Appendix B: ADDITIONAL TABULATED DATA	141

Universiti Malaya

CHAPTER 1: INTRODUCTION

1.1 Background

Thermal energy transport and conversion play a very significant role in more than 90% of energy technologies (Venkatachalam, Mariam, & Anchala, 2019). This fact increased attraction of researchers to investigate on thermal performance improvement of all applications such water heating, waste heat utilization, cooling and air-conditioning (Khanafar & Vafai, 2018). These years, one of the major research topics in this field is finding and improving the techniques and mechanisms for effective heat transfer. Heat transfer plays a main role in various types of industries; such as solar collectors, power generation, air conditioning systems, process plants, electronic devices etc.(Pei, Li, Zhou, Ji, & Su, 2012). Applying of high-performance materials and change of process parameters were performed to enhance the performance of solar collectors. At present, researchers have given emphasis on developing working fluids for solar thermal systems (Esfe, Saedodin, Mahian, & Wongwises, 2014a). Moreover, the most accessible, environmentally friendly and regular viable source of renewable energy on earth is solar energy. However, the earth receives millions of watts of energy daily coming from solar radiation, one third is reflected back into space, the natural world is used only a fraction of it in the form of photosynthesis and day lighting and the rest is absorbed by clouds, land and oceans (V. Tyagi, Kaushik, & Tyagi, 2012). Therefore, it is very practical to collect solar energy and utilize it efficiently to produce heat, electric power and for cooling purposes in a feasible way. In terms of environment, the effect of using solar energy for a variety of applications is minimal as it produces no harmful pollutants. In addition, environmental consciousness, dwindling of conventional energy sources marks solar energy as the appropriate and sustainable form of energy source to meet the growing demand of energy worldwide (Jacobson & Delucchi, 2011). Due to these facts, various studies and researches are aimed to developed technologies on how to harvest solar energy to serve human beings and are still considering new methods and technologies to maximize the

collection and increase also cooling and heating performance of working fluids in solar collectors (V. Tyagi et al., 2012). Various types of particles such as metallic, non-metallic and polymeric have been suspended into fluids to form suspensions containing millimeters or micrometer sized particles. However, they are not applicable for practical application due to problems such as sedimentation, erosion of pipelines, clogging of flow channels and increase in pressure drop, due to their momentum transfer. Furthermore, they often suffer from rheological problems and instability (Han, Meng, Wu, Zhang, & Zhu, 2011). In particular, the particles tend to settle rapidly. However, these increase in thermal conductivity of the liquid enhances their practical importance. Among the nano and micro matter sized suspensions as heat exchanging liquids, the nanofluids are preferable (Esfe, Saedodin, Bahiraei, et al., 2014). A research group at Argonne National Laboratory was the first who continuously studied the use of Nano-sized particles around a decade ago. A nanofluid is a suspension of ultra-fine particles with extremely high thermal conductivity compare to conventional base fluid. Nanofluids have the potential increase of heat transfer characteristics in comparison to the original fluid (Hadadian, Samiee, Ahmadzadeh, & Goharshadi, 2013). The importance and benefits of nano-sized particles compared to micro particles have been studied and its advantages are listed:

1. Longer suspension time (High stability)
2. Much higher surface area
3. Higher thermal conductivity
4. Significant energy saving
5. Lesser corrosion, erosion and clogging
6. Larger surface area/volume ratio (1000 times larger)
7. Reduction in inventory of heat transfer fluid
8. Lower demand for pumping power

Many researches have been carried to increase the thermal properties of the heat transfer within the fluids by adding high thermally conductive nanoparticle with quantities ranging from 0.001wt% to 50wt% (Mohammad Mehrali, Emad Sadeghinezhad, et al., 2014b).

Over the last several years, significant researches have been carried out leading to the development of using of the heat transfer enhancement liquids. Generally, additives have been used to increase the heat transfer performance of the base fluid. Furthermore, these nanofluids are expected to ideally suit in practical application as their use incurs little or no penalty in pressure drop but changes the transport properties and heat transfer characteristics of the base fluid. Due to ultra-fine nature of these nanoparticles, nanofluids behave as a single-phase fluid rather than multiphase, i.e., solid-liquid mixture (Esfe, Saedodin, Mahian, & Wongwises, 2014c). It is worth noting that good and proper dispersion of nanoparticles and also high stability of the nanofluids are essential for their extensive applications (Togun et al., 2014). Recently, a lots of taxation have been carried on the use of carbon-based nanostructures to prepare nanofluids (Moghaddam, Goharshadi, Entezari, & Nancarrow, 2013). Hence, a variety of applications of graphene have come to the fore front (Mehrali, Latibari, Mehrali, Indra Mahlia, & Cornelis Metselaar, 2013; Mehrali, Latibari, Mehrali, Mahlia, et al., 2013). Graphene has received much attention since it has been discovered by Novoselov et al. (2004) due to its unique atomic structure. It's a single-atom-thick sheet of hexagonally arrayed sp^2 -bonded carbon atoms. Graphene Nanoplatelets are flakes composed of multilayer graphene sheets in a "platelet" morphology. The unique shape with a high aspect ratio of thinness to width give them excellent electrical and thermal conductivity and make them ideal for applications such as strengthening composites and matrix materials. In the last few years, a significant number of studies have been conducted with graphene due to its unique thermal, electrical, optical, mechanical and other favorable characteristics. One of the

most important part of graphene investigation is characterization of graphene and involves measurements based on various microscopic and spectroscopic techniques (Graphene: Synthesis, Properties, and Phenomena, 2013).

World energy demand is increasing and expected to accelerate more in the future due to development and rise in human population (Hadadian et al., 2013). However, the sources and production of fossil oil are depleting. Renewable energies are becoming more important in the world economy today because they are sustainable, safe and clean. Therefore, there is a large effort in using solar thermal energy as solution to replace oil as a source of heat energy. There are particular challenges in the effective collection and storage of solar energy though it is free for taking. As solar radiation is only available during daytime, the energy must be collected in an efficient manner to make use of most of the daylight hours and then must be stored. Solar thermal collectors are the existing components to capture solar radiation which is then turned to thermal energy and transferred to a working fluid subsequently. Therefore, solar collectors are the main and most critical components of any solar system (Singh, Kumar, Hasan, Khan, & Tiwari, 2013).

Basically, there are two types of collectors, tracking and stationary (Kalogirou, 2004) Figure 1.1. In the stationary or non-concentrating type such a flat-plate and evacuated-tube solar collectors, the collector area (i.e., the area that intercepts the solar radiation) is the same as the absorber area (i.e., the area absorbing the radiation). In these types the whole solar panel absorbs light while in tracking or concentrating collectors have a bigger interceptor than absorber.

Different collector configurations can assistance to gain a large range of temperature. For example, 20–80 °C is the working temperature range of a flat plate solar collectors

(FPSCs) (Sharma & Diaz, 2011) and 50–200 °C is for an evacuated tube solar collector (Kalogirou, 2013).

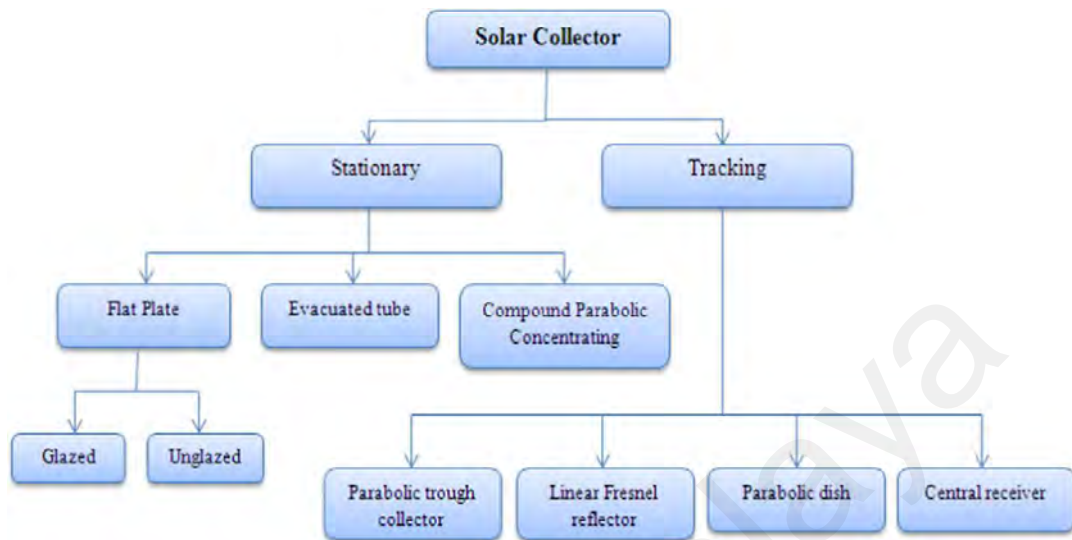


Figure 1.1: Types of solar collectors

ETSCs have significantly lower price and heat loss to compare to the standard flat plate solar collector ,FPSCs (Kalogirou, 2004). On the other hand, an ETSCs overcomes both these obstacles due to the existence of vacuum in annular space between two concentric glass tubes, which eliminates sun tracking by its tubular design. Conventional FPSCs are generally designed for warm and sunny climates. Their performance decreases during cold, windy and cloudy days and they are greatly influenced by the weather as moisture and condensation cause early erosion of internal materials which might cause system failure. In contrast, ETSCs have outstanding easy transportability, thermal performance and expedient installation. Moreover, ETSCs are suitable for unfavorable climates (Tang, Li, Zhong, & Lan, 2006).

According to researchers (Kalogirou, 2004; Morrison, Budihardjo, & Behnia, 2004; Zubriski & Dick, 2012) evacuated tube solar collectors have much higher efficiencies than flat plate solar collectors. ETSCs be able to collect both diffuse and direct radiations. Apart from very good thermal performances, ETSCs have easy transportability convenient installation.

Thermodynamics analysis is one of the preferred methods to analyze the performance of a solar collector. In thermodynamics analysis, the energy equation alone is insufficient to evaluate the evacuated tube solar collector efficiency. The second law or exergy analysis is more effective to determine the source and magnitude of irreversibilities and can be used to improve the efficiency of the system. Exergy is the maximum output that can be achieved relative to the environment temperature (Cengel & Boles, 2002). Some exergy analysis studies have been conducted by (Mahbubul, Saidur, & Amalina, 2012) on various solar energy applications and (Sabiha, Saidur, Mekhilef, & Mahian, 2015) on evacuated tube solar collectors. However, to the best of the author's knowledge, experimental studies on evacuated tube solar collector using GNP nanofluid have not appeared in the open literature even though a lot of simulation works have been done and all the studies on the exergy analysis on evacuated tube solar thermal collectors are either simulation or theoretical. Therefore, this thesis will focus on the thermodynamics performance and heat transfer characteristic of evacuated tube solar collector when applying GNP nanofluid to fill up those gaps.

1.2 Significance of study

Heat transfer fluids such as water, ethylene glycol, Freon and mineral oil play an important role in many industrial processes such as power generation, heating and cooling processes, chemical productions, transportations and microelectronics (Mangal, Lamba, Gupta, & Jhamb, 2010). The primary problem to the high compactness and effectiveness of the solar collectors is the poor heat transfer characteristics of these working fluids. An improvement in thermal conductivity of these conventional fluids is a key idea to improve the heat transfer characteristics (Gao, Zhang, Fan, Lin, & Yu, 2013). Thus, the essential initiative is to seek solid particles especially nano-sized particles having thermal conductivity several thousand orders higher than those of conventional fluids

(Sadeghinezhad et al., 2014). A substantial amount of research has been performed on thermo-physical properties of metal and oxide nanofluids and also applying these working fluids in different solar collectors, but little has been done on non-metallic nanoparticles nanofluids. This study focuses on experimental investigation of heat transfer characteristics of GNPs nanofluid and thermodynamics performance of evacuated heat pipe tube solar collector by applying GNPs nanofluid.

Up to date, no work has thus far been conducted to investigate the influence of this nanofluids on heat transfer and exergy analysis in the evacuated heat pipe tube solar collector. Moreover, the carbon base nanoparticles could protect the pipelines of the collector from the damage and corrosion problems due to the size of nanoparticles and less effect on pH. Therefore, the purpose of this study is to experimentally measure the heat transfer of this nanofluids and study second law characteristics of nanofluids in the ETSC. 3-Dimensional computational fluid dynamic analysis has been conducted to predict the outlet nanofluid temperature.

1.3 Objectives of present research

The main objectives of this research can be summarized as follows:

- 1- To optimize the thermal conductivity and viscosity of GNP nanofluids by using Design of Experiment (DOE)
- 2- To investigate the thermal efficiency enhancement of an evacuated tube solar collector (ETSC) using GNP nanofluid.
- 3- To analyze the thermodynamic performance of ETSC by using GNP nanofluid such as exergy efficiency and destruction, entropy, bejan number and pumping power.

- 4- To simulate the outlet nanofluid temperature of ETSC system by using a 3-Dimensional computational fluid dynamic (CFD) analysis.

1.4 Scope of this study

Solar collectors are low in efficiency. Applying nanofluid in solar collector can address this issue. The present investigation is an attempt to provide the efficiency, heat transfer and thermophysical analysis of solar collector when applying nanofluid as working fluid. The thermo physical properties, rheological behavior and stability of proposed GNP/water nanofluid were considered. The prepared nanofluid was applied in an evacuated tube solar collector where parameters such as solar radiations, inlet temperatures, outlet temperatures, absorber surface temperatures and ambient temperatures were recorded. All these data were then used to perform efficiency and heat transfer of nanofluid solar collectors and comparison was made with distilled water solar collectors.

1.5 Layout of thesis

The thesis starts with Chapter 1 which is focusing on giving a general idea of different mechanisms of energy transport in nanofluids and the importance of renewable energy sources such as solar thermal energy systems. In Chapter 2 a literature survey is presented. In Chapter 3, the methodology of the statistical approach and analytical method that are applied to calculate efficiency, exergy, pumping power, heat transfer, energy analysis and also simulation is discussed. The results that have been obtained from the experiments, calculations and software are discussed in Chapter 4. Also, the uncertainty analysis of the experimental set-up and analysis of tables and graphs by detailed are well discussed in Chapter 4. Chapter 5 contains a summary of the work done and proposed recommendations for future work.

CHAPTER 2: LITERATURE REVIEW

2.1 Background

With the development of solar application and similar devices, the requirement for improved heat transfer became more important. Solar collectors, heat transfer fluids or other components related to heat transfer were invented and improved with thriving technology. Usage of more compact, larger heat transfer area heat transfer devices are common in today's industry. At this point, increasing the heat transfer area of a device may no longer be a solution because the practical limitations of manufacturing (Sarkar, Ghosh, & Adil, 2015).

Researchers targeted two different ways to overcome these problems in the heat transfer research world, which are improving micro or nano sized channels and different types of heat transfer fluids (Sarkar et al., 2015). The second alternative includes nanofluid improvement and usage in heat transfer applications such as solar application.

Choi and Eastman (1995) first presented the term nanofluids referring to fluids containing dispersed nano sized particles having substantially higher thermal conductivity. Nanoparticles have unique potential to enhance the thermal transport properties of heat transfer systems than micrometer and millimeter sized particles. This is mainly due to the tininess of nanoparticles and its nanostructures, which not only improves the stability and the applicability of liquid suspensions, but also increases the thermal conductivity, specific surface area and the diffusion mobility of Brownian motion of the particles (Choi & Eastman, 1995).

Nanoparticles are generally considered to be a discovery of modern science; however, their history is long and rich. Naturally occurring nanoparticles and nanostructures of all types are as common as the macro-sized objects that surround us (J.-C. Yang, Li, Cai, Zhang, & Yu, 2014). Indeed, the universe itself was built from the bottom up, and that by

necessity, dictates that an astoundingly complex micro-world exists. Nanoparticles are common in nature as trace metals, organics, and inorganics formed through varied natural processes. These include the production of carbon structures such as fullerenes, through the combustion of any complex carbon molecule, and the creation of organic, inorganic, and metallic nanostructures through thermal, chemical, biological, and physical processes. Truly, the collection of naturally occurring nanoparticles is noteworthy and can be reviewed further in the literature.

The first truly scientific study of nanoparticles was done by Michael Faraday in 1857 when he discussed the optical properties of nanoscale metals (Esfe, Saedodin, Sina, Afrand, & Rostami, 2015). Since that time, a great deal of scientific research has focused on the physical and transport properties of nanoparticles. Indeed, the entire field of Nano science and nanoparticles has blossomed along with their applications and potential.

The heat transfer improvement by applying nanofluids is important because of the reasons mentioned above. The heat transfer enhancement was defined as proportion between heat transfer coefficient of nanofluid and heat transfer coefficient of base fluid at a constant parameter (Badar, Buchholz, & Ziegler, 2012).

Thermal conductivity enhancement was explained as ratio between nanofluid thermal conductivity and base fluid thermal conductivity. A comparison can be made between the base fluid and the nanofluid, thus; it can be observed that how much heat transfer coefficient improvement is achieved. The challenging topic on this issue is accurate prediction of heat transfer enhancement.

In this chapter, a literature survey on the studies about the solar energy, different solar collectors, heat transfer properties, design of experiment and simulation studies on solar collectors with different nanofluids are presented.

2.2 Solar Energy

The sun is a hot sphere gaseous matter with a diameter of 1.39×10^9 m. The distance from the sun to the earth is about 1.5×10^8 km. After leaving the sun thermal radiation travels with the speed of about 300,000 km/s and reach the earth in 8 min and 20 s. Total energy output of the sun is 3.8×10^{20} MW and equal to 63 MW/m^2 . This energy radiates in all directions and only a fraction of about 1.7×10^{14} kW reaches the earth. However, this small fraction of energy in 84 min can meet the need of the world energy demand for a year (Kalogirou, 2009).

The path of the sun as seen from the earth varies throughout the year. Knowing the sun path is important to determine the solar radiation falling on a surface so that proper orientation and placement of solar collectors can be made to avoid shading (Kalogirou, 2009). Geographically Malaysia is situated at the equatorial region with an average solar radiation of $400 - 600 \text{ MJ/m}^2$ per month (Mekhilef et al., 2012). The annual average solar radiation in Malaysia is presented in Table 2.1.

Table 2.1: Solar radiation in Malaysia (average value throughout the year) (Mekhilef et al., 2012)

Irradiance	Yearly average value (kWh/m ²)
Kuching	1470
Kuala Lumpur	1571
Petaling Jaya	1571
Seremban	1572

2.3 Solar Collectors

Solar collector is the major component, most important part of a solar energy system (Kalogirou, 2009). Solar collector is a device to absorb solar radiation and heat the fluid that flows through the collector. The heat can be used directly or be stored for nighttime

or on cloudy days. Solar collectors are classified into low temperature, medium temperature and high temperature heat exchangers. Mainly, there are three types of collectors which are flat plate, evacuated tube, and concentrating (Foster, Ghassemi, & Cota, 2009). Kalogirou (2009) divide solar collectors into non-concentrating or stationery and concentrating. Table 2.2 shows a list of collectors available (Kalogirou, 2004).

Table 2.2: Solar Energy Collectors (Kalogirou, 2004)

Motion	Collector Type	Absorber Type	Indicative Temperature Range (°C)
Stationary	Flat Plate Collector (FPC)	Flat	30-80
	Evacuated Tube Collector (ETC)	Flat	50-200
	Compound Parabolic Collector (CPC)	Tubular	60-240
Single axis tracking	Linear Fresnel Reflector (LFR)	Tubular	60-250
	Cylindrical Trough Collector (CTC)	Tubular	60-300
	Parabolic trough collector	Tubular	60-400
Two-axis tracking	Parabolic Dish Reflector (PDR)	Point	100-1500
	Heliostat Field Collector (HFC)	Point	150-2000

2.3.1 Evacuated tube solar collectors (ETSCs)

Evacuated tube collectors consist of a heat pipe inside a vacuum-sealed tube. The vacuum will reduce convection and conduction heat loss. The efficiency is higher than flat-plate collectors, but the cost is relatively expensive (Kalogirou, 2009).

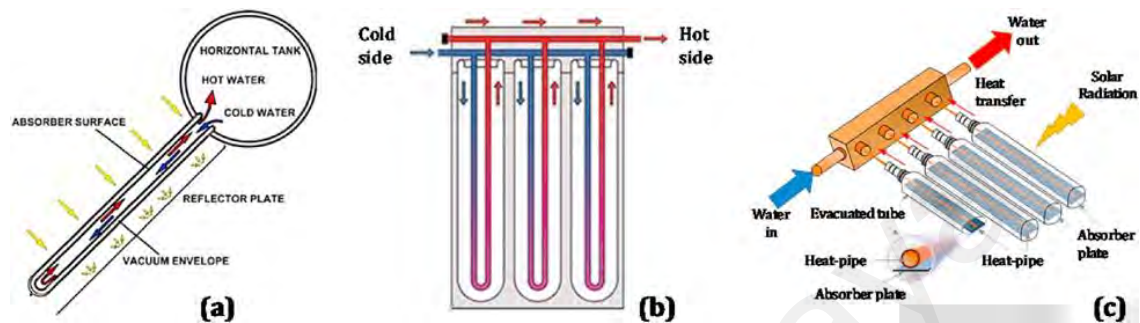


Figure 2.1: Representations of a water-in glass collector (a), of a U-type collector (b) and of a heat-pipe collector (c) (Evangelisti, Vollaro, & Asdrubali, 2019).

According to Gao et al. (2013) available types of evacuated tube solar collectors can be categorized into two groups; one is the single-walled glass evacuated tube and the other is the Dewar tube. Also, there are three typical evacuated tube collectors exist (Evangelisti et al., 2019) (Figure 2.1):

1. Water-in glass:

This collector consists of waterlogged tubes (characterized by a single end) connected to a horizontal tank. The pipes are characterized by two concentric glass tubes closed at one end with a vacuum in the annular space between the pipes and a selective surface treated on the external surface of the internal tube. The heat transfer mechanism is determined by a water's natural flow by the single-ended opening into the horizontal tank. Solar radiation heats up the water, which progressively rises along the higher part of the pipe. Warmer water is substituted by colder water deriving from the tank. A representation is provided in Figure 2.1a.

2. U-type:

The thermal fluid flows directly into the absorber, placed inside the tube vacuum. The plate is substituted by metal cylinders (e.g. made of copper), possibly finned, treated on the surface with black selective paints; each of these tubes is inserted, in turn, into an outer glass tube. During the assembly of the collector, air is drawn in between the two glass tubes to obtain the vacuum conditions. The different tubes are connected to each other as shown in the simplified picture of Figure 2.1b.

3. Heat-pipe:

These collectors can be equipped with a heat-pipe system for the recovery of heat from the absorber. Inside each tube, made of glass, there is an additional pipe made of copper, filled with an alcoholic solution able to evaporate at low temperatures. The alcoholic solution, by heating up itself, goes back along the heat-pipe. Then, it condenses giving heat to the heat-carrying fluid that flows into the collector. A schematic representation is reported in Figure 2.1c.

2.3.1.1 Single walled glass evacuated tube

The single-walled glass evacuated tube is popular in Europe. Badar et al. (2012) studied the thermal performance of an individual single walled evacuated tube with direct flow type coaxial piping based on analytical steady state model. Kim and Seo (2007) investigated the thermal performance of an ETSC with four different shaped absorbers both experimentally and numerically. Four different shapes are: finned tube (Model I), tube welded inside a circular fin (Model II), U tube welded on a copper plate (Model III) and U tube welded inside a rectangular duct (Model IV) as illustrated in Figure 2.2.

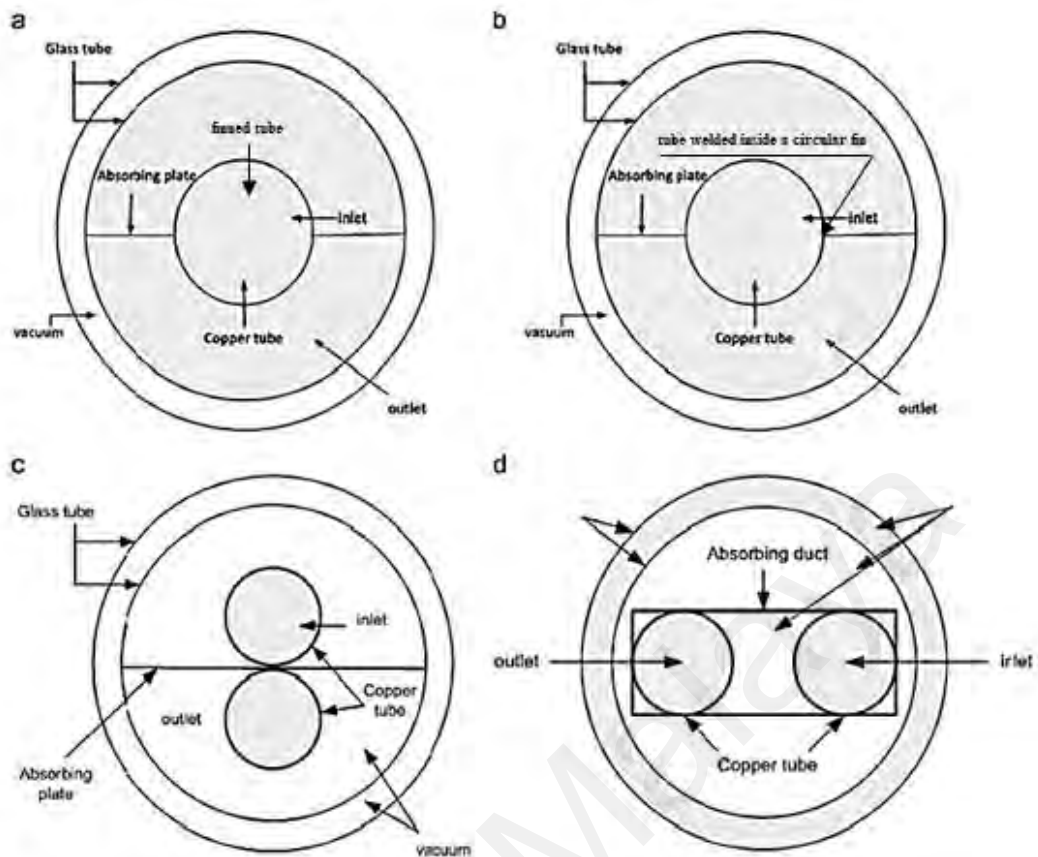


Figure 2.2: Cross-section of (a) Model I, (b) Model II, (c) Model III and (d) Model IV (Kim & Seo, 2007)

Firstly, by considering only the beam radiation, the performance of a single collector tube was observed, and it was found that the incidence angle has great influence on the collector efficiency. Model III had the highest efficiency with small incidence angle but the efficiency of model II became higher than model III with the increment of incidence angle. The incidence angle has negligible impacts on collector performance while prototype of solar water heating system with looped heat pipe single walled evacuated tube was designed and both experimental and theoretical research have been carried out by Zhao, Wang, and Tang (2010). Nkwetta, Smyth, Zacharopoulos, and Hyde (2013) demonstrated a solar collector which combines single walled evacuated tubes, heat pipe and an internal or external concentrator for improving output temperatures.

2.3.1.2 Dewar tube

Dewar tube consists of inner and outer tubes which are made of borosilicate glass and selective absorbance is used to coat the outside wall of the inner tube to collect solar energy. The heat loss is reduced in by evacuating the layer between the inner and outer tubes. Tang, Yang, and Gao (2011) investigated on dewar tubes and mentioned that the cheap price of dewar water in glass evacuated tube solar collector (WGETSC) makes it popular than dewar tube with U pipe evacuated tube (UPETSC) with heat pipe. Qi (2007) investigated the thermal performance of dewar ETSC with an inserted U pipe. Yan, Tian, Hou, and Zhang (2008) studied about the unsteady state efficiency of the dewar tube solar collector having heat pipe inserted. Xu, Wang, Yuan, Li, and Ruan (2012) tested the thermal performance of dewar tube solar collector under various dynamic conditions and they used air as the heat transfer fluid. They investigated the performance of dewar tube where the inner tube was filled with coaxial fluid and the outer tube was filled with an antifreeze solution and a one-dimensional mathematical model was established.

2.3.2 Flat-Plate Collectors

A flat-plate solar collector is shown in Figure 2.3. Solar radiation will pass through the transparent cover and will be absorbed by the absorber plate and be transported to the fluid in the tube and carried for use. The transparent cover purpose is to reduce convection losses from the plate and radiation losses from the collector. Flat-plate collector is cheap, fixed and without sun tracking (Kalogirou, 2009).

The performance of a flat plate solar collector can be influenced by several factors such as material, shape, coating of absorber plate, type of glazes, number of tubes, distance between tubes, and collector's insulation material. The collector's performance can also be affected by operating condition such as flow rate, ambient temperature, wind

speed and solar radiation. Lots of researches focus on these parameters for improving flat plate solar collectors.

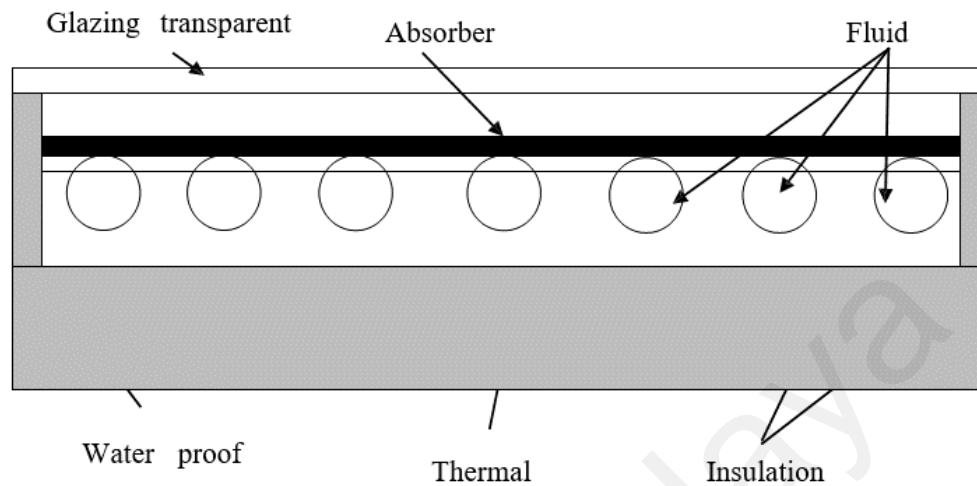


Figure 2.3: Flat Plate Collectors (Kalogirou, 2009)

2.3.3 Linear Fresnel reflector (LFR)

A linear Fresnel Reflector collector is made from an array of linear mirror strips that concentrate light onto a linear receiver as shown in Figure 2.4. On top of the receiver, a small parabolic mirror can be attached for further focusing the light. These systems aim to offer lower overall costs by sharing a receiver between several mirrors (as compared with trough and dish concepts), while still using the simple line-focus geometry with one axis for tracking. This is similar to the trough design (and different from central towers and dishes with dual axis). The receiver is stationary and so fluid couplings are not required (as in troughs and dishes).

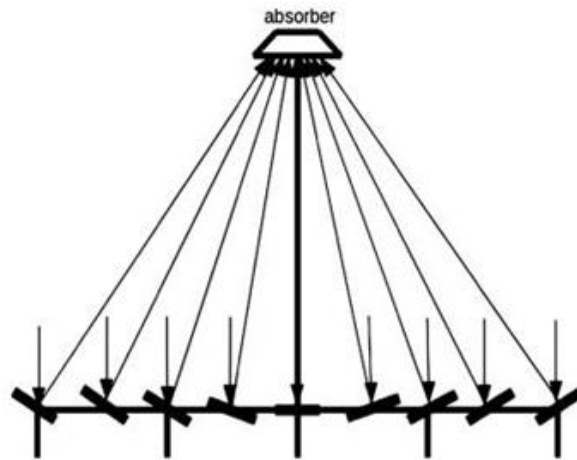


Figure 2.4: Linear Fresnel reflectors (Larsen, Altamirano, & Hernández, 2012)

2.3.3.1 Parabolic trough collector

Parabolic trough collectors parabolic shape reflector is made by bending a sheet of reflective materials where a black metal tube that is covered with a glass tube to reduce losses is used as the receiver. The system consists of low cost, light structure; single axis tracking and can effectively obtained heat up to 400°C (Kalogirou, 2009) as shown in Figure 2.5.

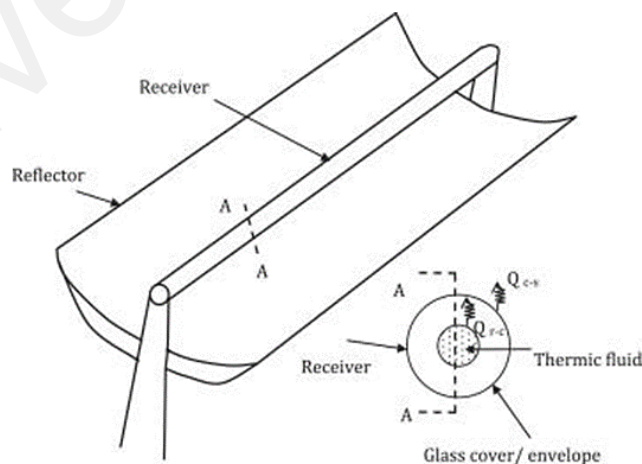


Figure 2.5: Parabolic trough collectors (Reddy, Kaushik, & Tyagi, 2012)

2.3.3.2 Parabolic dish reflector (PDR)

A parabolic dish reflector will concentrate solar energy at focal point receiver and tracks the sun in two axes as shown in Figure 2.6 Parabolic dish reflector can be used for electricity generation using parabolic dish engine system with temperature generated more than 1500°C. Advantages of parabolic dishes are (De Laquil III, Kearney, Geyer, & Diver, 1993):

- The most efficient collectors because it always pointing at the sun.
- Highly efficient at thermal energy absorption and power generation because of very high concentration ratios of 600 to 2000.
- Can function either independently or as part of a larger system.

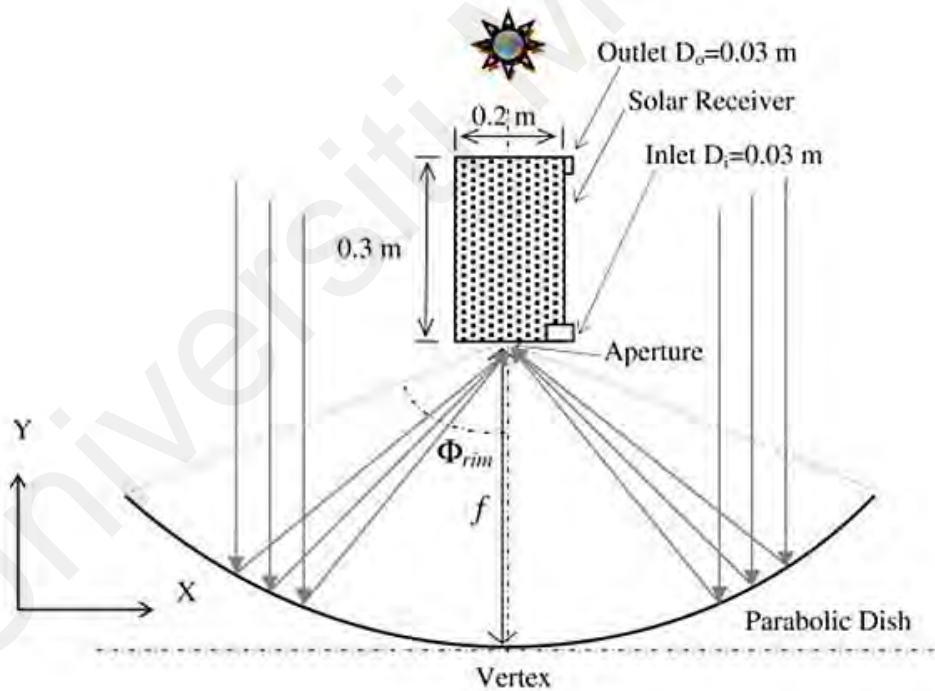


Figure 2.6: Parabolic dish reflectors (Z. Wang, 2010)

2.3.3.3 Heliostat field collector (HFC)

Heliostat collector use slightly concave segment, multiple flat mirrors that direct large amount of heat energy into the cavity of a steam generator to produce electricity (Figure

2.7). They have single receiver, with concentration ratios of 300 to 1500, can store thermal energy and quite large in size generally more than 10 MW (De Laquil III et al., 1993). Energy collected by the system will be converted to electricity using a steam turbine generator that is similar with the conventional fossil-fuelled thermal power plants (Romero, Buck, & Pacheco, 2002).

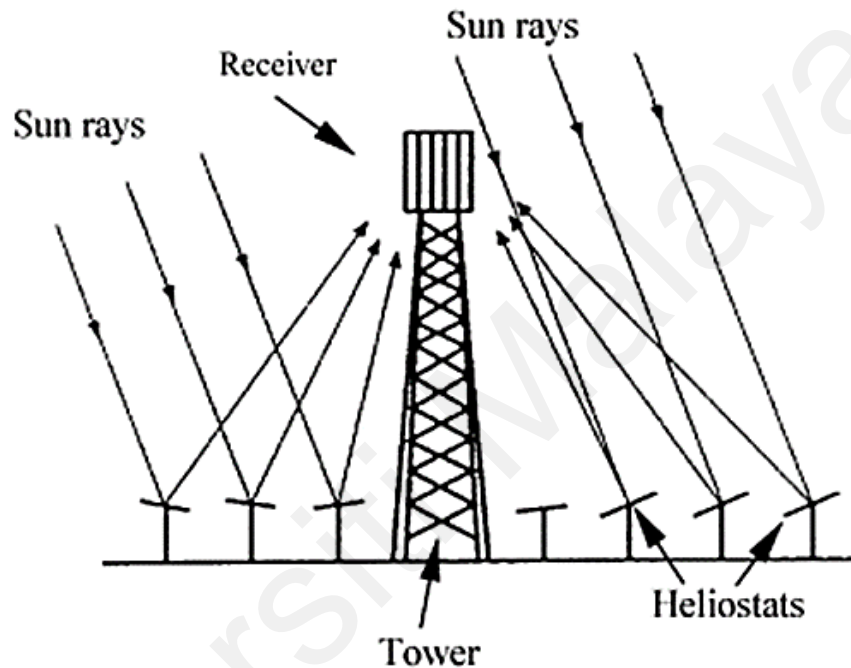


Figure 2.7: Heliostat field collectors (Kalogirou, 2004)

2.4 Heat transfer in evacuated tube solar collectors

The major drawback of the evacuated tube solar collectors is extracting heat from the evacuated tube and reducing the useful energy gain of the system. The enhancement of heat transfer rate in solar collectors could improve the overall performance of the heating system. Enhancement of heat transfer rate can be achieved by increasing the heat transfer coefficient by disrupting boundary layer, increasing the Reynolds number or increasing the temperature gradient.

In the effort of raising the efficiency of solar collector, the values of the convective and radiative heat transfer coefficients are often of interest to many researchers. An ETSC is made of parallel evacuated glass pipes. Each evacuated pipe consists of two tubes, one is inner, and the other is outer tube. The inner tube is coated with a selective coating while the outer tube is transparent. Light rays pass through the transparent outer tube and are absorbed by the inner tube. Both the inner and outer tubes have minimal reflection properties. The inner tube gets heated while the sunlight passes through the outer tube and to keep the heat inside the inner tube, a vacuum is created which allows the solar radiation to go through but does not allow the heat to transfer. In order to create the vacuum, the two tubes are fused together on top and the existing air is pumped out. Thus, the heat stays inside the inner pipes and collects solar radiation efficiently. Therefore, an ETSC is the most efficient solar thermal collector (Moorthy Mahendran, Ali, Shahrani, & Bakar, 2013).

2.5 Nanofluids

Nanofluids are made from generally one, two or more type of nanoparticles can be dispersed in base fluid and remain suspended in the fluid. As it is mentioned above, the aim is to surge the thermal conductivity of the fluid matrix for using in heat transfer applications. Many researches have been carried to increase the thermal properties of the heat transfer fluids by adding high thermally conductive nanoparticle with quantities ranging from 0.001wt% to 50wt% (Mohammad Mehrali, Emad Sadeghinezhad, et al., 2014b). More common nanoparticles and base fluid exploited in synthesis are presented in Figure 2.8.

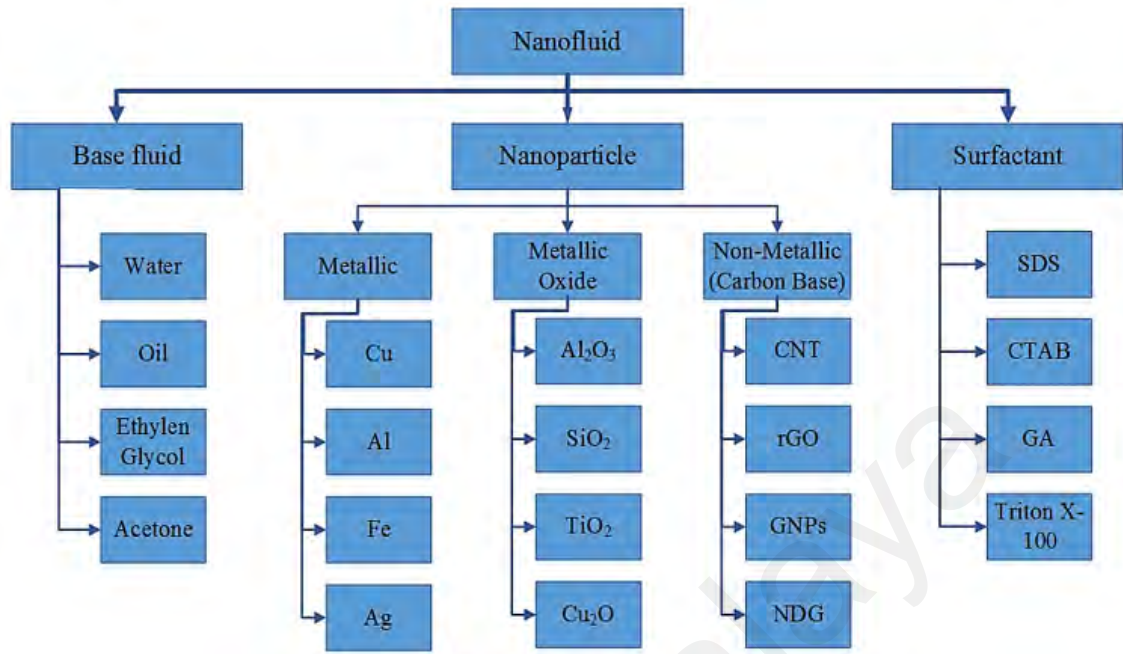


Figure 2.8: Common base fluids, nanoparticles, and surfactants for synthesizing nanofluid

Common heat transfer fluids can also be used as the base fluid of the nanofluid. The important point of the choice of the base fluid is still rely on suitability for a specific heat transfer application. All heat transfer base fluids can be used for nanofluid production as long as they are suitable for production techniques. However, it is important to note that the addition of suspended particles in a base fluid provides more enhancement if the fluid has poor heat transfer capabilities. In other words, it is much more beneficial to use the nanoparticle addition technology while the working fluid of a system has no good thermal conductivity.

2.5.1 Base fluids

As it was mentioned earlier, motion of particles especially Brownian motion can affect thermal conductivity of nanofluids. One noticeable parameter, which is in direct relationship with motion of particles, is viscosity of base fluid (Çağlar & Yamalı, 2012). Effect of electric double layer around nanoparticles could be considered as one influential

parameter on thermal conductivity of nanofluids, depending on base fluid. Table 2.3 Minea and Luciu (2012) denotes thermophysical properties of common heat transfer base fluids, which are important in nanofluid heat transfer phenomena.

Table 2.3: Selected base fluid properties affecting nanofluid heat transfer at 20°C.

Fluid Type	C_p (J/kg·K)	ρ (kg/m ³)	k (W/m·K)	Boiling Point(°C)	Freezing Point(°C)
Water	4184	998	0.599	99.97	0
EG (ethylene glycol)	2383	1117	0.250	102.2	-7.9
EO (engine oil)	1881	888	0.145	220	-30
Propylene Glycol	960	1006	0.147	213	-8

2.5.2 Carbon based nanoparticle

Carbon is a nonmetallic element. It is the sixth most abundantly available element in the universe and is commonly obtained from coal deposits. The three naturally occurring allotropes of carbon are graphite, diamond, and amorphous carbon. The morphology of carbon nanoparticles is spherical, and they appear as a black powder. Black surface or fluid is commonly used as light absorber in any heating application (Esfe, Saedodin, Mahian, & Wongwises, 2014b). Graphene, carbon nanotubes (CNT), and fluorescent carbon quantum dots (CQDs) pertain to carbon materials family. They have attracted much attention in the scientific community and engineering due to their extraordinary physical, chemical, optical, mechanical and thermal properties. Carbon nanotubes are tube-shaped carbon material and can be divided into two types: single-walled carbon nanotubes (SWCNTs) and multi-walled carbon nanotubes (MWCNTs) (Amrollahi, Hamidi, & Rashidi, 2008). Graphene is the thinnest two-dimensional material comprised

of a one-atom-thick planar sheet of sp^2 -bonded carbon atoms, while carbon nanotubes have a cylindrical nanostructure which also consisted of sp^2 -bonded carbon atoms. Graphene can be perceived as the basic structure of graphite, carbon nanotubes, and fullerene.

Many research has been carried to improve the thermal properties of the heat transfer fluids by adding amounts ranging from 0.001wt% to 50wt% of great thermally conductive particles of various nano-materials containing oxides (Minea & Luciu, 2012), nitrides (Zhi, Xu, Bando, & Golberg, 2011), metals (Sundar & Sharma, 2007), diamond (Yeganeh et al., 2010), carbon fiber (K. J. Lee, Yoon, & Jang, 2007), carbon black (Dongxiao, Zhaoguo, Daxiong, Canying, & Haitao, 2011), carbon nanotubes (CNT) (Nasiri, Shariaty-Niasar, Rashidi, & Khodafarin, 2012), single-walled carbon nanotubes (SWNTs) (Nanda et al., 2008), double-walled carbon nanotubes (DWCNT) (Assael, Chen, Metaxa, & Wakeham, 2004), multi-walled carbon nanotubes (MWNTs) (Chen, Xie, & Yu, 2012), graphite (Y. Yang, Zhang, Grulke, Anderson, & Wu, 2005), graphene oxide (GO) (S. W. Lee, Kim, & Bang, 2013), graphene (Yu, Xie, Wang, & Wang, 2011), graphite flakes (Zheng et al., 2011), graphene nanoplatelets (GNPs) (G.-J. Lee & Rhee, 2014; Mohammad Mehrali, Emad Sadeghinezhad, et al., 2014b) and hybrids (Baby & Ramaprabhu, 2011) of different shapes and forms (particle, disk, tube, sheet, etc.) (Goharshadi & Berenji, 2006).

2.5.2.1 Graphene

Latterly, a numerous researches and investigations have been carried on graphene due to its exceptional thermal and electrical conductivity and also excellent optical and mechanical characteristics. Whiles a number of other forms of sp^2 orbital hybridization nano-structured materials such as carbon nanotubes (Kroto & Heath, 1985) and fullerene

(Iijima, 1991) have been produced. Graphene contain a single-atom-thick sheet. It possesses arranged hexagonal carbon units, while each carbon is sp^2 -bonded. In 2004, this thinnest material was developed by peeling off graphite using adhesive tape (Novoselov et al., 2004).

2.5.2.2 Graphene nanoplatelets (GNP)

Graphene nanoplatelets are two-dimensional (2D) with an average thickness of 5 to 10 nm and a specific surface area of 50 to 750 m^2/g ; they can be produced at different sizes, from 1 to 50 μm . These interesting nanoparticles, including short stacks of platelet-shaped graphene sheets, are identical to those found in the walls of carbon nanotubes but in planar form (Tang et al., 2011). Graphene nanoplatelets (GNPs) have drawn a lot of interest due to their excellent electrical conductivity and high mechanical properties; the in-plane thermal conductivity of GNPs is reported to be as high as 3,000 to 5,000 $W/m\cdot K$ (Qi, 2007). Further, as this is a 2D material, the heat transfer properties are expected to be much different from the zero-dimensional nanoparticles and one-dimensional carbon nanotubes. Moreover, since GNP itself is an excellent thermal conductor, graphene-based nanofluids are normally expected to display a significant thermal conductivity enhancement (Yan et al., 2008). Graphene nanoplatelets are also offered in granular form which could be dispersed in water, organic solvents, and polymers with the right choice of dispersion aids, equipment, and techniques.

Already there has been significant investigations and research into the use of carbon-based nanostructures particles to prepare nanofluids (Moghaddam et al., 2013). Therefore, a wide variety of applications and devices for graphene has come to the fore front (Mehrali, Latibari, Mehrali, Indra Mahlia, et al., 2013; Mehrali, Latibari, Mehrali, Mahlia, et al., 2013).

2.6 Thermal conduction of carbon-based materials

There is a discrepancy in the degree of thermal conductivity enhancement along with the progress of research in thermal property of nanofluids. Some researchers found abnormal thermal conductivity enhancement in nanofluids; on the other hand, researchers participated in International Nanofluid Property Benchmark Exercise, they tested the same type of nanofluids from the same source and found no abnormal thermal conductivity enhancement.

Earlier measurements by several investigators indicated that the thermal conductivity of nanofluids could be influenced by many parameters. Such parameters are: type of base fluids, particle size, shape of particles, pH value in aqueous fluids, and temperature. Table 2.4 shows selected study of different carbon-based nanofluids and some parameters effect on thermal conductivity enhancement in latest investigations.

Table 2.4: Selected study of different carbon-based nanofluids and some parameters effect on thermal conductivity enhancement.

Working base fluid	particle	Average Particle size (μm)	Concentration	Thermal conductivity enhancement /ratio	Reference	Remarks
DW	MWCNT	10–50	1-3 vol%	3-7%	(Y. Hwang et al., 2007)	Concentration and particle size effect
DW+ sodium dodecyl benzene	MWCNT	20–60 (diameter)	0.04–0.84 vol%	1.04–1.24	(Wen & Ding, 2004a)	Two-step method
DW+GA	MWCNT	-	0.05–0.49 wt%	1.18–1.8	(Shanbedi, Heris, Baniadam, Amiri, & Maghrebi, 2012)	Temperature effect
Diesel Oil (Shell Rotella 15W-40)	SWCNT	0.3–10	0.25–1.00 wt%	1.10–1.46	(Marquis & Chibante, 2005)	Two-step Method
Ethylene Glycol (EG)	MWCNT	OD 1-4 ID 0.8-1.1	2.5 vol%	20%	(Amrollahi et al., 2008)	Temperature effect

DW	carbon black	-	4-8 vol%	0.8-6%	(Dongxiao et al., 2011)	Concentration effect
EG	GO nanosheet +GO	-	0-21 wt%	4.1-123%	(B. Wang, Hao, & Li, 2013a)	Concentration effect
DW	Graphite	1-2	2-2.5 wt%	1-1.23	(Y. Yang et al., 2005)	Heat Transfer effect
EG	graphene nanosheet	0.7-1.3	0.01-11.03 wt%	20-86%	(Yu et al., 2011)	Concentration effect
DW	graphene nanosheets	1-3	0.05–0.2 vol%	2-27%	(Sen Gupta et al., 2011)	Concentration effect
EG	xGnP	1.7–300	0.5-4 vol%	1.030-1.332	(G.-J. Lee & Rhee, 2014)	Concentration effect
EG and DW	silver nanoparticles decorated graphene	-	0.01-0.07 vol% 0.005-0.05 vol%	2-14% 7-86%	(Baby & Ramaprabhu, 2011)	Concentration effect
DW	GNPs	2 (diameter)	0.025-0.1 wt%	14.8-27.6%	(Mohammad Mehrali, Emad Sadeghinezhad, et al., 2014b)	Concentration and temperature effect
DW + Triton X-100	NDG	3–5	0.01-0.06 wt%	22.15-36.78%	(Mohammad Mehrali, Emad Sadeghinezhad, Sara Tahan Latibari, Mehdi Mehrali, et al., 2014)	Concentration and temperature effect

The effect of base fluid on thermal conductivity of nanofluid is reported by Pawel Keblinski, Eastman, and Cahill (2005). They dispersed treated carbon nano tube in three different kinds of base fluids (Decene, Distilled water and Ethylene Glycol). Their results showed that Decene based nanofluids have the highest thermal conductivity enhancement, Ethylene Glycol based nanofluids are the second best, and Distilled water based nanofluids have the least improvement in thermal conductivity. Particle size effect

on thermal conductivity enhancement is documented by Ganguly, Sikdar, and Basu (2009).

The three-dimensional form of carbon, diamond has remarkably high Young's modulus, record high thermal conductivity, chemical inertness, high mobility of charge carriers and high electron emission at low fields. Crystalline diamond is known to have the highest thermal conductivity among all bulk solids. At room temperature, it varies between 1000 - 2200 W/mK depending on the quality. These properties make diamond a preferable candidate for heat removal application (Pawel Keblinski et al., 2005).

However, diamond's scarcity and hence cost makes this unappealing. Graphite is a layered material formed by stacks of two-dimensional sheets of carbon atoms. It has one of the highest in plane thermal conductivity (2000 W/mK). But the thermal conductivity along c-axis is smaller compared to that along graphite basal plane (Kazemi-Beydokhti, Namaghi, & Heris, 2013). Again, carbon nanotube (CNT) is a unique one-dimensional form of carbon which has high thermal conductivity (ballistic conduction) along the tube. It is predicted that experimentally determined room temperature value of thermal conductivity for an individual MWCNT is 3000 W/mK and 3500 W/mK for an individual SWCNT. Theoretical calculations of the thermal conductivity of CNTs mostly support the experimental results for individual CNTs, although some discrepancy exists (Esfe, Saedodin, Biglari, & Rostamian, 2015).

2.7 Preparation of nanofluids

A good stability of nanofluids is one of the most important partial issues to achieve (Özerinç, Kakaç, & Yazıcıoğlu, 2010). It is worth noting that excellent dispersion of nanoparticles and high stability of the nanofluids are essential for their extensive applications (Togun et al., 2014). Also, as stated previously in the introduction, preparation of nanofluids is the essential step in the use of nanoparticles to increase the

thermal conductivity of the base liquid. There are two main production techniques, the single-step and the two-step method, which have been occupied in producing nanofluids.

2.7.1 The single-step preparation process

The production of a nanofluid is not a simple process. Indeed, the final behavior of any nanofluid is greatly influenced by the synthesis steps taken in production of nanofluid. Nanofluid production can be broken up into two broad categories, One-step and two-step methods. The first is that of creating the nanofluid and its inclusion particles in one step. This often involves chemical, electrical, or explosive dispersion/condensation/reduction process. Physical vapor deposition technique or chemical reduction technique can be used for preparation of the nanoparticles. The processes such as drying, storage, transportation, and dispersion of nanoparticles into the base fluid are avoided in this method, therefore the agglomeration of nanoparticles is minimized, and the stability of fluids is improved (Roslan, Saleh, & Hashim, 2011).

A single-step technique is usually applied for metal nanofluid preparation. But the main disadvantages of this process are that the only low vapor pressure fluids are compatible with the method and low concentration of nanoparticles. Therefore, this limits the application of single-step process.

2.7.2 The two-step preparation process

In the two-stage techniques, the nanoparticles are firstly prepared and then introduced into the base liquid. Metal oxide nanoparticles, nano-fibers or nanotubes consumed in this technique are first prepared as a dry powder by chemical vapor deposition method, inert gas condensation, mechanical alloying or other proper methods, and the nano-sized

powder is then dispersed into a liquid in a second processing step (Meibodi et al., 2010). This step-by step method isolates the preparation of the nanofluids from the preparation of nanoparticles. Consequently, agglomeration of nanoparticles due to attractive Van der Waals Forces may occur in both steps, especially in the process of drying, storage, and transportation of nanoparticles. The agglomeration will not only cause the settlement and clogging of micro-channels, but also decrease the thermal conductivity. Several techniques such as use of ultrasonic agitation equipment, pH control or addition of stabilizers to the fluids are often applied to minimize particle aggregation and improve dispersion behavior (Ranakoti, Irtisha, Kosti, & Nemade, 2012). Since nano-powder synthesis techniques have already been scaled up to industrial production levels by several companies, there are prospective economic advantages in using two-step synthesis techniques that depend on the use of such powders. But an important problem, which needs to be solved is the stability of the prepared suspension.

Another part of the two-step process is the chemical-dispersion method. This method is aimed to disrupt the long-range attractive Van der Waals forces. This is prepared by methods such as functional group coating process, electrostatic and steric dispersion techniques.

2.8 Stability of nanofluid

Stability of nanofluids for long term is the major issue for the engineering applications (Z.-h. Liu & Liao, 2008). Nanoparticles in the base fluid naturally will aggregate and sediment. In theory, there are existence of both attractive and repulsive forces between particles (Ise & Sogami, 2005). The attractive force is the van der Waals force and the repulsive force is the electrostatic repulsion when particles get too close together. If the repulsive force is stronger than the attractive force,

nanoparticles in the base fluid can remain stable or otherwise it will aggregate, and serious aggregation will lead to sedimentation. Adding surfactants to the nanofluid can enhance the electrostatic repulsion of nanoparticles. Surfactants such as sodium dodecyl benzene sulfonate, sodium dodecyl sulfate or Triton X-100 had been tested and proven to stabilize nanofluid (B. Wang, Hao, & Li, 2013b). However, the effect might be weakened when the Brownian motion of nanoparticles is too strong or when the nanofluid is heated. Another way to stabilize nanofluid is by changing the pH value of the solution (T. Yousefi, Veysi, Shojaeizadeh, & Zinadini, 2012). The pH of isoelectric point for nanoparticles carries no electrical charge and therefore causes no interparticle repulsion force which in turn causing more aggregated solution. The more differences between the pH of nanofluid and pH of isoelectric point may cause less aggregation and better dispersion. The third method for stabilized nanofluid is by dispersing nanoparticles into base fluid by using ultrasonicator and high-pressure homogenizer (up to 2000 bar capacity) to obtain a homogeneously dispersed solution. Based on the literature (Goharshadi, Ding, Jorabchi, & Nancarrow, 2009; Mehdi Mehrali et al., 2014; Sun et al., 2013), the sonication time is an important parameter for dispersing the aggregated nanoparticles. As it was mentioned before, all three methods might be used for one specific sample during synthesis and preparation; yet, it is difficult to make stable nanofluid and rare to maintain nanofluids synthesized by the traditional methods in a homogeneous stable state for more than 24h.(Mohammad Mehrali, Emad Sadeghinezhad, Sara Tahan Latibari, Mehdi Mehrali, et al., 2014).

2.9 Efficiency enhancement of solar collector when using nanofluid

There are particular challenges in the effective collection and storage of solar energy though it is free for taking. As solar radiation is only available during daytime, the

energy must be collected in an efficient manner to make use of most of the daylight hours and then must be stored. Solar thermal collectors are the existing components to capture solar radiation which is then turned to thermal energy and transferred to a working fluid subsequently. Therefore, solar collectors are the main and most critical components of any solar system (X.-Q. Wang & Mujumdar, 2007).

To improve the efficiency of solar collectors, researchers have mainly focused on several structural changes such as changing the structure of solar collectors or changing the coating to improve absorptivity but from the literature, only few studies focused on changing the working fluid in order to improve the collectors' efficiency (Selvakumar, Somasundaram, & Thangavel, 2014).

From recent studies, it is found that the working fluid can influence the performance of solar collector significantly. Water, oil, and air are the most common working fluids used in solar energy system but the thermal conductivity of these fluids is relatively low (T. Yousefi et al., 2012). Recently, researchers are investigating on other working fluids such as nanofluids rather than water and air to improve the collector's efficiency. Nanofluids consist of base liquid and nanomaterials that have enhanced thermophysical properties such as higher thermal conductivity, thermal diffusivity and convective heat transfer coefficients (Colangelo et al., 2015). Besides improving the effectiveness of heat transfer, nanofluids also improve optical properties, transmittance as well as extinction coefficient of solar collectors. Experimental investigation conducted by T. Yousefi et al. (2012) on the effect of Al_2O_3 based nanofluid shown that the increase of 28.3% efficiency of flat-plate solar collectors. Lenert and Wang (2012) presented a modeling and experimental study of concentrated solar power application using carbon-coated cobalt (C-Co) nanoparticles and Therminol VP-1 base fluid and concluded that the efficiency is more than 35% with nanofluid and the efficiency will increase with

increasing nanofluid height. Xiao et al. (2011) shown that the application of Copper Oxide (CuO) nanoparticles in evacuated tubular solar collector will significantly enhance the thermal performance of evaporator and evaporating heat transfer coefficient increased by 30% compared to water as working fluid. 5% improvement in efficiency was found out by Otanicar, Phelan, Prasher, Rosengarten, and Taylor (2010) by using diversity of nanoparticles with water as base fluid for micro-solar-thermal collector. Shin and Banerjee (2011) applied novel nanomaterials in molten salts base fluid for concentrated solar power coupled with thermal storage and experienced an enhancement in operational efficiencies. They also concluded that the cost of electricity will be reduced. Taylor, Phelan, Otanicar, Adrian, and Prasher (2011) used graphite based nanofluid in high flux solar collectors resulting with 10% increase in efficiency. Zamzamian, KeyanpourRad, KianiNeyestani, and Jamal-Abad (2014) performed an experimental study to investigate the effect of Cu nanoparticle on the efficiency of a flat-plate solar collector in different volume flow rates of the nanofluid from 0.016 to 0.050 kg/s.

The weight fractions of the nanoparticles tested in the study 0.2% and 0.3% and have average diameter of 10 nm. The Cu nanoparticles were suspended in ethylene glycol as the solvent. From their study, it was found that the optimum point for solar collector efficiency can be reached for 0.3 wt% Cu nanofluid at 1.5 L/min.

By using nanomaterials, the efficiency of an FPC has increased up to 10% and the incident radiation is found to be 9 times higher than a conventional FPC. For a direct absorption solar collector, the efficiency increased up to 10% using nanofluids (Verma & Tiwari, 2015).

2.10 Efficiency enhancement of ETSC when using nanofluid

A recent study, Ghaderian and Sidik (2017) used Al_2O_3 water nanofluid in an ETSC. They varied the volume fractions of nanoparticles and mass flow rates. They observed higher efficiency with increasing nanoparticle concentrations and mass flow rates. Again, the similar trends were observed by Ghaderian et al. (2017) when they studied the effect of CuO distilled water nanofluid on the performance of an ETSC water heater with internal coil under thermosiphon system. They used 0.03 and 0.06 vol% of nanoparticle and mass flow rate was varied from 20 to 60 L/h. Even for air heating, higher performance was observed by using CuO nanofluid in an ETSC. Table 2.5 represents the summary of the previous studies regarding the performance of ETSCs based on different working fluids.

Table 2.5: Performance of evacuated tube collectors based on working fluids

Type of nanoparticle	Base fluid	Researcher	Type of investigation	Research findings
SWCNT	Water	(Sabiha, Saidur, Hassani, Said, & Mekhilef, 2015)	Experimental	-The efficiency of the collector is higher for SWCNTs nano fluid compared to water. -The collector efficiency surges up to 93.43% for 0.2 vol.% SWCNTs nanofluid which is 71.84% higher compared to water at a flow rate of 0.025 kg/s.
MWCNT	Water	(Tong, Kim, & Cho, 2015)	Experimental	-Heat transfer coefficient increased by 8% using 0.24 vol.% MWCNT/water nanofluid compared to water -Collector efficiency increased 4% using nanofluid than water

CNT	Water	(Chougule, Pise, & Pardeshi, 2012)	Experimental	<ul style="list-style-type: none"> -The performance of collector using nanofluid is better -The average collector efficiencies at tilt angle 31.5 were 25% and 45% and at tilt angle 50 were 36% and 61% for water and nanofluid respectively -The maximum instantaneous efficiency obtained by using nanofluid was 69% at 50 tilt angles -Solar heat pipe collector (overall efficiency 25–69%) gave better performance over conventional FPC (overall efficiency 12–20%)
CuO	Water	(Y. Liu et al., 2013)	Experimental	<ul style="list-style-type: none"> -Using nanofluid, the maximum value of collecting efficiency of open thermosyphon had an increment of 6.6% -The mean value of collecting efficiency of open thermosyphon had an increment of 12.4%
TiO ₂	Water	(M Mahendran, Lee, Sharma, Shahrani, & Bakar, 2012a)	Experimental	<ul style="list-style-type: none"> -Compared to water, 2.0% TiO₂ nanofluids increased the efficiency of ETC by 42.5% -The efficiency of collector showed greater enhancement at low volume flow rate and concentration of nanofluids compared to its base fluid which was water

Al ₂ O ₃	Water	(Al-Mashat & Hasan, 2013)	Experimental	<p>-The efficiency increased 7.08% with using flat plate reflector, and 16.9% with using curved plate reflector</p> <p>-The volume concentration of Al₂O₃ was proportional to ETC performance, efficiency enhanced 28.4% with 1% of Al₂O₃ and 6.8% with 0.6% of Al₂O₃, for 0.3% of Al₂O₃ did not make sensible enhancement</p>
CuO	DW/ Water	(L. Q. Lu & Wang, 2011)	Experimental	<p>-The CuO nanoparticles had the potential to increase evaporation heat transfer coefficient by about 30%</p> <p>-The wall temperature of the open thermosyphon decreased due to the use of the CuO nanofluid</p>
Ag/ZrO ₂	Water	(Hussain, Jawad, & Sultan, 2015)	Experimental	<p>-The evacuated collector performed better using both Ag and ZrO₂ nanofluids with higher nanoparticle concentration (5 vol.%)</p> <p>-The performance of the collector was same as water for nanofluids lower concentration of nanoparticles (1 vol.%)</p>

2.11 Different modes of energy transports in nanofluids

There are two different types of studies concerning nanofluids. The first one concerns itself with the study of the effective thermal conductivity and the other with the study of

convective heat transfer enhancement. In the study of the effective thermal conductivity, correlations are developed for the thermal conductivity, which are then used in the study of heat transfer enhancement.

The thermal conductivity of the nanofluid is a function of both the thermal conductivity of the nanoparticle and base fluid as well as the volume fraction, surface area, shape of the nanoparticle, the distribution of the dispersed particles and the thermal conductivity of the nanolayer. The heat transfer coefficient of the nanofluid depends on a number of factors such as thermal conductivity and heat capacity of the base fluid and nanoparticles, the flow pattern, the viscosity of the nanofluid, the volume fraction of the suspended particles, the dimensions and the shape of these particles as well as on the flow structure. The methods, which are mentioned above, consider the nanofluid as a single-phase fluid. The size of the dispersed particles presents some difficulty in analyzing the interaction between the fluid and the solid particles during heat transfer.

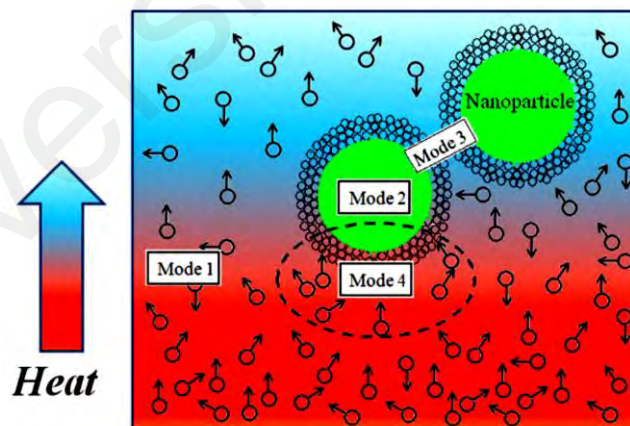


Figure 2.9: Modes of energy transport in nanofluids

Jang and Choi (2004) derived four modes of heat transport in nanofluids as shown in Figure 2.9. The first mode of heat transport is the collision between base fluid molecules, which physically represents the thermal conductivity of the base fluid. The second mode is the thermal diffusion in nanoparticles. The thermal diffusion is carried by phonon's which are created at random, propagate in random directions through the particles and are

scattered by each other or by defects in the particles, thus justifying the macroscopic description of heat transport.

The third mode is Brownian motion, which is the collision between nanoparticles. This enables direct solid to solid transport of heat from one to another, but it is a very slow process and can be neglected. Brownian motion could, however, have an important indirect role in producing particle clustering which significantly enhances the thermal conductivity, since the particles are much closer together and thus enhance consistent phonon heat transfer among the particles. The last mode is the thermal interactions of the nanoparticles with the base fluid molecules, which translates into conduction at the macroscopic level. Hence the nano layer forms a thermal bridge between the liquid base fluid, where the solid nanoparticles enhance the effective thermal conductivity (Grote, 2013).

2.12 Thermo-physical properties of nanofluid

Thermo-physical properties are crucial parameters to the knowledge of the convective heat transfer performance of nanofluids. The key thermo-physical properties of heat transfer fluids for thermal system include density, specific heat capacity, thermal conductivity and viscosity. Various researchers have published the properties of nanoparticles and thermal properties of nanofluids as the basis of research on nanofluids applications. Table 2.6 shows the indicated specific heat, thermal conductivity and density of different nanoparticles.

Table 2.6: Properties of different nano particles (Kamyar, Saidur, & Hasanuzzaman, 2012; Namburu, Kulkarni, Dandekar, & Das, 2007)

Material	Specific heat, Cp (J/kgK)	Thermal conductivity, k(W/m K)	Density, ρ (kg/m ³)
Alumina (Al ₂ O ₃)	773	40	3960
Copper oxide (CuO)	551	33	6000
Titanium oxide (TiO ₂)	692	8.4	4230
Silicon dioxide (SiO ₂)	765	36	2330
Carbon Nanotube (CNT)	-	3000	1350
Graphite	0.71	120	2160
Diamond	0.509	3300	3530
Single wall carbon nanotube (SWCNT)	841	6000	2100
Water (H ₂ O), base fluid	4182	0.60	1000

Improvement in thermal properties of nanofluids such as thermal conductivity and convective heat transfer that have been described in the previous section had a few mechanisms contributing to it as listed by (Phillbot Koblinski, Phillpot, Choi, & Eastman, 2002) such as Brownian motion, particle and liquid interface nanolayer and heat transfer in nanoparticles. However, all this special characteristic cannot be achieved unless the nanoparticles are properly dispersed and stable. Surfactants can play a major role in achieving better dispersion and stability of nanofluids (Ghadimi, Saidur, & Metselaar, 2011; S. S. Murshed, De Castro, Lourenço, Lopes, & Santos, 2011). However, some researchers did not add any surfactants or dispersants in the fluid because the addition of it could influence the thermal conductivity of the fluid and can deteriorate the thermal conductivity enhancement (Trisaksri & Wongwises, 2007).

2.13 Thermal conductivity enhancement in nanofluids

Thermal conductivity is the potential of a material to carrying energy in the form of heat (energetic vibrations) (Jiang, Xia, Zhai, Zhang, & Liu, 2019). Generally, in solids, the form of this transport is the free electron diffusion and direct energy exchange through atomic level lattice vibrations, while for fluids/gases it takes the form of molecular diffusion and direct molecular contact (Davoudi, Nicola, & Vlassak, 2012). It is a natural and fundamental property of any physical material and is defined as energetic power per unit temperature and per unit length over which the thermal conductivity is acting. Eventually, a material's thermal conductivity is based upon the physical structure of the material, and its current state. Based on literature, the thermal conductivity of nanofluids will be affected by:

1. Nanoparticle Morphology

In material science, morphology would be defined as study of particle's shape, size, texture and phase distribution of physical objects (Penn, 2017). The study of the effect of nanoparticles size has been conducted by several researchers and they have declared significant influence of nanoparticle size on thermal conductivity of nanofluid. Specific surface area (SSA) is other characteristic of nanoparticle, which is supposed to be taken into account by investigators during preparation since it will affect the thermal conductivity of nanofluid (Sadeghinezhad et al., 2016).

2. Temperature

According to the recent research, it has been proven that thermal conductivity and temperature have direct relationship which means when temperature rises, thermal conductivity of nanofluid increases as well (Pryazhnikov, Minakov, Rudyak, & Guzei, 2017).

3. Nanoparticle Concentration

The concentration of nanoparticles inside the basefluid is the other key issue that can highly affect the thermal conductivity of nanofluid (Etefaghi et al., 2017). In different articles, concentration has been stated in both types including weight percentage as well as volume.

4. Particles Motion

Three types of motion have been much argued in literatures called:

- Thermophoretic motion (The motion produced by temperature gradient)
- Brownian motion (force)
- Osmophoretic motion (Motion in concentration gradient)

Thermophoretic motion is the motion of particles caused by temperature gradient. Though, most effective type of motion which influenced in increasing thermal conductivity of nanofluids is called Brownian motion (Makinde & Animasaun, 2016). The osmophoretic motion can be explain as motion in concentration gradient and fluctuate by concentration of particles.

5. Thermal conductivity of nanoparticles

Inside one specific base fluid, thermal conductivity of particles would significantly impact on the thermal conductivity of the fluid. In this case, higher thermal conductivity of particles is expected to lead in higher thermal conductivity of nanofluid (Naddaf & Heris, 2018). This fact has been proved by different researches and experiments.

6. Thermal conductivity of base-fluid

As it was mentioned earlier, motion of particles especially Brownian motion can affect thermal conductivity of nanofluids (Makinde & Animasaun, 2016). Effect of electric double layer around nanoparticles could be

considered as one influential parameter on thermal conductivity of nanofluids, depending on base fluid.

7. Clustering

Clustering is other feature which always can be taken into account that effecting thermal conductivity of nanofluids (Karthikeyan, Philip, & Raj, 2008). It is interesting to note that in different models presented by different researches, regarding thermal conductivity of nanofluids, the effect of clustering has been regarded by some researchers.

8. Acidity (pH)

Literature survey reveals that there are not a lot of researches investigating influence of pH of base fluid on thermal conductivity of nanofluid (Ghadimi et al., 2011).

9. Additives

Additives are utilized to keep nanoparticles in suspension and prevent them from agglomeration. Therefore, they are expected to cause thermal conductivity of nanofluids increased (Korayem, Tourani, Zakertabrizi, Sabziparvar, & Duan, 2017).

According to the parameters mention above one of the most important thermal transport characteristics of a material is thermal conductivity, which plays a significant role in lots of design problems. Thus, a great deal of work has gone into measuring and characterizing, thermal conductivity over the last few centuries.

Experimental investigation on the thermal conductivity of nanofluids has been reported by many researchers. All the studies indicate that nanofluid have higher thermal conductivity than base fluids. Y. Lee et al. (1999) shown that more than 20% enhancement of thermal conductivity achieved by using 4% volume fraction of CuO nanoparticles in ethylene glycol. Eastman, Choi, Li, Yu, and Thompson (2001) observed

that up to 40% increase in thermal conductivity of ethylene glycol containing 0.3% volume fraction of Cu nanoparticles with mean diameter less than 10 nm compared to pure ethylene glycol. Xie et al. (2002) investigated experimentally the thermal conductivity of Al_2O_3 nanoparticles suspended in deionized water, ethylene glycol and pump oil and found out that small amount of Al_2O_3 in the solution have higher thermal conductivity than the base fluid and the enhancement increased by increasing the volume fraction of nanoparticles. Das, Putra, Thiesen, and Roetzel (2003) shown that 1% of volume concentration of CuO nanoparticles suspended in water have increased the thermal conductivity ratio from 6.5% to 29%. S. Murshed, Leong, and Yang (2005) reported that the thermal conductivity of TiO_2 /water nanofluid increased remarkably with increasing volume fraction of nanoparticles. Mintsa, Roy, Nguyen, and Doucet (2009) presented in his experimental data of Al_2O_3 /water and CuO/water nanofluids that the effective thermal conductivity increased with increasing volume fraction, decreasing particle size and at higher temperatures. From all the reports in many publications it has been confirmed that adding nanoparticles in fluid can increase the thermal conductivity of the base fluid and the enhancement in thermal conductivity of nanofluids influenced by some factors including temperature, size and volume concentration of nanoparticles.

2.14 Convective heat transfer of nanofluids

The forced convective heat transfer of working fluids is a very important mechanism in solar collectors. Nanofluids, with enhanced thermal conductivity are very attractive in this area. By adding a very small amount of nanoparticles in a base fluid, the convective heat transfer are expected to be enhanced while making little or no undesired effect in pressure drop that had been the major problem for micro-sized particles before.

Xuan and Li (2003) investigated experimentally the convective heat transfer of Cu nanofluids in a 10mm straight tube and showed that heat transfer rate had been enhanced by using nanofluids and low concentration nanofluids friction bring no significant penalty in pumping power. Wen and Ding (2004b) tested the convective heat transfer of Al_2O_3 nanofluids in a copper tube under laminar flow regime and found an enhancement in heat transfer is quite significant in the entrance region. They suggested that enhancement in thermal conductivity might not be the only reason for increase in convective heat transfer but particle migration that result in non-uniform distribution of thermal conductivity and viscosity that will then reducing the thickness of thermal boundary layer might be the caused as well. Similarly, (Meyer, McKrell, & Grote, 2013) tested the amorphous carbonic-water nanofluid that have almost the same thermal conductivity with water but managed to increase the convective heat transfer coefficient by 8% under laminar flow. Ding et al. (2007) experimentally investigated forced convective heat transfer using aqueous and ethylene glycol-based spherical titania nanofluids, and aqueous-based titanate nanotubes, carbon nanotubes and nano-diamond nanofluids and found out that all the tested nanofluids shown a higher effective thermal conductivity than the one predicted by theories. However, at low Reynolds numbers, the convective heat transfer for TiO_2 /ethylene glycol nanofluid and nano-diamond/water nanofluid was observed to be deteriorated due to the competing effects of particle migration on the thermal boundary layer thickness and the effective thermal conductivity might be the caused for it. K. S. Hwang, Jang, and Choi (2009) tested the convective heat transfer coefficient and pressure drop of Al_2O_3 /water nanofluids and shown that the convective heat transfer coefficient for 0.3% nanofluid concentration increased by 8% compared to pure water. Duangthongsuk and Wongwises (2010) tested and presented the values for the heat transfer coefficient and friction factor of TiO_2 /water nanofluids in the turbulent flow condition and concluded that the heat transfer coefficient of nanofluids

at 1% concentration has 26% greater than pure water whereas increasing the concentration to 2% reduces the heat transfer coefficient to 14% lower than the base fluid under the same condition. At lower particle volume fraction, the pressure drops only incurred very slightly however, the pressure drops in nanofluids increased by increasing concentration due to increase in viscosity of the fluid. Fotukian and Esfahany (2010) experimentally investigated the turbulent convective heat transfer coefficient and pressure drop for a very low concentration of less than 0.24% CuO/water nanofluid in a circular tube and observed that the increase in heat transfer coefficient was to be on average of 25% with 20% reduction in pressure drop. Haghighi et al. (2014) investigated independently the turbulent convective heat transfer coefficients of 9 wt% Al₂O₃/water and TiO₂/water nanofluids inside a circular tube. In the investigation, the heat transfer coefficients of nanofluids were compared with those of the base fluids at the same Reynolds number or at the same pumping power. The same Reynolds number requires higher flow rate of nanofluids therefore such comparison shows up to 15% increase in heat transfer coefficient but at equal pumping power, the heat transfer coefficient of Al₂O₃ nanofluid was practically the same with water while was about 10% lower for TiO₂. It had been concluded that comparing performance at equal Reynolds number is clearly misleading since the heat transfer coefficient can always be increased by increased pumping power and so, the comparison between the fluids should be done at equal pumping power.

2.15 Viscosity of nanofluids

Viscosity of nanofluids is a property as important as thermal conductivity for investigation of solar collector's performance although less attention was given for viscosity than thermal conductivity over the past few years (Mahbubul et al., 2012).

Adding nanoparticles additive in fluid will increase the viscosity of the fluid and lead to increase in pumping power required. Nguyen, Roy, Gauthier, and Galanis (2007) have investigated experimentally the influence of both the temperature and the particle size on the dynamic viscosities Al_2O_3 and CuO nanofluids. Dynamic viscosities was measured using a 'piston-type' calibrated viscometer based on the Couette flow inside a cylindrical measurement chamber and the results shown that viscosity of nanofluid increases with increasing of particle volume concentrations but it decreases with the increase in temperature. Namburu et al. (2007) presented an experimental investigation of rheological properties of nanofluid containing CuO nanoparticles. The nanofluids tested have volume percentage ranging from 0% to 6.12% in temperatures ranging from $-35\text{ }^\circ\text{C}$ to $50\text{ }^\circ\text{C}$ to demonstrate their applicability in cold regions. The test results indicate that the viscosity increased with increasing concentration and exponentially decreased with temperature. Phuoc and Massoudi (2009) displayed experimental observations on the effects of the shear rates and particle volume fractions on the shear stress and the viscosity of Fe_2O_3 nanofluids using Polyvinylpyrrolidone (PVP) or Polyethylene oxide (PEO) as a dispersant. At volume fractions beyond 0.02, a non-Newtonian law exhibiting shear-thinning was observed indicating that shear viscosity depends on the shear rate and concentration of nanofluids. Other researchers, such as S. W. Lee, Park, Kang, Bang, and Kim (2011) on SiC nanofluids for high temperature heat transfer applications, Aladag et al. (2012) on CNTs and Al_2O_3 nanofluids at low temperatures application and Elias et al. (2014) on the thermo-physical properties of Al_2O_3 nanofluids in car radiator application also indicated that nanofluid viscosity increases with increasing volume fraction.

Based on the literature, understanding viscosity of nanofluids is the one of fascinating challenge and the most critical parameters in heat transfer properties of nanofluids. It follows two important characteristics: (a) increase in viscosity with increases of nano-

particle concentration and the internal viscous shear stress increases, (b) decrease in viscosity with temperature (Sadri et al., 2014). With increasing of the temperature, the nanoparticles are motivated more, hence inter-particle and inter-molecular adhesion forces become weaken. Meanwhile, with the rise of temperature, thermal movement of molecules and Brownian motion intensifies and viscosity of the nanofluids decreases (Mohammad Mehrali, Emad Sadeghinezhad, et al., 2014b).

The researchers have highlighted the different factors which can influence the viscosity. (Mohammad Mehrali, Emad Sadeghinezhad, Sara Tahan Latibari, Mehdi Mehrali, et al., 2014).

1. Temperature
2. Volume fraction
3. Morphology
4. Shear rate
5. Dispersion method, stabilizers and Clustering

2.16 Evaluation of thermal conductivity and viscosity of nanofluids by design of experiment (DOE)

Nanofluids, comprising highly thermally conductive nanoparticles dispersed in a quiescent fluid at low volume fractions, will probably be the future heat transfer media (Hatami, Ganji, & Gorji-Bandpy, 2014; Mondragon, Julia, Barba, & Jarque, 2012; Park, Lee, Bang, & Park, 2011). Different mechanisms have been proposed for effective thermal conductivity enhancement (ETCE) of nanofluids: Brownian motion of nanoparticles, molecular layering, the nature of heat transport in nanoparticles, particle interface (Williams, Buongiorno, & Hu, 2008), nanoparticle aggregation, clustering and specific surface area (Esfe, Rostamian, Shabani-samghabadi, & Arani, 2017).

Theoretically, the nanoparticles are very efficient in enhancing the performance of thermal applications. Recent studies show that nanofluids are able to enhance thermal efficiency; however, there are some restrictions, such as instability, agglomeration, erosion and corrosion of thermal equipment systems. Apparently, by choosing the adequate shape, type and size of nanoparticles, most of the desired thermophysical properties can be achieved (Garg et al., 2009).

Viscosity of the adjacent layer of fluid offers frictional resistance against shearing stresses. One of the most critical parameters in nanofluids is viscosity, which plays a very important role to determine the quality of heat transfer (Garg et al., 2009). Viscosity of nanofluids generally increases with rises in concentration of nanoparticles and decreases with temperature. K. J. Lee et al. (2007) explored that particle to particle interaction is responsible for nonlinear relation between viscosity and volume concentration. Studies performed by many researchers suggested that apart from particle size and volume concentration, the temperature of working fluid also plays an important role in viscosity variation (Nam, Kim, Chung, & Lee, 2015). Buschmann (2013) indicated that the increases in nanofluid temperature affect nanofluid viscosity.

Thermal conductivity of nanofluid is one of the crucial factors, which governs heat transfer capability of nanofluids in various thermal applications. Hence, a number of mathematical model according to the experimental data and theoretical analysis about the thermal conductivity of nanofluid have been accomplished by many researchers over the last two decades (Garg et al., 2009). A lot of studies indicated that desired thermal conductivity of nanofluid can be achieved by selecting the optimized concentration and temperature, proper size, shape and type of nanoparticles and base fluid materials (Nkwetta et al., 2013; Zhao et al., 2010).

Recently, researchers have been encouraged to estimate and predict accurately variables such as viscosity and thermal conductivity of nanofluid in different temperature, particle diameters, density, sonication time and concentration by using soft computing methods. A.Kazemi-Beydokhti et al. (Kazemi-Beydokhti et al., 2013) have been determined the most important variables on thermal conductivity of CuO nanofluid using the fractional factorial design approach. Hemmat esfe et al. (Esfe, Saedodin, Akbari, et al., 2015) modeling the dynamic viscosity and thermal conductivity of ferromagnetic nanofluid using artificial neural network.

Several statistical methods have been proposed to minimize the experimental measurement and provide correlations for predicting the variables of nanofluids such as genetic algorithms, fuzzy logic and respond surface methodology, etc. A classical experimental design method, which is not only time-consuming and laborious but also expensive in terms of its considerable material. Moreover, the use of traditional methods of experimentation neglects the effects of interaction between factors and leads to low efficiency in process optimization. Therefore, the application of statistical experimental design in nanofluids seems to be the best methodology for optimization.

Response surface methodology (RSM) and factorial design analysis are proper tools to determine the optimal process conditions (Gheshlaghi, Scharer, Moo-Young, & Douglas, 2008). In many experimental settings, it is not desirable or feasible to assess all factors and their joint effects; thus, it is only the dominant factors that need to be identified.

2.17 Statistical software for optimization

Statistically designed experiments are a powerful tool for improving the efficiency of experimentation (Buschmann, 2013). Through an iterative process, they allow us to gain

knowledge about the system being studied with a minimum number of experiments. Inclusion of replicate test conditions allows the estimation of random, experimental variation. Statistical analysis of data generated from the experiment clearly establishes the relationship between the measured parameter of interest (response) and the process parameters (input factors or factors) being studied. The factors may have individual, simple effects on the response (referred to as main effects) or may have effects that are interdependent (referred to as interaction effects). Since the designed experiments are generated on the basis of statistical theory, confidence in the results obtained and conclusions drawn are clearly defined (Shirvan, Mamourian, Mirzakhani, & Ellahi, 2016). Different types of designs are available; their choice is determined by the objectives of the experiment and the current state of knowledge about the experimental environment. They can be categorized as follows:

- Screening
- Fractional & full factorial
- Response surface

2.17.1 Screening

If there would be few data about the target, screening designs can be applied for exploring the experimental space. In this design, information of each factor can be derived, but interactions cannot be interpreted. The factors are run at two levels with only high and low levels as defined by the range of each factor. The number of factors can be as high as 15.

2.17.2 Factorial

Fractional designs are used when there is former information about which factors are significant. If a complicated design would be selected, the main effects and their interactions could be distinguished more precise. Two to six factors can be selected in this design in which two-level designs with variation of low and high level appears. Replicate experiments in the center (where all factors are simultaneously held at their midlevel) can detect the behavior of nonlinear factor. Meanwhile, another design of this series, fractional factorial, exist which can detect the interactions and significant factors by less number of experiments without losing a lot of information (see Figure 2.10).

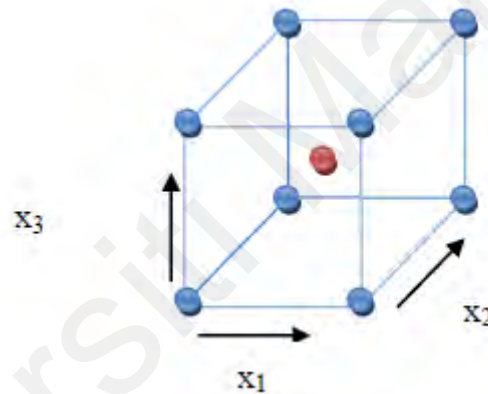


Figure 2.10: Three-factor full factorial design with center point

2.17.3 Response surface methodology (RSM)

Response surface designs are applied to gain accurate information about factor effects including magnitude and direction. Like factorial design, normally two to six factors with three levels design can be selected to estimate linear, two-factor interaction and nonlinear effects of all factors under study. If there would be a prior indication of nonlinear behavior or when a set of preliminary (factorial) experiments shows nonlinear behavior, selection of this method would be thoughtful.

They provide precise prediction of responses within the experimental region and are useful in identifying optimum conditions. Assay optimization in particular produces responses that are nonlinear. Figure 2.11 shows various response surface designs using three factors for illustration.

2.17.3.1 Central composite design (CCD)

The first approach in RSM is central composite design (CCD) where experiments are added to the factorial design after nonlinear behavior is detected (Figure 2.11). The next method is a modified CCD, called a face-centered cube design, where the added experiments lie on the faces of the space formed by the factorial design.

2.17.3.2 Box-Behnken Design (BBD)

BBD is used to further study the quadratic effect of factors after identifying the significant factors using screening factorial experiments. The Box-Behnken design (Figure 2.11) is an independent quadratic design in that it does not contain an embedded factorial or fractional factorial design. In this design the treatment combinations are at the midpoints of edges of the process space and at the center. These designs are rotatable (or near rotatable) and require 3 levels of each factor. The designs have limited capability for orthogonal blocking compared to the central composite designs.

Box-Behnken designs do not contain any points at the vertices of the experimental region. This could be advantageous when the points on the corners of the 45 cubes represent factor-level combinations that are prohibitively expensive or impossible to test because of physical process constraints.

A Box–Behnken design is run when there is prior information about the existence of nonlinear effects. The experiments are located on the edges of the experimental space. Box–Behnken and CCDs involving up to 10 numerical and 1–3 categorical factors are fast becoming popular because of nonlinear responses common in assay development (Altekar et al., 2006).

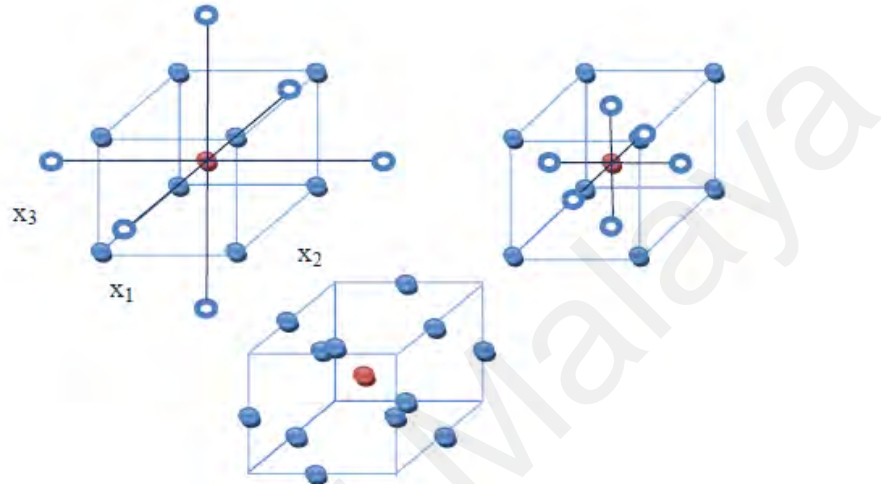


Figure 2.11: Graphic representations of central composite, face-centered cube and Box–Behnken designs

The effect of different parameters such as concentration of the surfactant, the ratio of organic phase to internal phase in the membrane and membrane to external phase ratio on process parameters were studied using Box-Behnken design and response surface method by (Nosrati, Jayakumar, & Hashim, 2011). Analysis of variance (ANOVA) provides the statistical results and diagnostic checking tests which enables researchers to evaluate adequacy of the models (Ghafari, Aziz, Isa, & Zinatizadeh, 2009; Nosrati et al., 2011).

2.18 3-dimensional computational fluid dynamics (CFD)

A very few researchers conducted 3D numerical modeling on ETSC because of difficulties. They used air and water as heat transfer medium. But no 3D numerical studies have been conducted using nanofluids on this device.

Karanth, Manjunath, and Sharma (2011) numerically simulated a solar flat plate collector using Discrete Transfer Radiation Model (DTRM) – a CFD approach. Dynamics (CFD) by employing conjugate heat transfer showed that the heat transfer simulation due to solar irradiation to the fluid medium, increased with an increase in the mass flow rate. Manjunath, Karanth, and Sharma (2011) studied comparatively solar dimple plate collector with flat plate collector to augment the thermal performance. Their result described that the average exit water temperature showed a marked improvement of about 5.50C for a dimple solar collector as compared to that of a flat plate solar collector. CFD analysis of solar flat plate collector was conducted by Hejazian and Moraveji (2013). His work attempted to present numerical simulation of solar collector developed exclusively for grape drying. CFD analysis of triangular absorber tube of a solar flat plate collector was performed by Basavanna and Shashishekar (2013) where the numerical results obtained using the experimentally measured temperatures are compared to the temperatures determined by the CFD model. 3D conjugate heat transfers through unglazed, glazed water-filled and gas-filled solar flat plate collectors with and without finned tubes were investigated by (Ekramian, Etemad, & Haghshenasfard, 2014; Manjunath et al. (2011); Tagliafico, Scarpa, & De Rosa, 2014; Vestlund, 2012).

Al-Ansary and Zeitoun (2011) investigated the parabolic trough collectors using CFD simulation. Numerical modeling was used for calculating the conduction and convective heat losses from the receiver of the collector. Table 2.7 shows some researchers conducted 3D numerical modeling of solar collectors.

Table 2.7 Summary of some researchers conducted 3D numerical modeling of solar collectors

Reference	Summary
(Fan, Shah, & Furbo, 2007)	Collector pipes only – no absorber. Heat flux applied through pipe walls.
Selmi, Al-Khawaja, and Marafia (2008)	Single Pipe CFD with radiative and convective heat transfer. Heat loss did not increase at higher temperatures.
(Reynolds, Jance, Behnia, & Morrison, 2004)	Simulation of single large trapezoidal cavity. Convective and radiative heat transfer.
Iordanou (2009)	Single pipe investigation of mesh inside collector tubes
Manuel, Omar, Antonio, and Armando (2013)	Rectangular and cylindrical pipe network – no absorber.
(Dović & Andrassy, 2012)	Corrugated absorber where flow ran either through the plate or connected pipe work.
Martinopoulos, Missirlis, Tsilingiridis, Yakinthos, and Kyriakis (2010)	Flat polymer collector with absorbent ink suspended in water as the heat removal fluid. Numerous rectangular risers.
Manjunath et al. (2011)	Single pipe connected to an absorber.
(Sadeghi, Safarzadeh, & Ameri, 2019)	Energetic and exergetic numerically analysis of a constructed evacuated tube solar collector using Cu ₂ O/distilled water nanofluid.
(Kaya & Arslan, 2019)	An evacuated U-tube tube solar collector (EUSC) was designed and simulated numerically. Ag, ZnO and MgO nanoparticles in 30%:70% (by volume) ethylene glycol-pure water (EG-PW) mixture and different nanoparticle volumetric concentrations were used as working fluids
(Bianco, Marchitto, Scarpa, & Tagliafico, 2019)	A numerical investigation to study laminar convection flow of Al ₂ O ₃ -water nanofluids within a three-dimensional rectangular section channel asymmetrically heated.

Sultana, Morrison, and Rosengarten (2011) used CFD software to investigate the thermal performance of a solar collector by predicting the heat loss, radiation, and convective heat transfer coefficient inside the collector and maximized the overall thermal efficiency. A numerical study for single glazed flat plate collector was reported by Selmi et al. (2008) and CFD software was used to predict outlet water temperature. Their study revealed good agreement between the CFD results and experimental data. Gertzos, Pnevmatikakis, and Caouris (2008) and Gadi (2000) used CFD and found that the developed model predicted system performance with minimal error. Martinopoulos et al. (2010) investigated polymer solar collector using CFD analysis. In their study the effect of operating parameters such as flow rate, temperature, solar insolation, etc. on thermal efficiency were carried out and found good agreement between the experimental and simulation result.

2.19 Summary

More than ever before, cooling and heating are the most pressing challenges of many technologies nowadays. Nanofluids are promising for heat transfer enhancement due to their high thermal conductivity. Presently, discrepancy exists in nanofluid thermal conductivity data in the literature, and enhancement mechanisms have not been fully understood yet. The major efforts are to determine the physical properties of nanofluid and to evaluate the effect of graphene nanoplatelets nanofluids on the performance enhancement of an evacuated tube solar collector.

In addition, literature shows that there is an enhancement in heat transfer when working with nanofluids. The enhancement mainly depends on the thermal conductivity and heat capacity of the base fluid and nanoparticles, the flow pattern, the viscosity and density of the nanofluid, the volume fraction of the suspended particles, the dimensions and the shape of these particles as well as on the flow structure. The thermal conductivity

of the nanofluid is a function of both the thermal conductivity of the nanoparticle and base fluid as well as the volume fraction, surface area, shape of the nanoparticle, the distribution of the dispersed particles and the thermal conductivity of the nano layer. Many studies were done on the convective heat transfer enhancement of nanofluids containing metallic oxide particles and only a few containing carbons based.

Universiti Malaya

CHAPTER 3: METHODOLOGY

3.1 Introduction

This chapter is aimed in providing the detail description of methods and procedures in this study. In order to achieve the objectives this study has been divided into four part. Design of experiment by Analysis of variance and preparation of nanofluids (stability and aggregation) is described in the first subsection followed by investigation of thermophysical properties. An evacuated tube solar collector set up is used to obtain the energy and exergy analysis as well as the pumping power, entropy generation and bejan number. The last step is focused on the CFD modeling of outlet nanofluid temperature during convective flows. Flowchart of the experimental and analytical step is presented in Figure 3.1.

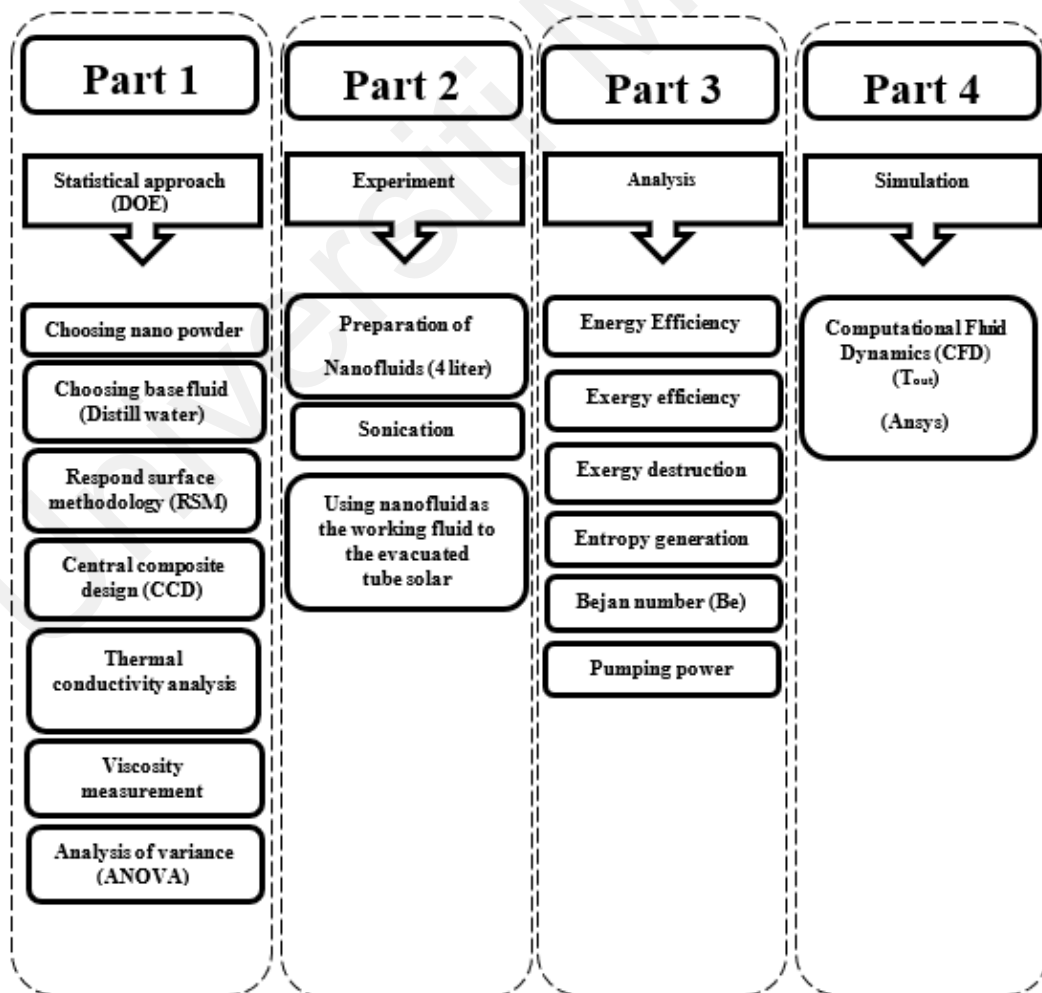


Figure 3.1: Flowchart of experimental and analytical analysis

3.2 Part I: Experimental design by DOE

Design-Expert software version 9.0.5 was applied to analyze the statistical results. The impact of three factors as most effective parameters on thermophysical properties of nanofluids, including: temperature (A), concentration (B) and specific surface area of nanoplatelets (C) were examined by Analysis of variance (ANOVA). It is well suited for fitting a quadratic surface using a standard RSM design called a central composite design (CCD), which usually works well for process optimization. Table 3.1 shows the variable factors, including: the coded and actual values at two levels high (+1), low (-1), and the center points (coded level 0).

Table 3.1: Variable factors and their specifications

Factor (Unit)	Level		
	(-1) Low	(0) Centre Point	(+1) High
Temperature (A) (°C)	20	40	60
Concentration (B)(wt%)	0.05	0.075	0.1
	Categorical		
Surface Area (C) (m ² /g)	500		750

A total of 26 experiments with 10 center points and 8 axial points were designed by software (Table 3.2).

Table 3.2: Experimental design.

		Factorial input variable		
Std	Run	A	B	C
20	1	+1	0	750
25	2	+1	-1	500
7	3	0	-1	750
9	4	0	0	500
17	5	0	0	750
14	6	-1	+1	500
23	7	+1	+1	500
26	8	0	0	750
24	9	-1	0	750
19	10	0	0	500
11	11	0	0	500
1	12	0	0	500
21	13	0	+1	500
22	14	+1	+1	750
8	15	+1	-1	750
4	16	0	+1	750
16	17	0	0	500
15	18	0	0	750
13	19	-1	-1	500
3	20	+1	0	500
6	21	-1	0	500
12	22	0	0	750
10	23	-1	-1	750
18	24	0	0	750
2	25	0	-1	500
5	26	-1	+1	750

3.3 Part II: Experimental

3.3.1 Material and nanoparticles dispersion in liquid

GNP with special properties (Table 3.3) was purchased from XG Sciences, Inc., USA. The dispersion of GNP into the base fluid is an essential process and needs special attention. The specified amount of GNP weight was measured by an analytical balance (Precisa balance, Switzerland) and then was mixed with distilled water (DW). Then, the ultrasonication probe (QSonica, USA) was used to prepare a homogeneous and stable GNP nanofluid with concentrations of 0.05, 0.075, and 0.1 wt%. The graphene nanoplatelets were dispersed in distilled water using a high-power ultrasonication probe (Sonics Vibra Cell, Ningbo Kesheng Ultrasonic Equipment Co., Ltd., Ningbo, China) having a 1,200-W output power and a 20-kHz frequency power supply. In this investigation 4 liter of nanofluid prepared that each 500 ml was sonicated for 60 minutes. All concentrations of GNP nanofluids were under observation for 3 months. The stable homogeneous GNP nanofluids were prepared without using any surfactant.

Table 3.3: GNP specifications

Property	Specification
Color	Black granules/powder
Carbon content	>99.5
Bulk density	0.2-0.4 g/cm ³
Relative gravity	2.0-2.25 g/cm ³
Specific surface area	500 and 750 m ² /g
Particle diameter	2 μm
Thickness	2 nm
Thermal conductivity (parallel to surface)	3000 W/m.K
Thermal conductivity (perpendicular to surface)	6 W/m.K

3.3.2 Thermo-physical properties measurements

As stated earlier, it is important to be able to measurement of thermos-physical properties of nanofluids specimen for heat transfer enhancement study. In order to understand the effect of GNP on base fluid, details of the methods for finding these experimental results, are stated the following sections.

3.3.3 Thermal conductivity measurement

The Decagon Devices KD2 thermal properties analyzer (KD2 Pro, Decagon Devices, Inc., USA), is used on all nanofluids at room temperature as a first inspection for the conductivity. The accuracy of the KD2 is given as 5% by the manufacturer over a span of temperatures of 0 to 60°C. A schematic of the KD2 setup with the isothermal bath is shown in Figure 3.2.

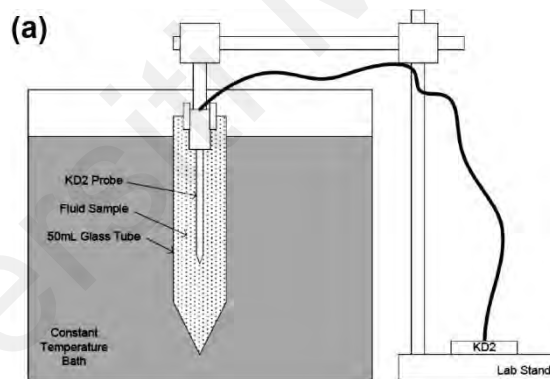


Figure 3.2: Schematic setup of KD2 thermal properties analyzer

In this work, the used analyzer device has 5% accuracy between 5°C and 40°C. The thermal conductivity measurements are repeated ten times and the average values were reported.

3.3.4 Viscosity measurement

Viscosity of nanofluids is one of the most critical parameters, which determines the quality of the heat transfer fluid. As with simple fluids, the viscosity of a nanofluid

depends largely on the temperature (Mohammad Mehrali, Emad Sadeghinezhad, Sara Tahan Latibari, Mehdi Mehrali, et al., 2014). Moreover, the viscosity of nanofluids is measured at different rotor RPMs to investigate if the nanofluids are Newtonian or non-Newtonian fluids. The rheological behavior of nanofluids with amounts of nano sized particle was measured on Anton Paar rheometer (Physica MCR 301).

3.3.5 Stability analysis

Although the stability of nanofluids is very important to practical application, there are limited studies on estimating the stability of a suspension (Mohammad Mehrali, Emad Sadeghinezhad, Sara Tahan Latibari, Mehdi Mehrali, et al., 2014). Sedimentation photograph capturing was introduced as a basic method to evaluate stability of nano suspensions inside the fluid. After preparation of nanofluid, it would be kept in a stationary standing condition inside glass tubes and settlement of particles would be recorded continuously by capturing photos.

3.3.6 Thermal analysis

Differential scanning calorimetry (DSC) is a powerful tool to measure the heat capacity of nanofluids. The maximum heating rate for not modified PC DSC is up to 500K/min and the maximum cooling rate is up to 400 K/min. Temperature range of measurement is up to 400 °C with time constant of only 1.5 s or lower. The difference in the amount of heat flow required for heating up a sample pan and reference pan are measured as a function of temperature. During the whole process, the sample and reference pans are maintained at nearly the same temperature throughout the experiment. By measuring the difference in heat flow, the heat capacity of the sample is obtained. The heat capacity of GNP nanofluids was obtained on a differential scanning calorimeter

(METTLER TOLEDO 820C-Error $\pm 0.25-1^{\circ}\text{C}$) at a heating rate of $5^{\circ}\text{C}/\text{min}$ in purified nitrogen atmosphere.

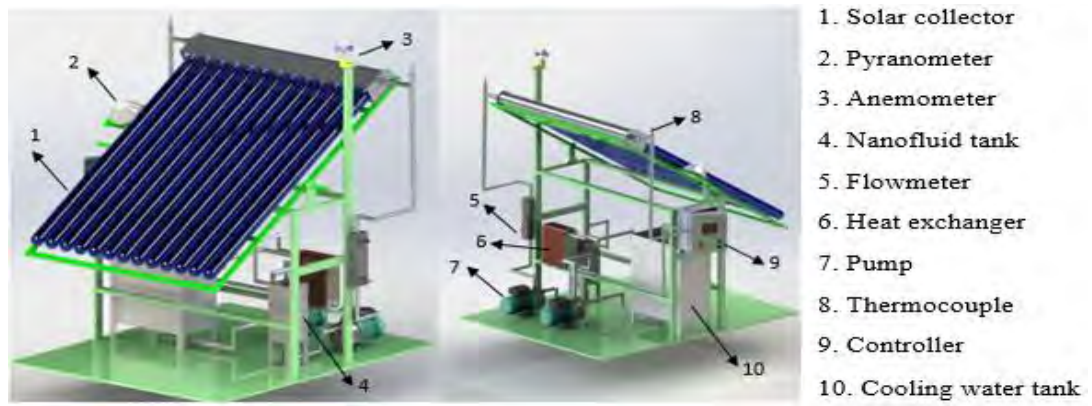
3.4 Morphology study

Transmission electron microscopy (TEM) is the primary technique to verify single particle dimensions and to identify agglomerations of particles. The electron beam can be used to see features on the nanometer level. A major drawback to the use of TEM is that samples must be dried out of solution in order to be attached to the carbon matrix and placed in the vacuum chamber of the TEM; therefore, the particles are not exactly in the colloid state and agglomeration might occur during drying. However, TEM can be used in combination with dynamic light scattering to acquire exact sizing in nanofluid form. Transmission electron microscopy (TEM) measurements were conducted on a CARL ZEISS-LIBRA120 microscope.

3.5 Specification of the ETCS apparatus

The schematic diagram of the experimental setup for this work is shown in Figure 3.3. It consists of a circulation pump, nanofluid tank, cooling water tank (with capacity of 50 liters) and controlling units. The tilt angle of this ETSC is taken as 33° for the maximum solar daily radiation absorption and flow rate of 0.5, 1 and 1.5 l/min were used in this study. Four RTD sensor (PT-100) were installed to measure the inlet (T_i) and outlet (T_o) temperature of manifold, storage tank and environment.

The wind speed and solar radiation was measured by anemometer and pyranometer, accordingly. A data logger with 10 channels were connected to all sensors and the data were recorded by the computer.



1. Solar collector
2. Pyranometer
3. Anemometer
4. Nanofluid tank
5. Flowmeter
6. Heat exchanger
7. Pump
8. Thermocouple
9. Controller
10. Cooling water tank

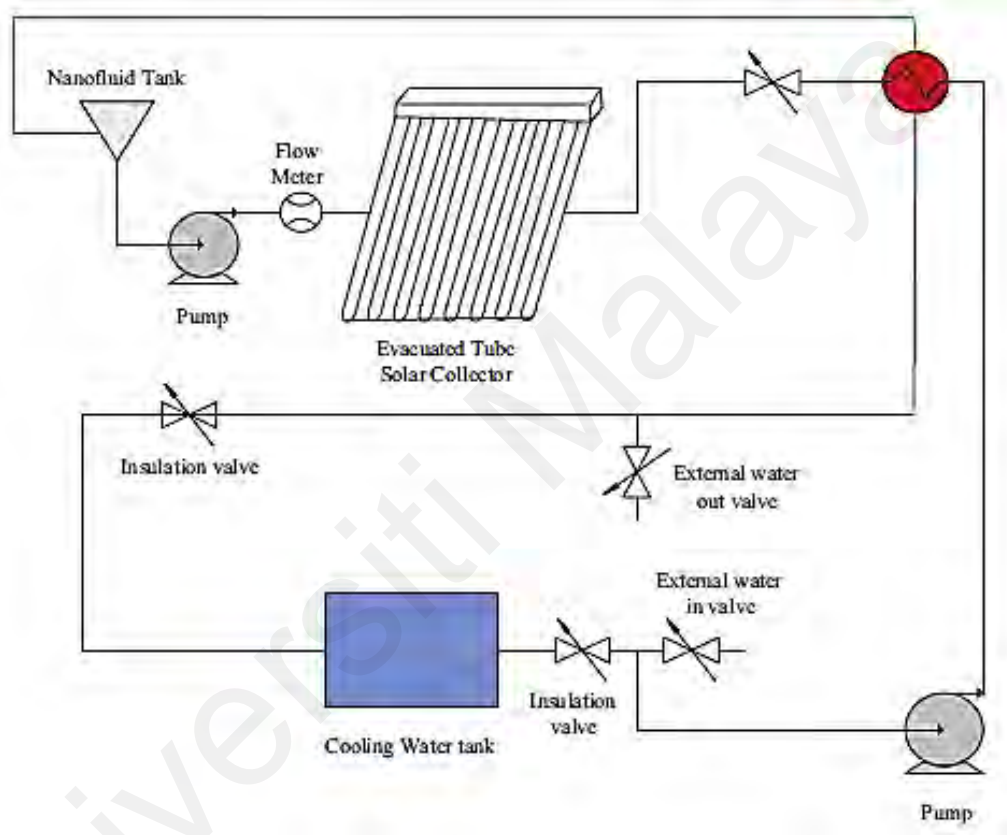


Figure 3.3: A schematic of evacuated tube arrangement

The dimensions and specifications of the evacuated tube solar collector (ETSC) is listed in Table 3.4 and Figure 3.4 shows the real setup and copper manifold arrangements.

Table 3.4: Specifications and details of the ETSC experimental set up

Specification	Dimension
Outer diameters of glass tube	0.058 m
Inner diameters of glass tube	0.047 m
Length of glass tube	1.8 m
Thickness of the glass	0.0016 m
Material	Borosilicate glass 3.3
Number of evacuated tubes	12 pcs
Working fluid of evacuated tube	Ethanol
Collector area	1.92 m ²
Absorbance area	1.14 m ²
Absorbance of collector	0.93
Transmittance of collector	0.89
Distance between 2 tubes	0.0750 m
Heat transfer coefficient of evacuated tube	2.360 W/m ² .K
Frame material	Aluminum alloy, anodized
Riser tube material	Copper TP2

The metal evacuated tube (heat pipe) was attached to a curved fin and was inserted to a glass tube. The heat pipes transferred the solar heat to the copper manifold that is filled with working fluid. The heat was transferred via fluid flow to the storage tank; thus, the hot water can be used at night or the next day due to the insulating properties of the tank.



Figure 3.4: Photograph of the experimental setup (front and back view)

3.6 ASHRAE standard

Existing standards for testing the performance of solar collectors are documented in ASHRAE 93-2003(2003) (Table 3.5). The ASHRAE 93 standard requires an experimental determination of the steady-state collector efficiency under prescribed environmental conditions for a range of collector fluid temperatures.

Each test requires a minimum of 20 min and 22 tests are required to fully characterize a collector's thermal performance. The ASHRAE 93 testing procedure is further complicated by the fact that the prescribed weather conditions do not often occur in some locations, which prolongs the time required to conduct the performance tests for a given collector. The EN12975-2 collector test procedure provides an alternative transient test method that can be conducted over a larger range of environmental conditions.

Table 3.5: ASHRAE standard that used in this experimental test

Variable	Absolute limits	Deviation	Units
Global solar irradiance (G)	>700	±50	W/m ²
Diffuse fraction (G _d /G)	20	-	%
Surrounding air speed (u)	3	±1	m/s
Incidence angle of beam irradiance θ	<20	-	Degree (°)
Surrounding air temperature (T _a)	-	±1	°C
Collector inlet temperature (T _{in})	-	±0.1	°C

3.7 Uncertainty analysis

Uncertainty analysis is essential to verify the accuracy of each experimental set up. There are various kind of errors such as data reduction errors, instance calibration errors, data acquisition errors and individual instrument uncertainties. In present study, the errors were coming from the direct measurement of each parameters such as temperature, solar radiation, pressure and mass flow rate. The results are presented in Table 3.6 and it shows the maximum uncertainty ranges for each parameter.

Table 3.6: Uncertainty analysis for the ETSC collector

Variation name	Uncertainty analysis
Pyranometer	±1%
Pressure transducer	±0.3%
RTD sensor	±0.1°C
Flow meter	±2%
Anemometer	±3%

3.8 Part III: Analytical approach

This section explains the formulas used to calculate the analytical and theoretical value before the experimental investigation were being conducted. The value such as energy, exergy, pumping power, entropy generation, bejan number of evacuated heat pipe solar collector were explained.

3.8.1 Energy analysis (First law of thermodynamics)

First law of thermodynamics is about energy balance. It states that energy is a conservative property; which means that the energy entering into the system is equal to the energy leaving the system as steady state. Overall amount of conserved energy is the same, although different forms of energy, for example, mechanical, internal, potential, kinetic experience quantitative changes (Lepers, Davesne, Chiacchiera, & Urban, 2010). In the application of solar thermal collector, heat gain (Q_u) by absorbing medium is given by;

$$Q_u = \dot{m}C_p(T_{out} - T_{in}) \quad (3.1)$$

Where, T_{out} , T_{in} , \dot{m} and C_p symbolize the outlet and inlet fluid temperature, mass flow rate of working fluid and specific heat of absorbing medium, respectively. Where, A_c and S are the absorbance area of the evacuated tube solar collector (ETSC) and the global solar radiation, respectively the input energy can be calculated as (H. Yousefi, Nishino, Faezipour, Ebrahimi, & Shakeri, 2011):

$$Q_{in} = A_c S \quad (3.2)$$

The thermal efficiency of ETSC (η) was a proportional of useful energy and the energy input and it is expressed as follows:

$$\eta = \frac{Q_u}{Q_{in}} \quad (3.3)$$

3.8.2 Exergy analysis (Second law of thermodynamics)

First law of thermodynamics practically is not possible to convert the heat energy into an equivalent amount of work. Therefore, second law of thermodynamics is used to overcome the drawbacks of the 1st law. It started by considering that real processes are not reversible, and it will gain entropy through the processes. Some of the common irreversible processes are molecular diffusion, friction, hysteresis etc (Lepers et al., 2010).

The exergy can be performed from the first and second thermodynamic laws and has different behavior depending on the operation condition. In this experiment, the potential and kinetic energy are neglected. Totally, exergy analysis provides a better insight into how a physical process work to compare with energy analysis. The thermophysical properties of the nanofluids, both in and out from the apparatus are constant.

Therefore, if the heat transfer to the system and work transfer from the system consider positive, the exergy balance for steady flow process and steady state condition can be expressed in the rate form as given below:

$$\dot{E}x_{in} - \dot{E}x_{out} = \dot{E}x_{dest} \quad (3.4)$$

Where ($\dot{E}x_{in}$) and ($\dot{E}x_{out}$) are the total exergy input and output respectively and ($\dot{E}x_{dest}$) is the destruction rate. $\Delta\dot{E}x$ is the exergy rate and can be defined as (Faramarz, Said, Hossein, & Amin, 2010):

$$\Delta \dot{E}x = \dot{m}_{bf} [(h_{out} - h_{in}) - T_a (s_{out} - s_{in})] \quad (3.5)$$

The specific enthalpy of the fluid at outlet and inlet are h_{out} and h_{in} ($J \text{ kg}^{-1}$). The entropy generation of the fluid at outlet and inlet are s_{out} and s_{in} ($J \text{ kg}^{-1} \text{ K}^{-1}$) respectively. The ambient temperature is T_a (K) and it is equal 300 K in this study.

The changes in the entropy and enthalpy of the nanofluid in solar collector are expressed:

$$\Delta h = h_{out} - h_{in} = c_{p,nf} (T_{f,in} - T_{f,out}) \quad (3.6)$$

$$\Delta s = s_{out} - s_{in} = c_{p,nf} \ln \frac{T_{f,out}}{T_{f,in}} - R_f \ln \frac{P_{out}}{P_{in}} \quad (3.7)$$

The exergy collection rate in steady state is exergy gained by heat transfer fluid while the fluid temperature increases from $T_{f,in}$ at the inlet to $T_{f,out}$ at the outlet. The expression of the exergy collection rate, assuming that the fluid is incompressible, can be obtained by using of the following equation without considering mechanical exergy and equations (3.8) to (3.9) can be established as:

$$\dot{E}x_{dest} = \dot{m}_{bf} \left[c_{p,nf} (T_{f,in} - T_{f,out}) - T_a \left(c_{p,nf} \ln \frac{T_{f,out}}{T_{f,in}} - R_f \ln \frac{P_{out}}{P_{in}} \right) \right] \quad (3.8)$$

Equation (3.10) is reordered due to P_{out} and P_{in} pressure and new equation can be obtained as below:

$$\dot{E}x_{dest} = \dot{m}_f c_{p,nf} \left[(T_{f,out} - T_{f,in}) - T_a \ln \frac{T_{f,out}}{T_{f,in}} \right] \quad (3.9)$$

There are two important points that should be noted in considering the exergy available ratio for solar radiation. One is that the solar flux radiating on earth can be assumed as always being in a steady state but never in equilibrium state. The other is that the radiation of the sun is a kind of an open system which means banishment of photons cannot be recovered unlike equilibrium closed system. From these facts the Carnot's expression of $(1 - T_a/T_s)$ is appropriate for the solar radiation exergy which has the same form as Jeter's result (Jeter and Stephens 2012). The total rate of the exergy ($\dot{E}x_s$) received from the solar radiation is defined as follow:

$$\dot{E}x_s = SA_c \left(1 - \frac{T_a}{T_s}\right) \quad (3.10)$$

Where, T_a and T_s stand for ambient temperature and apparent sun temperature, respectively. The heat transfer process from the sun to the collector's working fluid consists of two main parts, absorbing the solar radiation by absorber plate and heat transfer from absorber plate to working fluid. The exergy destructions occur during these two processes including flowing parts (Suzuki, 1988):

1. Absorption exergy loss (radiation \rightarrow plate): an exergy annihilation process when the solar radiation at T_s , is absorbed by the absorber at T_c .
2. Leakage exergy loss (plate \rightarrow ambient): an exergy loss process accompanied with heat leakage from the absorber out into its surroundings.
3. Conduction exergy loss (plate \rightarrow fluid): an exergy annihilation process caused by heat conduction between the absorber and the heat transfer fluid.

Therefore, the solar collector exergy efficiency (η_{ex}) is defined here and is expressed using equation (3.12) as follows:

$$\eta_{ex} = \frac{\dot{m}c_{p,nf} [(T_{f,out} - T_{f,in}) - (T_a \ln \frac{T_{f,out}}{T_{f,in}})]}{SA_c(1 - \frac{T_a}{T_s})} \quad (3.11)$$

Also, the exergy destruction (\dot{E}_{xdest}), can be estimated as:

$$\dot{E}_{xdest} = T_a \dot{S}_{gen} \quad (3.12)$$

The exergy loss processes are closely related with the corresponding entropy generation rates through Gouy-Stodola's theorem (Bejan & Kestin, 1983). The entropy generation can be estimated through the following relation:

$$\dot{S}_{gen} = \underbrace{\eta_o GA_c \left(\frac{1}{T_p} - \frac{1}{T_s} \right) + \dot{m}c_{p,nf} \left(\ln \left(\frac{T_{out}}{T_{in}} \right) - \frac{(T_{out} - T_{in})}{T_p} \right) + U_L A_c \left(1 - \frac{T_a}{T_p} \right) \left(\frac{T_p}{T_a} - 1 \right)}_{\dot{S}_{gen\Delta T}} + \underbrace{\frac{\dot{m}\Delta P}{\rho_{nf}} \frac{\ln \left(\frac{T_{out}}{T_a} \right)}{(T_{out} - T_{in})}}_{\dot{S}_{gen\Delta P}} \quad (3.13)$$

Where ΔP is pressure drop (Pa), A_c is the surface area (m^2) of solar collector. In addition, T_s is apparent sun temperature, T_p is the mean temperature of absorber plate, T_a is the ambient temperature, \dot{m} is mass flow rate of nanofluid (kg/s), T_{in} and T_{out} are the inlet and outlet temperatures of the working fluids, respectively.

An alternative description of irreversibility is the Bejan number, which is a distribution parameter that is defined as ratio of entropy generation due to heat transfer to

the total entropy generation, which gives an idea whether the fluid friction irreversibility dominates over heat transfer irreversibility or the heat transfer irreversibility dominates over fluid friction irreversibility.

It is simply the ratio of entropy generation due to heat transfer to the total entropy generation. Bejan number (Be) can be described as:

$$Be = \frac{\dot{S}_{gen\Delta T}}{\dot{S}_{gen\Delta T} + \dot{S}_{gen\Delta P}} \quad (3.14)$$

3.8.3 Pressure drop and pumping power

The circulation of nanofluid through the system carried out by pump. The pressure drop was estimated:

$$\Delta P = f \frac{\rho V^2}{2} \frac{\Delta l}{d} + K \frac{\rho V^2}{2} \quad (3.15)$$

Where f is the friction factor, K is the loss coefficient and d is the diameter of the pipe. The velocity V is the velocity (m/s) of the working fluid and can be calculated from:

$$V = \frac{\dot{m}}{\rho_{nf} \pi D_H^2 / 4} \quad (3.16)$$

The density of nanofluid (ρ_{nf}) can be calculated:

$$\rho_{nf} = \varphi \rho_{np} + (1 - \varphi) \rho_{bf} \quad (3.17)$$

There are two expressions to calculate the fractional factorial (f). The first for laminar flows can be used equation (3.19) and the second for turbulent flows, equation (3.20):

$$f = \frac{64}{Re} \quad (3.18)$$

$$f = 0.079Re^{-1.4} \quad (3.19)$$

For assuming Reynolds number following relation can be used:

$$Re = \frac{\rho V D_H}{\mu} \quad (3.20)$$

The following relation can be used to estimate the pumping power:

$$\text{pumping power} = \left(\frac{\dot{m}}{\rho_{nf}} \right) \times \Delta p \quad (3.21)$$

3.9 Part IV: CFD Solver

3.9.1 Problem definition

The flow fluid and heat transfer into ETSC is a complex process. In consequence, the efficiency of a thermal CFD simulation depends on many factors. Creation of the model geometry and its integration in a physical domain, grid generation and choice of a suitable numerical computing scheme are significant factors that can determine the level of success of the simulation process. The main steps of the performed studies are described in the following paragraphs.

3.9.2 Physical properties and key parameters

The system configuration is shown in Figure 3.5. The unit consists of a manifold network, inlet & outlet of fluid and heat pipe condenser. The thermal energy received from the 12 heat pipes condenser that consider as heat engine on this simulation. The heat dissipation to the heat engine is simulated in manifold and outlet temperature are recorded to calculate the thermal performance enhancement of ETSC by using different fluid.

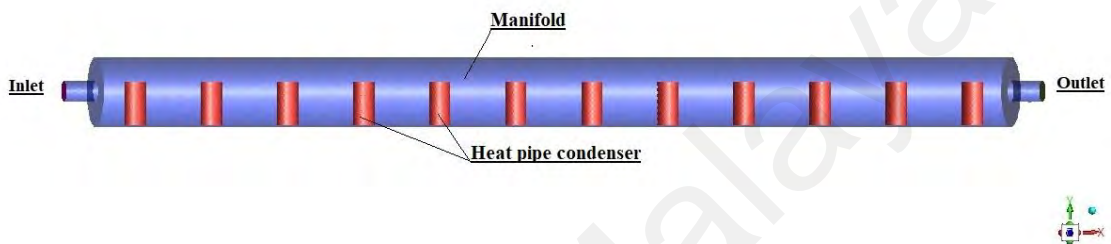


Figure 3.5: Schematic the manifold network of ETSC with 12 heat pipes.

3.9.3 Geometry Modeling

Figure 3.6 shows the geometry creation, which consists of inlet and outlet pipe diameter, manifold diameter and length are 30 mm, 100 mm and 1500 mm respectively, which is the same dimension of the experimental setup. The heat pipe condenser geometry simplifies to cylindrical shape with 30mm diameter and 60mm height.

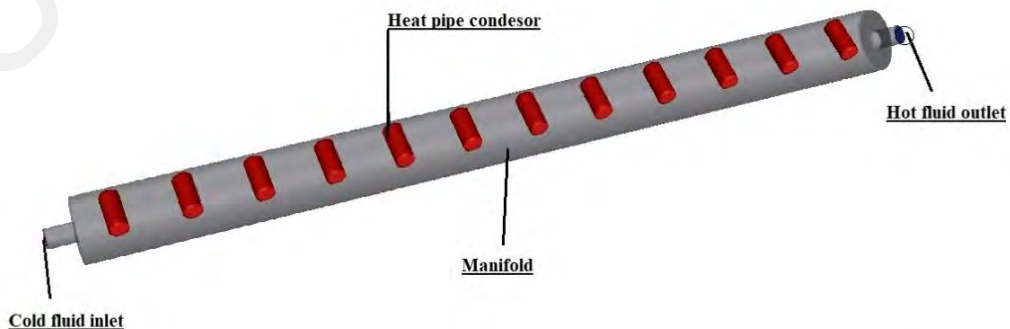


Figure 3.6: Geometry modeling of manifold network

3.9.4 Mesh generation

ANSYS Meshing was adopted to generate the meshes. Mapped meshing method with Quadrilateral element was used to mesh the surface bodies. Finer grids are applied in the wall of inlet and outlet and in the main condenser regions. The computational meshes for heat pipe and wall regions in the main condenser are shown in Figure 3.7 for the heat pipe.

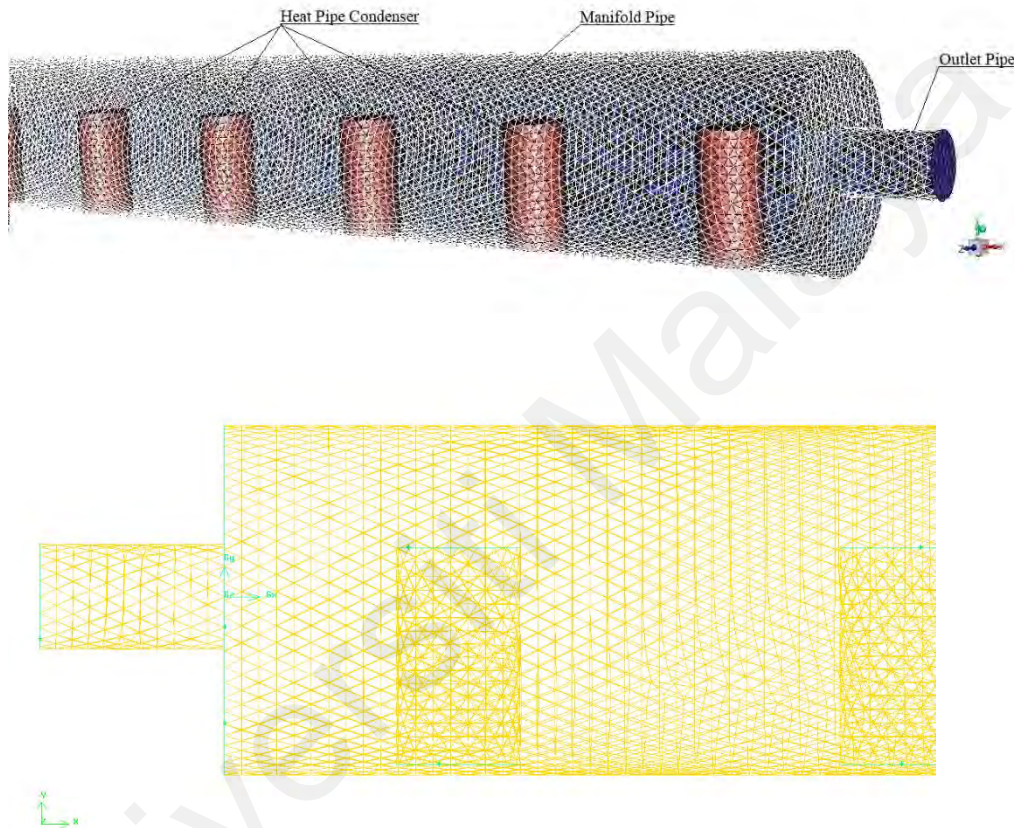


Figure 3.7: Magnified meshed part of the computational domain

3.9.5 Boundaries condition

It can be said that determining the boundaries conditions is one of the most basic and most important stages of numerical solution simulation which adjusted in ANSYS-FLUENT 19.00. The computational domain consists of a solid zone; representing the manifold and heat pipe, and a fluid zone; representing the liquid inside the manifold. The outer surface of the heat pipes condenser region is subjected to a heat flux boundary condition. The heat flux

corresponds to the varying heat input that shown in Table 3.7 are calculated with solar radiation and surface area of collector based on the data obtained from experiments. The inlet temperature of fluid is fix by 30 C° and flow rate 0.5 lit/min. The outlet was specified with an average static pressure of 0 Pa. The outer surface of the manifold, an adiabatic zone, is subjected to a zero heat flux boundary conditions.

Table 3.7 : Heat generation base on solar radiation and surface area in different time.

Time	Solar radiation	Area (m ²)	Heat flux Q(w)
10	500	1.14	570
11	700	1.14	798
12	900	1.14	1026
13	1100	1.14	1254
14	1300	1.14	1482
15	1000	1.14	1140
16	700	1.14	798
17	450	1.14	513

3.9.6 Governing Equations

The Boussinesq Approximation was chosen to take the lifting effect in the CFD simulations into account, and all physical and convection properties except density were assumed as fixed in this approach. In our model in which Boussinesq Approximation was used; the continuity, momentum and energy equations that will be used in our Finite Volumes Method solutions were expressed below.

Continuity equation:

$$\rho_{nf} \left(\frac{\partial u_x}{\partial x} + \frac{\partial u_y}{\partial y} + \frac{\partial u_z}{\partial z} \right) = 0 \quad (3.22)$$

Momentum equations:

x-component

$$u_x \frac{\partial u_x}{\partial x} + u_y \frac{\partial u_x}{\partial y} + u_z \frac{\partial u_x}{\partial z} = -\frac{1}{\rho_{nf}} \frac{\partial P}{\partial x} + \frac{\mu_{nf}}{\rho_{nf}} \left(\frac{\partial^2 u_x}{\partial x^2} + \frac{\partial^2 u_x}{\partial y^2} + \frac{\partial^2 u_x}{\partial z^2} \right) \quad (3.23)$$

y-component

$$u_x \frac{\partial u_y}{\partial x} + u_y \frac{\partial u_y}{\partial y} + u_z \frac{\partial u_y}{\partial z} = g_y \beta_{nf} (T - T_\infty) + \frac{\mu_{nf}}{\rho_{nf}} \left(\frac{\partial^2 u_y}{\partial x^2} + \frac{\partial^2 u_y}{\partial y^2} + \frac{\partial^2 u_y}{\partial z^2} \right) \quad (3.24)$$

z-component

$$u_x \frac{\partial u_z}{\partial x} + u_y \frac{\partial u_z}{\partial y} + u_z \frac{\partial u_z}{\partial z} = -\frac{1}{\rho_{nf}} \frac{\partial P}{\partial z} + \frac{\mu_{nf}}{\rho_{nf}} \left(\frac{\partial^2 u_z}{\partial x^2} + \frac{\partial^2 u_z}{\partial y^2} + \frac{\partial^2 u_z}{\partial z^2} \right) \quad (3.25)$$

Energy equation:

$$\rho_{nf} c_{nf} \left(u_x \frac{\partial T}{\partial x} + u_y \frac{\partial T}{\partial y} + u_z \frac{\partial T}{\partial z} \right) = k_{nf} \left(\frac{\partial^2 T}{\partial x^2} + \frac{\partial^2 T}{\partial y^2} + \frac{\partial^2 T}{\partial z^2} \right) \quad (3.26)$$

In the above equations, g denotes gravity acceleration. The change in the density was expressed by using the Boussinesq Approximation and this approach; are expressed as below. In this expression, ρ_0 denotes the density of the fluid while it was at the inlet of the system, β thermal-expansion-coefficient and T_0 the inlet temperature of the fluid.

$$\rho_{nf} = \rho_{nf0} [1 - \beta_{nf} (T - T_0)] \quad (3.27)$$

Analyzes and calculations were made by using the single-phase approach model in which nanoparticles are assumed to be distributed as homogenous in the fluid.

3.9.7 Solution procedure

The CFD package, ANSYS Fluent 18.0, was used for all the simulations performed in this study. The CFD model was developed to predict the outlet nanofluid temperature for the copper manifold attached at the top of the collector. The outlet nanofluid temperature is computed using general purpose CFD software. The convective heat transfer between the fluid zones and the corresponding faces are solved by coupling the momentum and energy equations. The SIMPLE method is used for the discretization of the pressure and second order upwind for momentum and energy equations.

Pressure-based solver is used for uncompromising flow and low speeds. But the Density-based solver is used for overcurrent and high-speed currents. In this regard, due to the incompressibility of the flow, pressure-based solver is used for this study. The velocity and temperature field for the nanofluid flow in the manifold is determined by solving the equations of continuity, momentum and energy. The grid independency test was done to check the quality of mesh on the solution. The solutions converged when the values of residuals in the computational domain fell below 1×10^{-6} . Further grid refining resulted in an error less than 0.6%. Also, the relative error between experimental results (X_{exp}) and simulation values (X_{sim}) is expressed by:

$$Error(\%) = \frac{|X_{sim} - X_{exp}|}{X_{sim}} \times 100 \quad (3.28)$$

CHAPTER 4: RESULTS & DISCUSSION

4.1 Introduction

This chapter will discuss the analytical approaches and experimental testing performed in laboratories and at roof top during this study. The data obtained throughout the investigation are interpreted and presented in tabular and pictorial format.

4.2 Design of Experiment

In the present study, three influential parameters including concentration, temperature and specific surface area of graphene nanoplatelets were investigated, which is the effective parameters on the viscosity and thermal conductivity of aqueous GNP nanofluids. A mathematical model developed by respond surface methodology (RSM) based on a central composite design (CCD). Also, the significance of the models was tested using the analysis of variance (ANOVA). The optimum results of aqueous GNP nanofluid showed that the concentration has a direct effect on the relative viscosity and thermal conductivity. Furthermore, predicted responses that proposed by the Design Expert software was compared with the experimental results. The statistical analysis of the predicted values was in satisfactory agreement with the empirical data and was performed the excellent predictability of the proposed models.

A total of 26 experiments with 10 center points and 8 axial points were designed by software with target of minimizing relative viscosity (μ_{nf}/μ_f) and maximizing relative thermal conductivity (K_{nf}/k_f) that have significant and direct effect on thermal applications (Table 4.1).

Table 4.1: Experimental results according to the design.

		Factorial input variable			Respond Variable	
Std	Run	A	B	C	k_{nf}/k_f	μ_{nf}/μ_f
20	1	+1	0	750	1.263	1.340
25	2	+1	-1	500	1.185	1.180
7	3	0	-1	750	1.199	1.201
9	4	0	0	500	1.187	1.144
17	5	0	0	750	1.234	1.243
14	6	-1	+1	500	1.205	1.219
23	7	+1	+1	500	1.287	1.380
26	8	0	0	750	1.232	1.285
24	9	-1	0	750	1.198	1.200
19	10	0	0	500	1.186	1.172
11	11	0	0	500	1.181	1.186
1	12	0	0	500	1.189	1.158
21	13	0	+1	500	1.250	1.243
22	14	+1	+1	750	1.307	1.440
8	15	+1	-1	750	1.218	1.260
4	16	0	+1	750	1.275	1.356
16	17	0	0	500	1.184	1.172
15	18	0	0	750	1.227	1.271
13	19	-1	-1	500	1.111	1.162
3	20	+1	0	500	1.212	1.280
6	21	-1	0	500	1.153	1.181
12	22	0	0	750	1.230	1.257
10	23	-1	-1	750	1.177	1.171
18	24	0	0	750	1.222	1.201
2	25	0	-1	500	1.152	1.102
5	26	-1	+1	750	1.234	1.248

4.2.1 Statistical analysis of relative thermal conductivity

Various statistic parameters for the thermal conductivity ratio responsible to the nanofluid system were computed from ANOVA. Table 4.2 shows the significant model

terms are those with p-values of less than 0.05 and implies A, B, C, AC, AB, BC, B2 and B2C with significant model terms. The results indicated that the concentration (B) has great influence on the thermal conductivity of GNP nanofluids.

Table 4.2: Analysis of variance table for relative thermal conductivity

Source	Sum of Squares	Df	Mean Square	F-Value	p-value Prob > F	
Model	0.048	10	4.755E-3	197.48	< 0.0001	significant
A-Temperature	0.013	1	0.013	543.85	< 0.0001	
B-Concentration	0.022	1	0.022	915.88	< 0.0001	
C-Specific Surface Area	5.626E-3	1	5.626E-3	233.64	< 0.0001	
AB	2.002E-4	1	2.002E-4	8.31	0.0114	
AC	1.120E-4	1	1.120E-4	4.65	0.0447	
BC	4.311E-4	1	4.311E-4	17.90	0.0007	
A²	2.011E-5	1	2.011E-5	0.84	0.3752	
B²	5.762E-4	1	5.762E-4	23.93	0.0002	
A²C	1.009E-5	1	1.009E-5	0.42	0.5272	
B²C	1.183E-4	1	1.183E-4	4.91	0.0426	
Residual	3.612E-4	15	2.408E-5			
Lack of Fit	2.457E-4	7	3.510E-5	2.43	0.1181	not significant
Pure Error	1.155E-4	8	1.443E-5			
Cor Total	0.048	25				
Std. Dev.	4.907E-3		R-Squared	0.9925		
Mean	1.21		Adj R-Squared	0.9874		
C.V. %	0.40		Pred R-Squared	0.9631		
PRESS	1.769E-3		Adeq Precision	59.310		

The value of R² (R-squared), which was used to measure the variation in the response around the mean and clarified by the proposed model. Base on the mathematical calculations for a good-fit model, the amount of the variation in the response must be close to one (Onsekizoglu, Bahceci, & Acar, 2010). As expected, the R² is 0.9925 and adjusted R² (R²-adj) is 0.9874, shows that our proposed model is in a good agreement with experimental results. These results value indicate that nearly 99% of the variability in the response can be verified by the model. This practical value can use for comparison between the degrees of variation from one data series to another. Generally, coefficient of variation should be less than 10% for an ideal fit to the selected model. The lack of fit seems to be desirable, thus, the “lack of fit F-value” of 2.43 implies that it is not significantly linked to the pure error.

4.2.2 Statistical analysis of relative viscosity

The ANOVA analysis in Table 4.3 provides the importance of each term in the regression model, such as checking the importance of the model. Significant terms that have considerable effect on viscosity of GNP nanofluid with ‘Prob.> F’ value of less than 0.05, include the first and second order effect of temperature (A, A²), concentration and specific surface area of nanoplatelets (B, C), interaction of second order effect of temperature and specific surface area of GNP (A²C) and (AB) two level interaction of temperature and concentration. The results show that the temperature plays the significant role on viscosity of GNP nanofluids in comparison to the other parameters. Table 4.3 shows the deference between predicted-R² and adjusted-R² and it was only less than 0.2. A ratio greater than 4 is desirable to demonstrate adequate model discrimination. The coefficient of variation (C.V.%) value that should not be greater than 10% for an ideal fit, was found to be 1.62% of Kratio response of the nanofluid system.

Table 4.3: Analysis of variance table for Relative Viscosity

Source	Sum of Squares	Df	Mean Square	F-Value	p-value Prob > F	
Model	0.15	10	0.015	37.85	< 0.0001	significant
A-Temperature	0.041	1	0.041	101.97	< 0.0001	
B-Concentration	0.055	1	0.055	136.88	< 0.0001	
C-Specific Surface Area	0.022	1	0.022	54.93	< 0.0001	
AB	7.606E-3	1	7.606E-3	19.04	0.0006	
AC	1.701E-3	1	1.701E-3	4.26	0.0568	
BC	1.446E-5	1	1.446E-5	0.036	0.8516	
A²	7.506E-3	1	7.506E-3	18.79	0.0006	
B²	7.832E-4	1	7.832E-4	1.96	0.1817	
A²C	3.884E-3	1	3.884E-3	9.73	0.0070	
B²C	2.469E-4	1	2.469E-4	0.62	0.4439	
Residual	5.991E-3	15	3.994E-4			
Lack of Fit	7.239E-4	7	1.034E-4	0.16	0.9877	not significant
Pure Error	5.267E-3	8	6.583E-4			
Cor Total	0.16	25				
Std. Dev.	0.020		R-Squared	0.9619		
Mean	1.23		Adj R-Squared	0.9365		
C.V. %	1.62		Pred R-Squared	0.9228		
PRESS	0.012		Adeq Precision	26.670		

4.2.3 Proposed Models

The Predicted Residual Error Sum of Squares (PRESS) is an important value that computes the difference between proposed model and the experimental data while it is

evaluating the model predictability. In this study, the PRESS value was calculated to be 1.769×10^{-4} and 0.012 for the relative thermal conductivity and relative viscosity in the model, respectively. In terms of code factors, the final equation presented in equations (4.1, 4.2, 4.3, and 4.4).

The final mathematical models between the response and independent variables can be represented as follows:

$$\frac{k_{nf}}{k_f}(500) = (1.11791) + (1.70596 \times 10^{-3} A) - (2.00742 B) + (0.01000 A^2) - (8.14875 \times 10^{-6} A^2) + (23.74480 B^2) \quad (4.1)$$

$$\frac{k_{nf}}{k_f}(750) = (1.13766) + (8.59895 \times 10^{-4} A) - (0.26592 B) + (0.010005 A^2) - (1.39142 \times 10^{-6} A^2) + (+8.93829 B^2) \quad (4.2)$$

$$\frac{\mu_{nf}}{\mu_f}(500) = (+1.36041) - (0.014984 A) - (1.06383 B) + (0.061667 AB) + (1.58452 \times 10^{-4} A^2) + (8.35379 B^2) \quad (4.3)$$

$$\frac{\mu_{nf}}{\mu_f}(750) = (+1.30139) - (3.18603 \times 10^{-3} A) - (4.18537 B) + (0.061667 AB) + (2.58621 \times 10^{-5} A^2) + (29.74946 B^2) \quad (4.4)$$

As shown in Figure 4.1, the predicted data versus actual value performed a comparison between the predicted model and the experimental data for viscosity and thermal conductivity. The graph should demonstrate random scatter about a 45° line and the line goes through the middle of each data over the whole range of the data. As shown in Figure 4.1, the RSM provides results in satisfactory agreement with experimental data. The scatter represented that the thermal conductivity and viscosity ratio can be predicted very precisely by the CCD model.

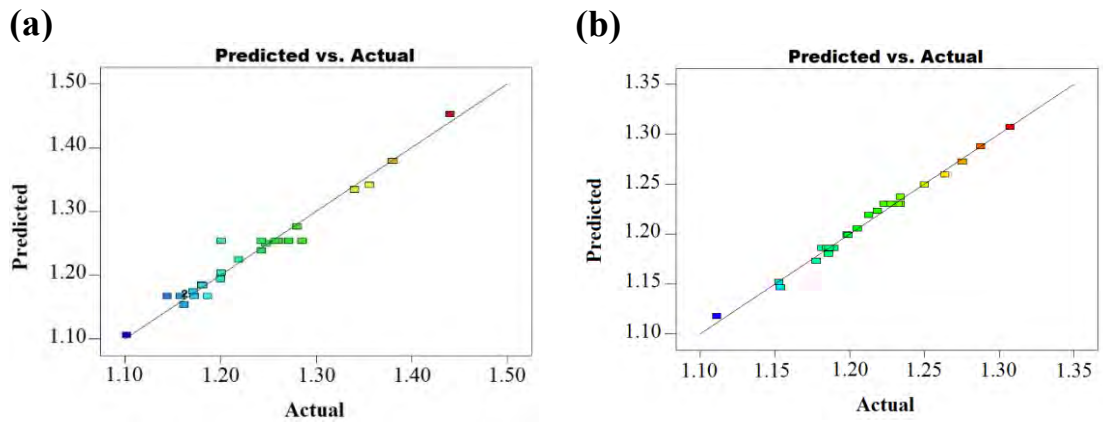


Figure 4.1: Correlation between experimental and predicted values for (a) viscosity (b) thermal conductivity

To evaluate the adequacy of our proposed model, the comparison results were performed between three predicted data results from software and actual experiment results is demonstrated in Table 4.4. The small error value between the actual value and experimental data in Table 4.4 supports the good agreement between experimental results and theoretical estimates.

Table 4.4: Confirmation experiments

No.	T (°C)	V (wt %)	SA (m ² /g)	Thermal conductivity (W/m.k)				Viscosity (m.Pa.s)			
				Actual	Predicted	Residual	Error (%)	Actual	Predicted	Residual	Error (%)
1	20	0.1	500	1.200	1.205	- 0.005	0.41	1.229	1.224	- 0.005	0.40
2	40	0.05	750	1.197	1.198	- 0.001	0.08	1.199	1.203	- 0.004	0.33
3	60	0.07	750	1.256	1.259	-0.003	0.23	1.34	1.334	0.006	0.44

The graphs Figure 4.2, show that thermal conductivity of GNP nanofluids enhanced with the temperature and concentration. It is clear that the GNP nanofluid with 0.1 wt% and specific surface area of 750 m²/g at 60°C provides the maximum thermal conductivity enhancement.

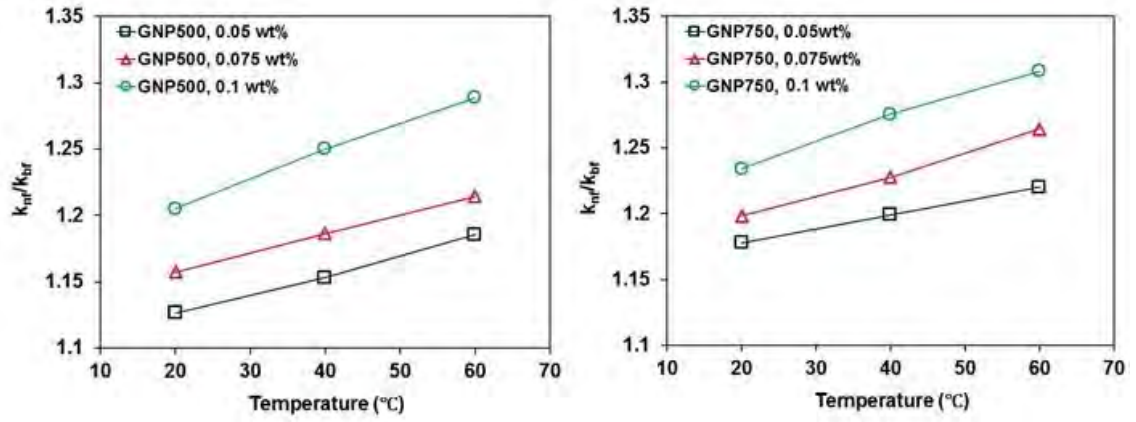


Figure 4.2: Relative thermal conductivity of GNP nanofluids versus temperatures, at three different concentration

Figure 4.3 shows the viscosity for GNP nanofluid at different specific surface area and concentrations versus temperatures. In general, temperature is the main effective factor on viscosity of nanofluids, similar to simple fluids. As shown in Figure 4.3, the viscosity was reduced for higher temperature. This behavior of all other varieties of nanofluids happen as a result of the flagging of the intermolecular adhesion force.

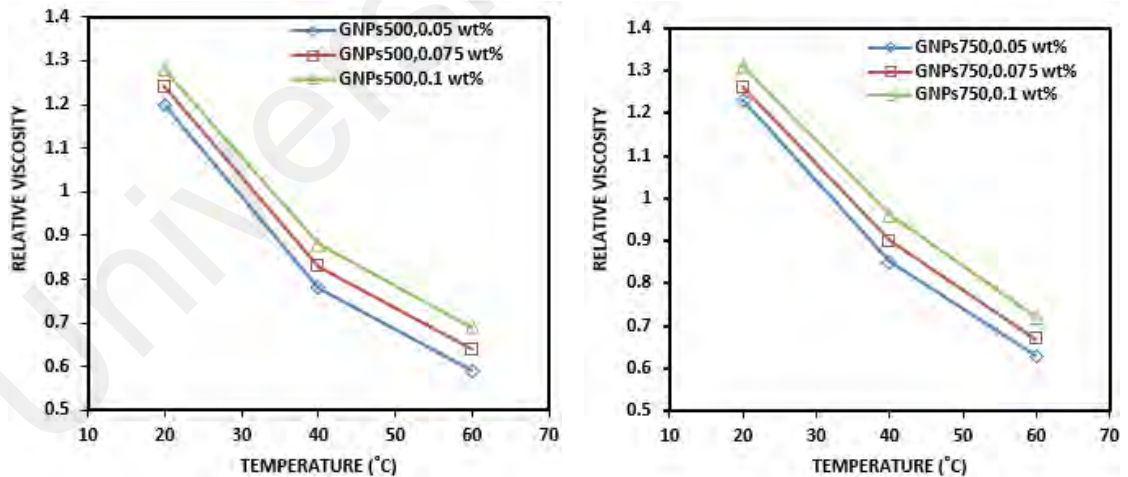


Figure 4.3: Relative viscosity of GNP nanofluids versus temperatures in different concentration

According to Table 4.2 and Table 4.3, the 3D surface and contour plots demonstrate the interaction effect of temperature and concentration for specific surface area of 750 m^2/g on the thermal conductivity ratio and viscosity of the GNP nanofluid system and

they are displayed in Figure 4.4. Figure 4.4 (a and c) show that the 3D surface graphs have a smooth profile in accordance with the two-factor interaction model while (b and d) show the contour plot for the response surface. Figure 4.4 (a and b) indicates that the enhancement in concentration plays higher influential role for thermal conductivity of GNP nanofluid while the Figure 4.4(c and d) illustrates the viscosity depend on temperature.

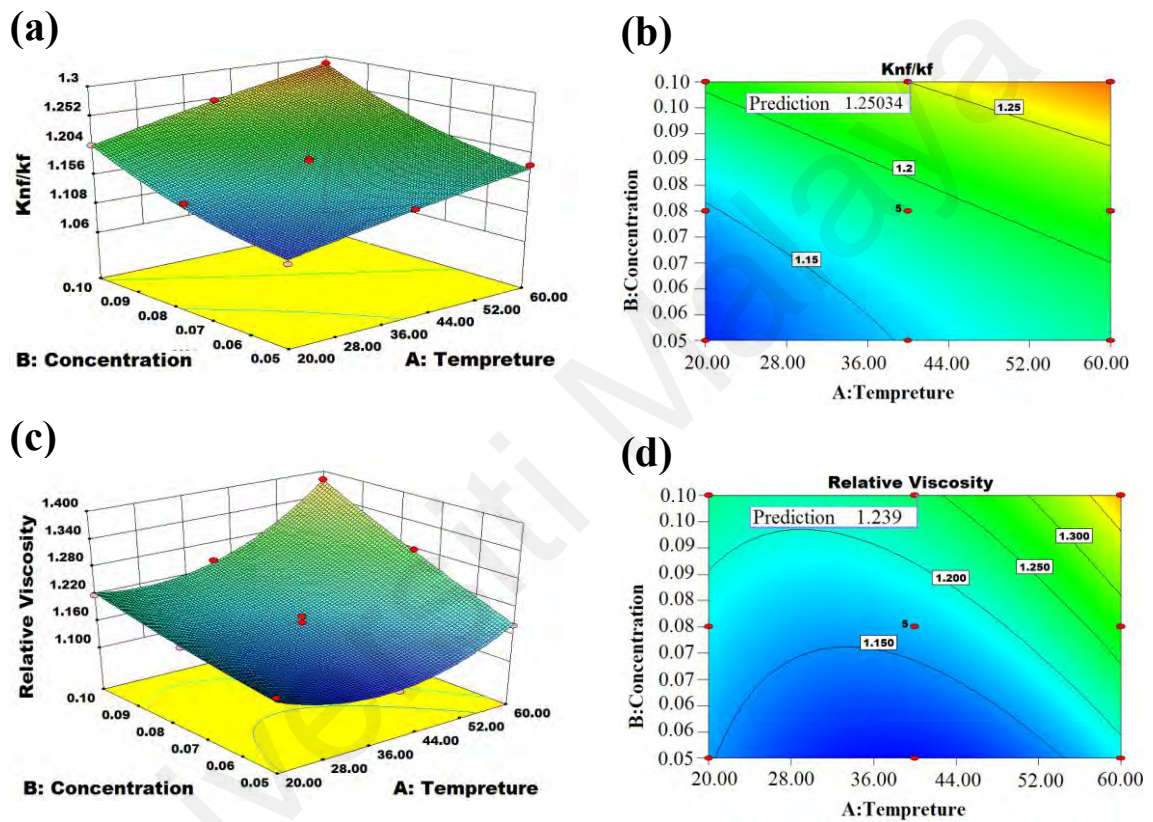


Figure 4.4: Interaction effect of temperature and concentration on thermal conductivity ratio response: (a) 3-D surface; (b) contour plot and Interaction effect of temperature and concentration on viscosity response: (c) 3D surface; (d) contour plot.

Figure 4.5 illustrate the independence verification of the errors that was clarified some plots of the residuals versus run order or predicted values and factors (Kazemi-Beydokhti et al., 2013). As shown in

Figure 4.5, the predicted values and run number of the responses versus studentized residuals are depicted. These graphs be able to lead to detect response variables. The observation from these figures indicated that there is no unusual configuration such as megaphone shape or sequences of positive and negative residuals.

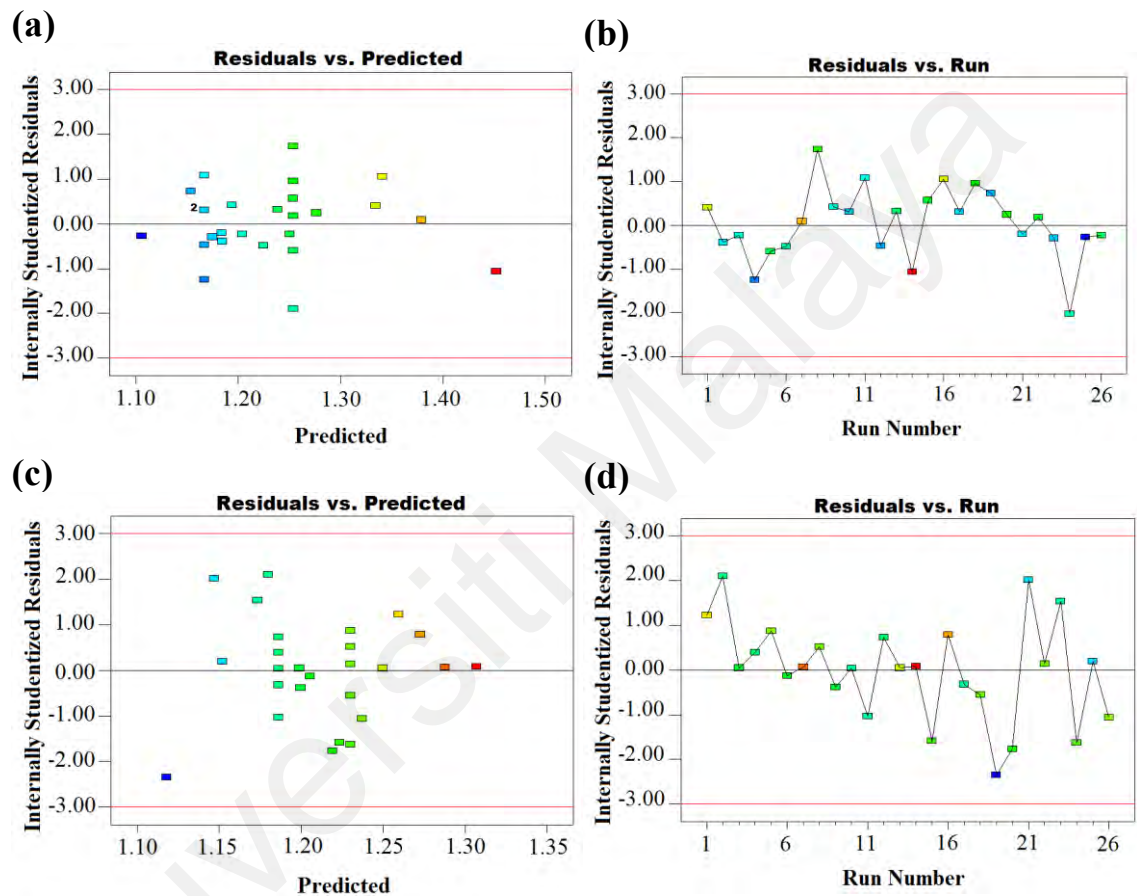


Figure 4.5: Studentized residuals versus (a) predicted response (b) run number for viscosity and (c) predicted response (d) run number for thermal conductivity

4.3 Nanofluid preparation without surfactant

Dispersion of nanoparticles into the base fluid is an important process requiring special attention. The prepared nanofluid should be an agglomerate-free stable suspension without sedimentation for long durations. Graphene nanoplatelets are offered in granular form that is soluble in water with the right choice of dispersion aids, equipment, and techniques. The graphene nanoplatelets were dispersed in distilled water using a high-

power ultrasonication probe (Sonics Vibra Cell, Ningbo Kesheng Ultrasonic Equipment Co., Ltd., Ningbo, China) having a 1,200-W output power and a 20-kHz frequency power supply. The concentrations of nanofluids were maintained at 0.025, 0.05, 0.075, and 0.1 wt.% for specimens of specific surface areas of 750 m²/g. The stable homogeneous GNP nanofluids were prepared without using any surfactant. Photos of four typical samples of GNP nanofluids at their concentration after 3 months are shown in Figure 4.6. In the picture observed that there is no sediment at the bottom of the container and GNP nanofluids at different concentration are stable.



Figure 4.6: Photograph image of prepared sample of GNP nanofluid after three months

4.4 Morphology of GNP dispersion

A drop of diluted solution was placed onto a carbon coated copper grid, air-dried, and observed under TEM. Figure 4.7 shows the image of dried GNP suspensions. The GNPs, the sheet-like structure with a lateral size at the micrometer length scale has been well captured. When GNPs were dispersed by ultrasonic treatment, the lateral size of GNPs was decreased. The edges of GNP layers are clearly seen as straight lines. The sonication process tends to break the flake: longer sonication time improves the exfoliation degree;

further sonication is advantageous from the aspect of dispersion and colloidal stability (Mohammad Mehrali, Emad Sadeghinezhad, et al., 2014a).



Figure 4.7: TEM images of GNP

4.5 Solar radiation and ambient temperature measurement

The solar radiation was measured with Pyranometer. Figure 4.8 demonstrates the variation of solar energy gain as a function of different tilt angle of solar collector. The results show that the best performance for ETSC occurs at 33° in Kuala Lumpur, Malaysia. Therefore, the tilt angle of this ETSC is taken as 33° for the maximum solar daily radiation absorption.

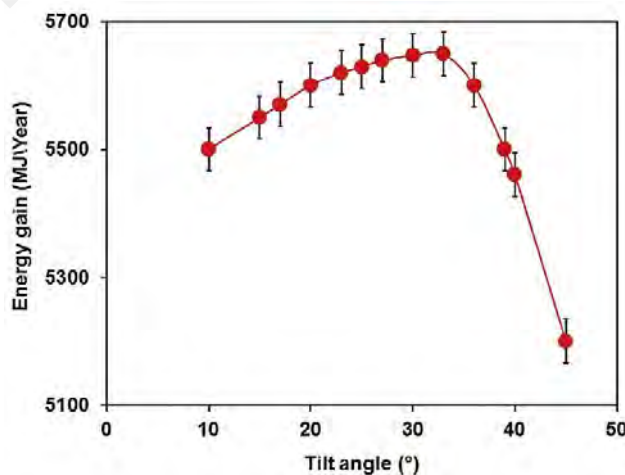


Figure 4.8: Variation of total energy gain of ETSC system as a function of different tilt angle

The experiments were carried out in consecutive days for the period of January to September. The hourly time range of the experiment was 9:30 a.m. to 5:00 p.m. (MST) in order to utilize the availability of the sun in Malaysia. Figure 4.9 demonstrates the average solar radiations (G) and ambient temperatures during the experimental procedure for the clear sky. The thermal performance of the system was estimated under steady-state conditions and transient affects were ignored.

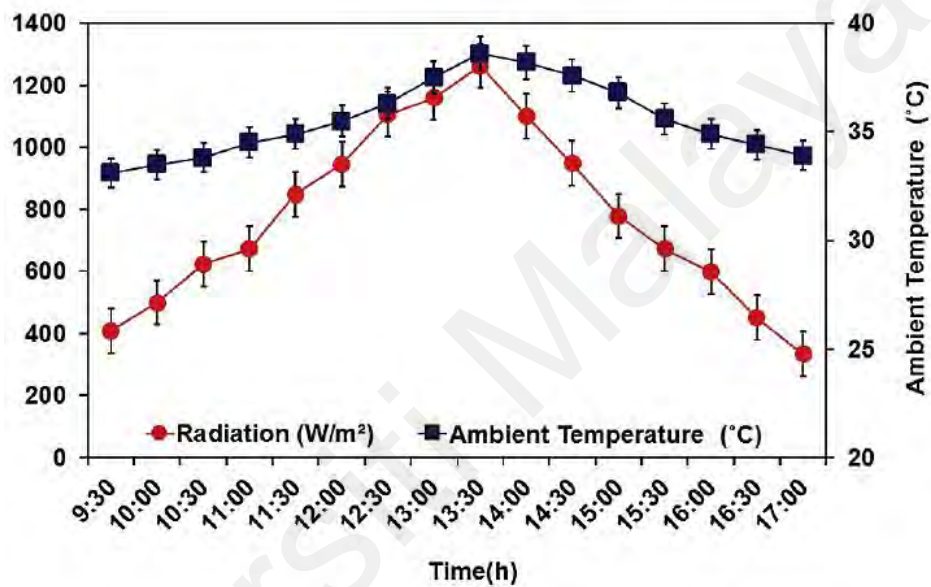


Figure 4.9: The average solar radiation versus time for the test period

4.6 Distilled water as working fluid

To validate the experimental setup for calculating experimental data and to providing a control to compare the GNP nanofluid data, an experimental test was conducted for DW. Figure 4.10 demonstrates the collector thermal efficiency at different mass flow rates for DW. The result show that thermal efficiency for DW improved with increasing the mass flow rate from 0.5 l/min to 1.5 l/min. When the flow rates are too low it is not able to remove the heat effectively from the collector, therefore the efficiency of set-up decrease. Figure 4.10 shows that efficiency enhancement has increasing trend at noon due

to rising ambient temperature, solar radiation, flowrate and consequently higher temperature different.

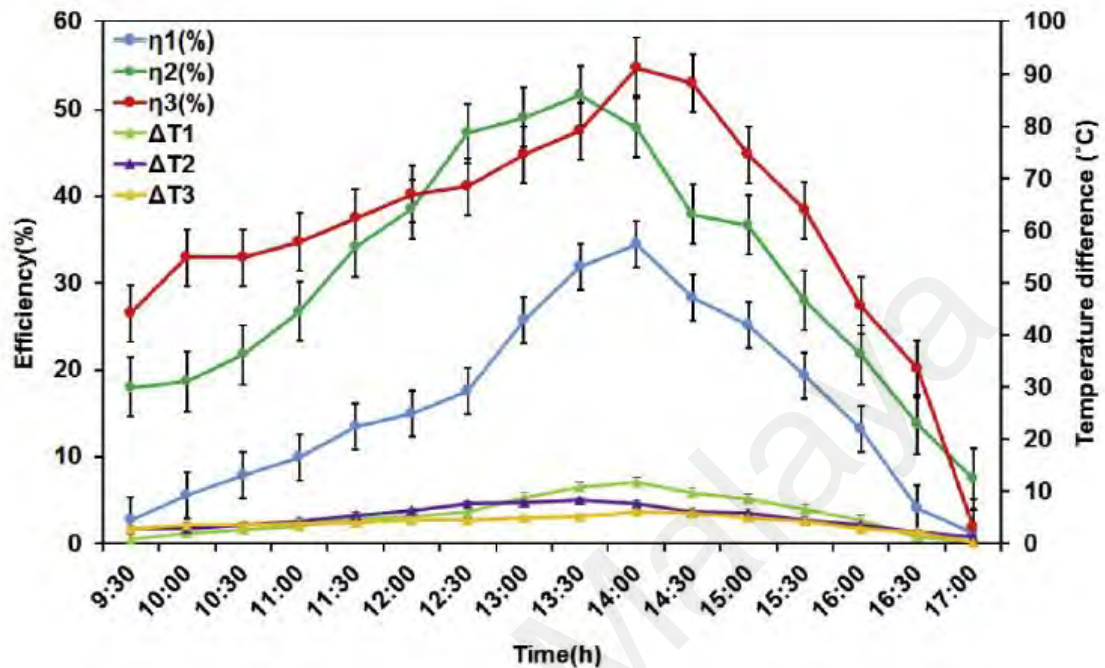


Figure 4.10: Efficiency of ETSC and temperature difference for Distilled water

4.7 Thermal performance of the ETSC with GNP nanofluid as working fluid

In order to improve the thermal performance of ETSC and compare the impacts of different concentrations and mass flow rates, each experiment was conducted for several cloudless days. The best ambient temperature, wind speed and solar radiation results have been chosen. The results indicated that mass flow rate plays an important effect on the thermal efficiency (η) of the ETSC, as shown in Figure 4.11(a-d). It shows the η_1 , η_2 , and η_3 of collector at mass flow rate 0.5, 1 and 1.5 l/min, respectively. The results show that the efficiency of the solar was dependent on solar intensity and ambient temperature, as well as flow rate and concentration of working fluid. Figure 4.11 shows that the thermal efficiency of the solar collector and the temperature of working fluid difference between inlet and outlet increase to the maximum at noon due to high ambient temperature and solar radiation.

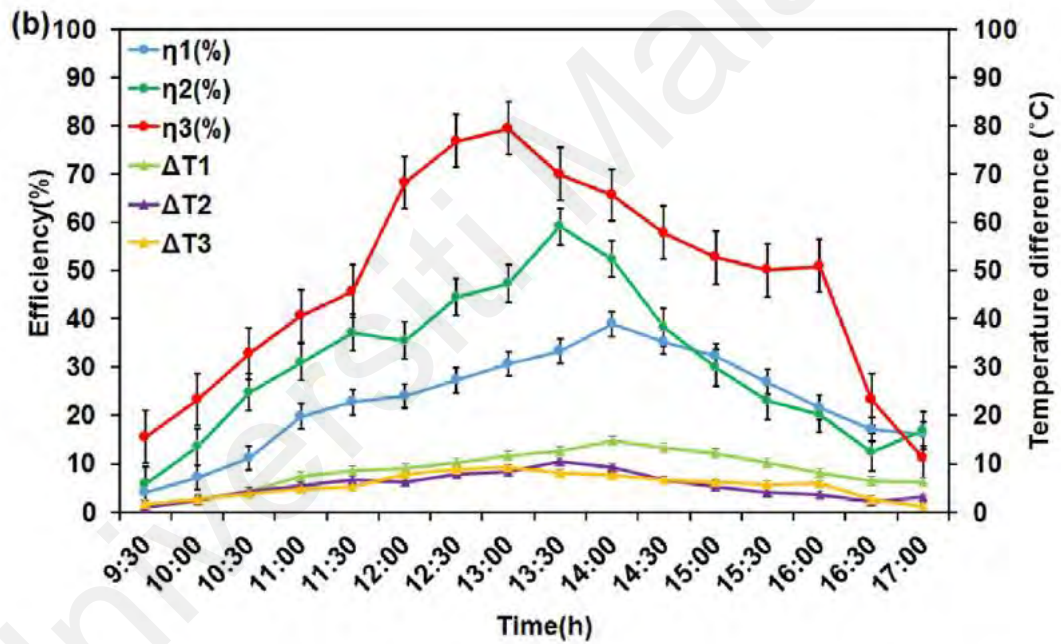
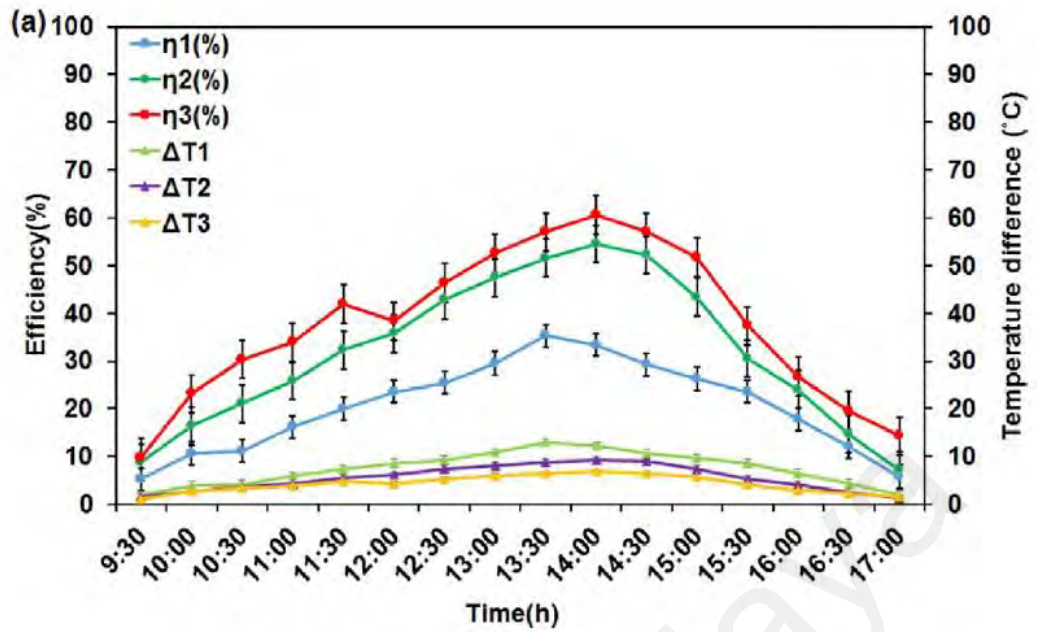


Figure 4.11: Thermal efficiency of ETSC versus time at different concentrations of GNP nanofluid (a) 0.025 wt%, (b) 0.05 wt%, (c) 0.075 wt% and (d) 0.1 wt%

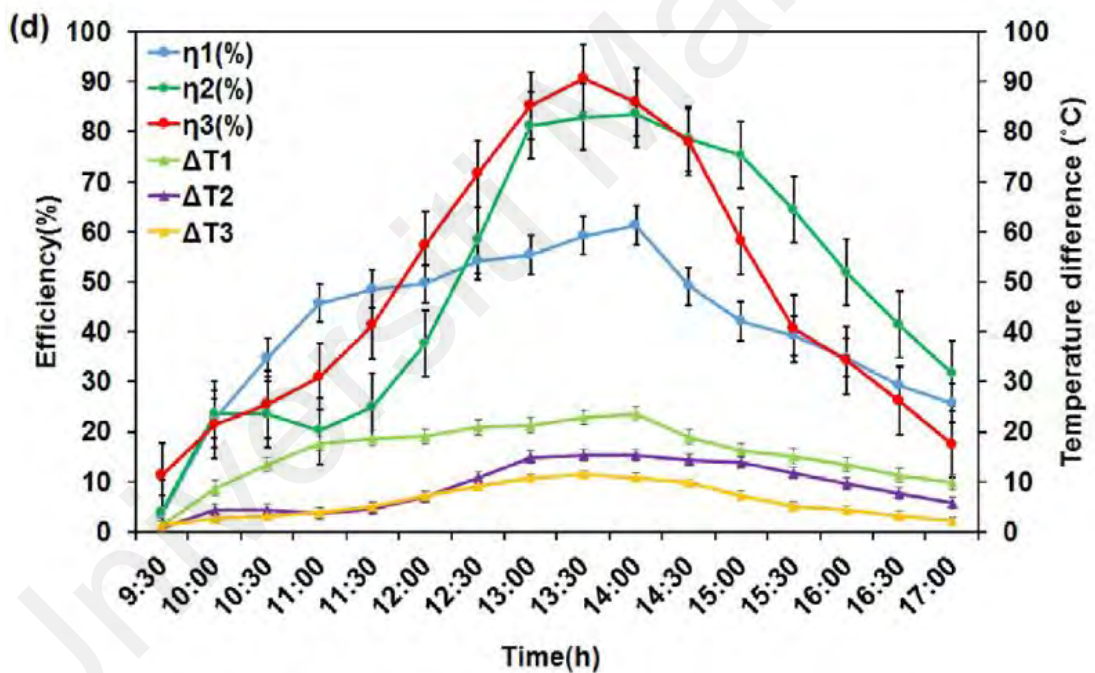
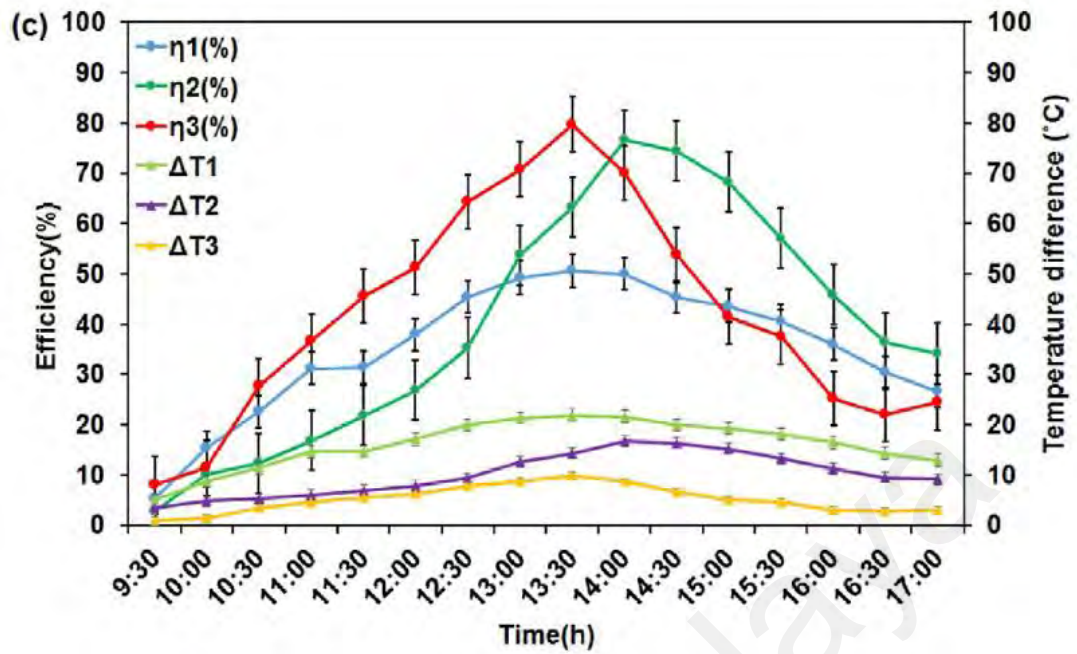


Figure 4.11, continued'. Thermal efficiency of ETSC versus time at different concentrations of GNP nanofluent (a) 0.025 wt%, (b) 0.05 wt%, (c) 0.075 wt% and (d) 0.1 wt%

Figure 4.12 demonstrates that the temperature difference is directly a proportional to the concentration of GNP. The results revealed that the difference between the inlet and outlet temperature of manifold was increased with the concentration of GNP nanofluent. The maximum value was attained by 12.9°C, 14.7°C, 18.8°C and 23.6°C for GNP nanofluent

at 0.025, 0.05, 0.75 and 0.1 wt%, respectively. The temperature difference increased considerably by the addition of small amounts of nanoparticles to the base fluid due to more solar energy absorption, compared to water. This prove that by using a correct additive in basefluid, the heat transfer can be further enhanced to 100% compare to water.

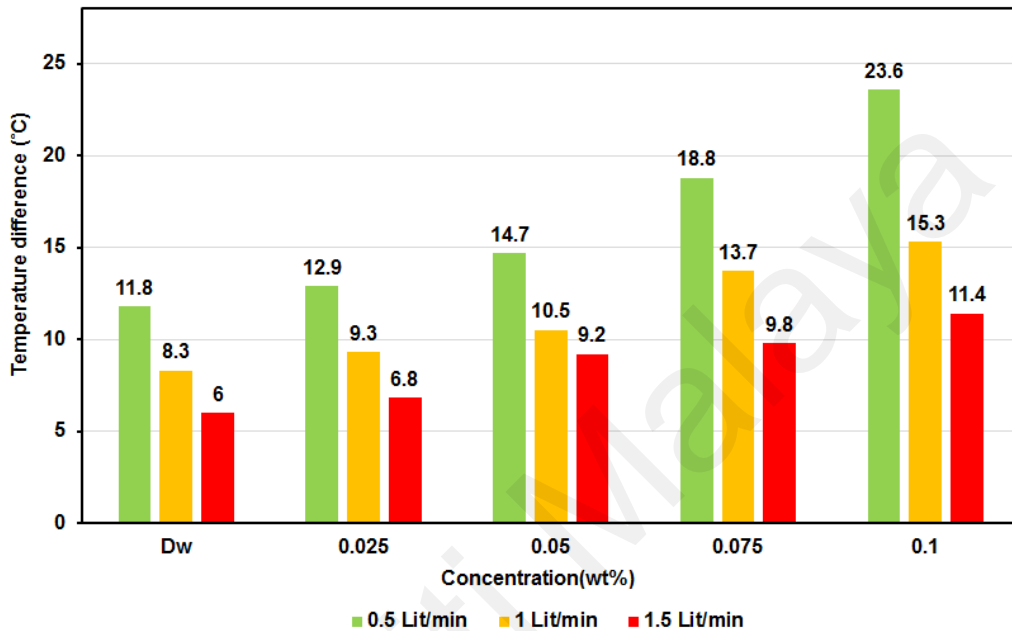


Figure 4.12: Effect of concentration and mass flow rate on temperature difference

The thermal efficiency of GNP nanofluid at different concentrations and velocities illustrated in Figure 4.13. It can be observed that the GNP nanofluids has excellent convective heat transfer properties due to nano-convection of GNP as the mechanisms of energy transport and it has heat conductivity due to the Brownian motion as a prime factor for enhancement of thermal conductivity. In addition, this figure shows that the efficiency is directly related to the concentration and the mass flow rate of GNP nanofluids. It can be clearly seen that efficiency improved 26.8 %, 31.9%, 35.9 % for 0.1 wt% concentration compared to distilled water at, 0.5,1 and 1.5 l/min mass flow rate respectively.

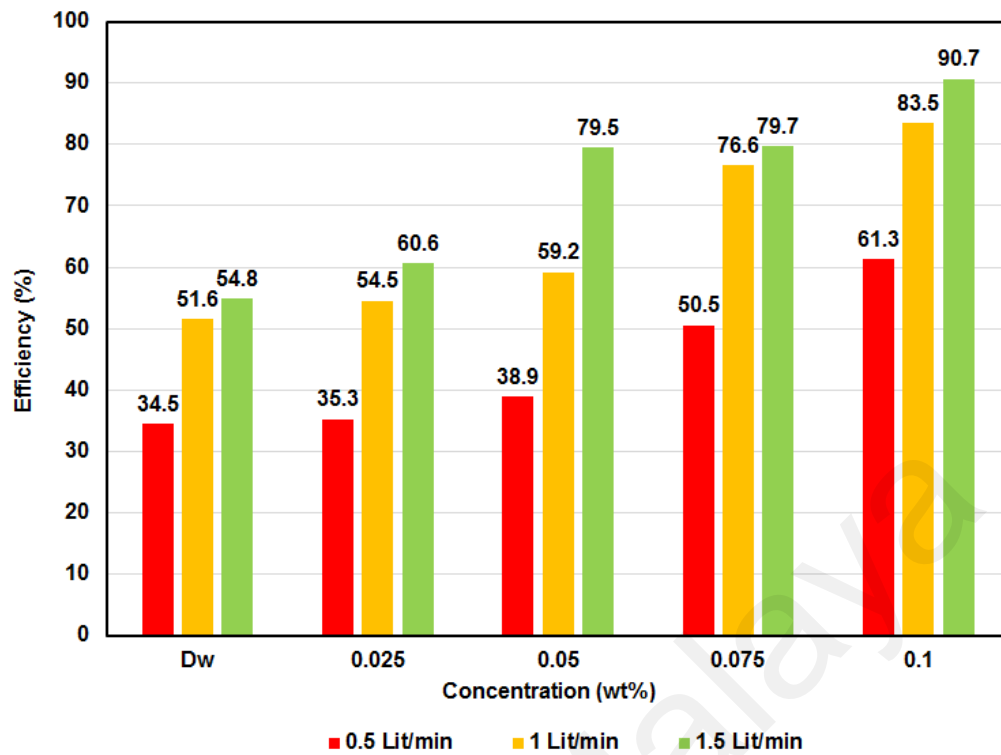


Figure 4.13: Thermal Efficiency with the enhancement of concentration

4.8 Correlation development between thermal efficiency and thermal conductivity

GNP nanofluid with a high thermal conductivity ratio compare to the DW was capable of absorbing more heat at the manifold section that led to the higher outlet temperature. For further investigation of thermal conductivity effects on the thermal efficiency of ETSC system, an empirical correlation was developed to calculate the thermal efficiency as a function of various influencing parameters (see Equation 5).

The mentioned empirical correlation was expanded by Vaschye Buckingham theory to create two p groups that were generated from several physical variables and can be expressed as (Sabiha, Saidur, Mekhilef, et al., 2015):

$$\eta = f(\dot{m}, C_p, \Delta T, A_c, S, k_{bf}, k_{nf}) \quad (4.5)$$

That two π groups and thermal efficiency can be explained as follows:

$$\pi_1 = \frac{\dot{m}C_p\Delta T}{A_c S} \quad (4.6)$$

$$\pi_2 = \frac{k_{nf}}{k_{bf}} \quad (4.7)$$

$$\eta = \alpha \pi_1 \pi_2^\beta \quad (4.8)$$

where, α and β are the empirical coefficients and can be calculated by a non-linear regression. The final form of this empirical correlation is expressed as follow:

$$\eta = 0.91 \pi_1 \sqrt{\pi_2} \quad (4.8)$$

Figure 4.14 shows that the empirical correlation has good agreement with the experimental results with the R^2 value of 0.9966.

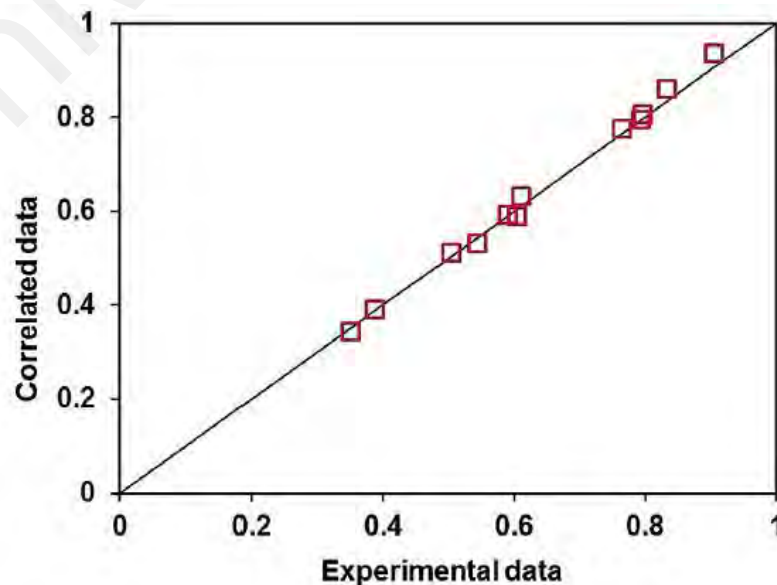


Figure 4.14: Experimental data versus predicted data of thermal efficiency

4.9 Energy and exergy efficiency

The thermal efficiency of solar collectors was calculated from the ratio of useful energy to the energy incident on the collector. Many research have shown that the efficiency for various types of nanofluids including CuO, Al₂O₃, SiO₂ and TiO₂ based nanofluids is proportional to the volume fraction of nanoparticles T. Yousefi et al. (2012) and H. Tyagi, Phelan, and Prasher (2009).

There are reasons for the higher efficiency of nanofluids solar collector compared to water. Output temperature of solar collector can be influenced by the specific heat of working fluids (T. Yousefi et al., 2012). As seen in Table 2.6, different nanoparticles have different specific heat therefore when added to base fluid, improve the heat capacity of liquid. Usually, the specific heat of the nanofluids increased compared to base fluids after adding dispersant in the mixtures. There are contradictory results among the effects of temperatures on specific heat of the nanofluids. But generally, if low specific heat capacitive nanofluid needed then nanoparticles with low specific heat capacity should be suspended in the base fluid and vice versa. Therefore, together required specific heat capacitive nanofluids, it is recommended to know the specific heat of the base fluids and nanoparticles (Shahrul, Mahbubul, Khaleduzzaman, Saidur, & Sabri, 2014).

In this study as shown in Figure 4.15 (a) it can be observed that with increasing the mass flow rate and particle concentration, the thermal efficiency of collector enhanced. It is clear that at mass flow rate 1.5 l/min, the efficiency of collector reached maximum.

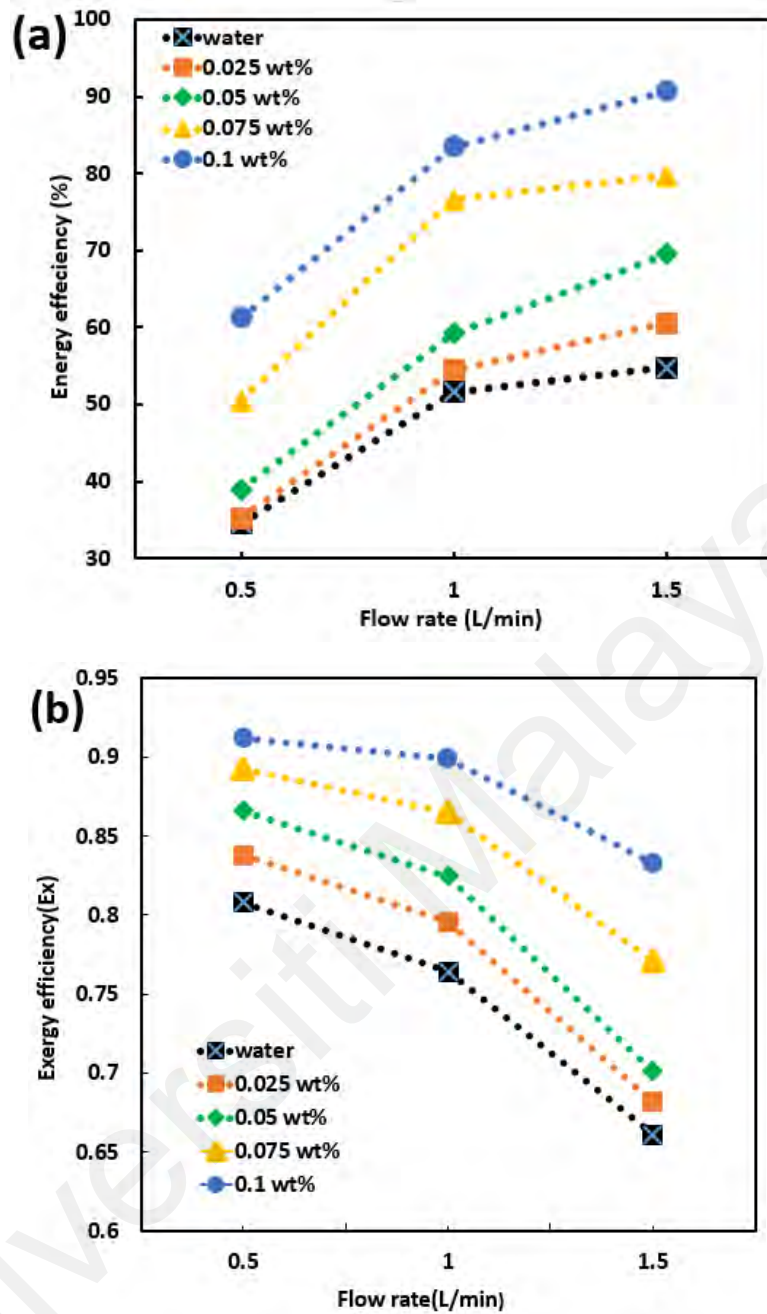


Figure 4.15: Impact of particle concentration and mass flow rate on energy efficiency (a) and exergy efficiency (b)

Figure 4.15(a) shows the solar collector thermal efficiency raised up to 90.7 % for 0.1 wt% and mass flow rate of 1.5 l/min, which is 35.8% higher than distilled water. Difference between the inlet and outlet temperature of fluid deduct with increasing the mass flow rate. This consequently results in the decrease of energy efficiency. Also, the temperature difference is directly a proportional to the concentration of GNP

nanoplatelets. The similar findings were reported from an experimental investigation on Al_2O_3 nanofluid by (T. Yousefi et al., 2012). It can be observed that the temperature difference was increased with the concentration of GNP nanofluid due to the high thermal conductivity of nanofluid. The maximum value between inlet and outlet temperature was recorded 23.6 °C for GNP nanofluid at 0.1 wt%. The stochastic motion of the GNP nanoplatelets is the main reason behind the observed improvement the heat transfer properties. Generally, the increase in the energy efficiency can be a result of the enhanced thermal conductivity, due to improvement of convective heat transfer coefficient. Comparison of results obtained for thermal efficiency from this study with other researches is shown in Table 4.5.

Exergy indicates conversion of available energy into useful work or energy in the thermal systems. The result presented in Figure 4.15 (b), shows that how exergy efficiency (E_x) enhance with particle concentration and simultaneously decrease with mass flow rate. Based on the results, it is observed that optimum exergy efficiency is 0.91 which occurred in 0.1 wt% and 0.5 l/min mass flow rate. Referring equation (3.11), the interaction of mass flow rate and heat capacity effect significantly on exergy efficiency

By using nanofluid in solar collector, exergy efficiency can be increased. Nanofluids may be a good choice as an absorbing medium because of their exergy efficiency is higher than water. From Hamilton and Crosser model (Hamilton & Crosser, 1962), it is stated that the thermal conductivity of nanofluid is directly related to the volume fraction and the shape of the nanoparticle. It can be explained that addition of more particles leads to increased effective surface area for heat transfer.

Table 4.5: Comparison of results obtained for thermal efficiency from this study with other researches

Nano particle	Efficiency improvement	Solar thermal system	Researcher
TiO ₂	16.67 %	Evacuated tube solar collector	(M Mahendran, Lee, Sharma, Shahrani, & Bakar, 2012b)
Copper Oxide (CuO)	30%	Evacuated tubular solar collector	(L. Lu, Liu, & Xiao, 2011)
SWCNT	21.59%	Evacuated tube solar collector	(Sabiha, Saidur, Mekhilef, et al., 2015)
CNT	25%	Evacuated tube solar collector	(Chougule, Pise, & Madane, 2012)
AL ₂ O ₃	28.4%	Evacuated tube solar collector	(Al-Mashat & Hasan, 2013)
GNP	35.8 %	Evacuated tube solar collector	(Iranmanesh et al., 2017)

Additionally, the inherently higher thermal conductivity of nanoparticles will improve the thermal conductivity of the nanofluid. This may cause an improvement in exergy efficiency. Thus, the analytical results indicated that in evacuated tube solar collector, there is a definite probability to get maximum exergy by using nanofluid as agent medium. The possible reason for this enhancement may be associated with the

following: (I) the nanofluid with suspended nanoparticles increases the thermal conductivity of the mixture and (II) it is also known that the convective heat transfer coefficient of the nanofluid is higher than that of the base fluid (water) at a given Reynolds number. The results complied with those obtained from (Duangthongsuk & Wongwises, 2009; Xuan & Li, 2003).

4.10 Pumping power

The enhancement of pumping power has adverse effect on thermal and exergetic efficiency. Therefore, according the equation 3.19, increase in pressure drop is not desirable. Figure 4.17 showed that the pumping power rises with enhancement of the mass flow rate and GNP nanofluid concentration. For 0.025 wt% particle concentration 1.1 % increase in pumping power observed at 0.5 l/min while 5.8 % increase in pumping power observed for 0.1wt% particle concentration at same mass flow rate. However, surge in pumping power depends both on mass flow rate and particle concentration and shows then nanofluid has been needed a very small amount of pumping power especially at low concentration.

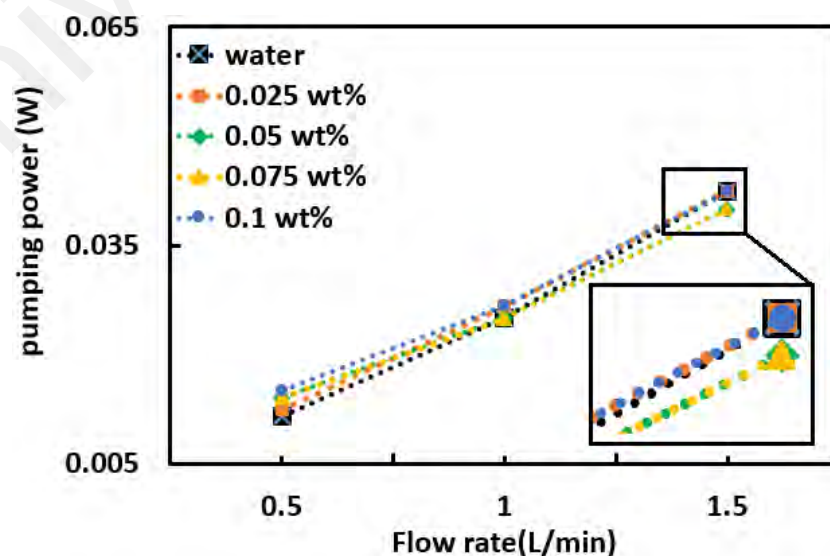
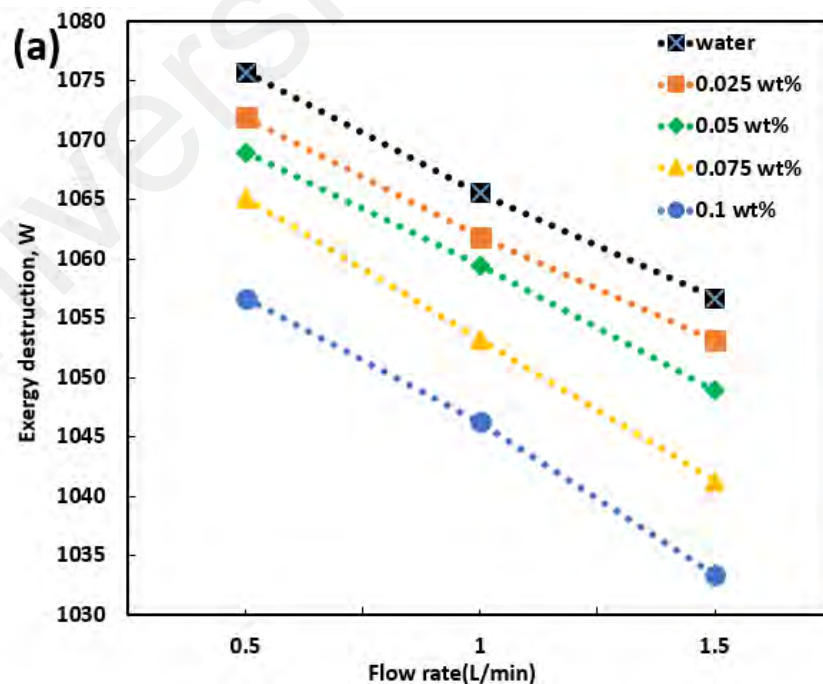


Figure 4.16: Effect of mass flow rate on pumping power and pressure drop at varying particle concentration

4.11 Exergy destruction, entropy generation and Bejan number

Based on the maximum second law efficiency, it is essential to estimate the exergy analysis of the system, which is related to the viscous friction loss and heat transfer parameters. It is obvious from Figure 4.17 (a), exergy destruction has similar pattern to compare to entropy generation in Figure 4.17(b).

According to the equation (3.20), entropy generation play the main role to analysis the exergy destruction of collector and it is the main tool for explaining the irreversibilities influence of a system. The maximization output power in solar collector can be achieved by minimization of the entropy generation. Figure 4.17(a) shows that the exergy destruction decreased with the enhancement of nanofluid concentration, which can be explained by the viscosity, entropy generation and irreversibility. Additionally, with enhancement of mass flow rate, the exergy destruction effect can be deducted, and entropy generation decreased.



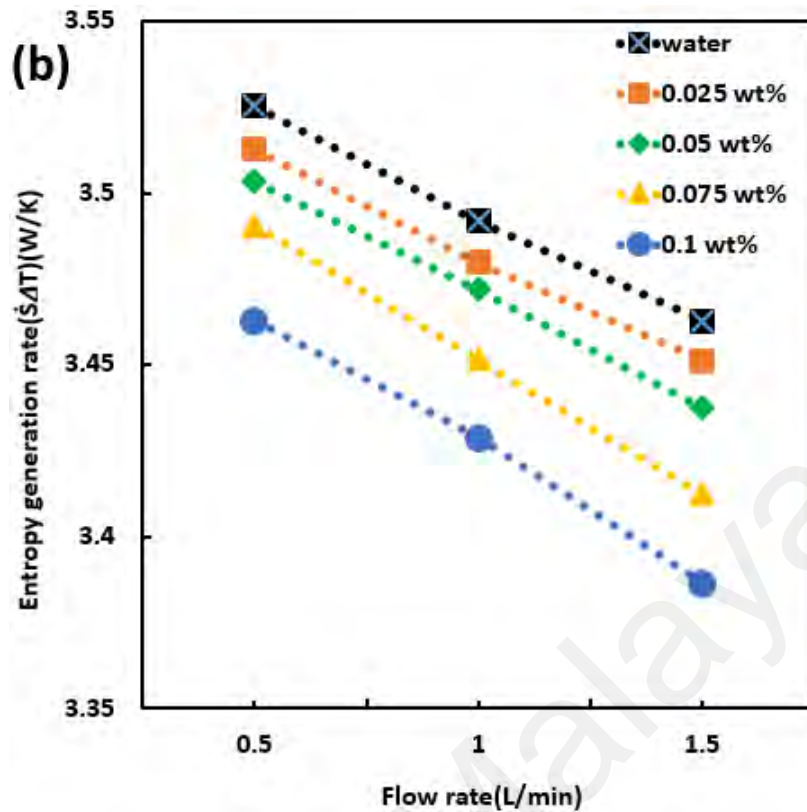


Figure 4.17: (a) Variation of exergy destruction with respect to mass flow and concentration and (b) effect of mass flow rate on entropy generation

Bejan number analysis plays a significant role on the thermal systems especially where entropy generation occurs, and it is related to internal irreversibility and fluid mass flow rates. It can be explained as ratio of heat transfer irreversibility to total irreversibility due to heat transfer and fluid friction. Figure 4.18(a) displays the effect of different mass flow rates and particle concentrations on Bejan number. It can be observed that the Bejan number enhances with increasing the particle concentration at constant mass flow rate. It indicates that by particle loading, the contribution of heat transfer to total entropy generation could be increased. At low particle concentration (0.025 wt%), nanofluid behaves like base fluid due to very weak Brownian interaction between base fluid and GNP. Figure 4.18(b) illustrated that the variations of Bejan number at the different GNP nanofluid concentration and mass flow rates. It also showed that the Bejan number reduced with increasing the mass flow rate and it means that the contribution of heat transfer to total irreversibility decreases with rise of the velocity of nanofluids in the solar

collector. Bejan number as an effective scientific criterion can be used for design and analysis of efficient thermal system which is involving fluid flow and higher of this number is desirable.

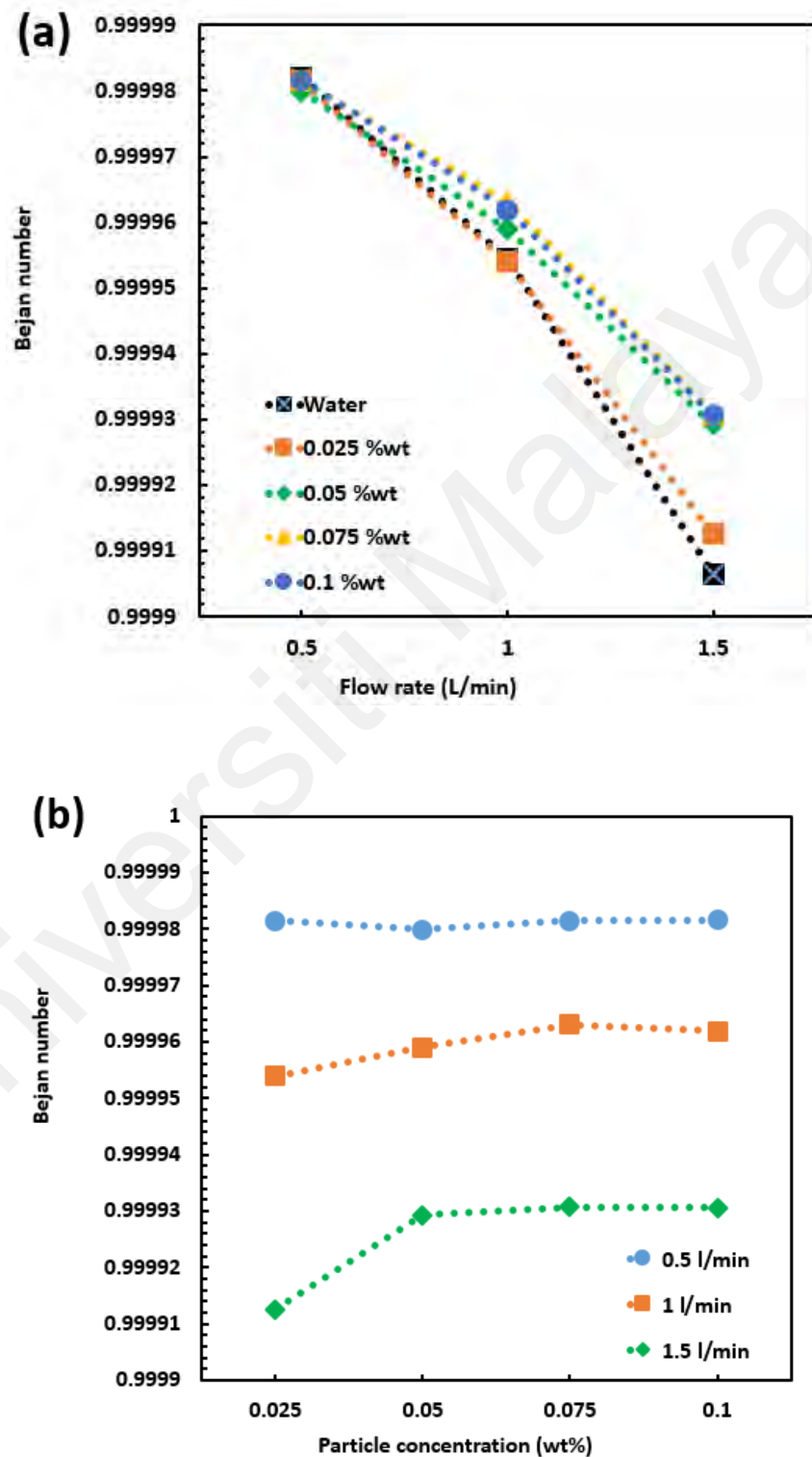


Figure 4.18: (a) Effect of mass flow rate on Bejan number and (b) Effect of nanofluid concentration (wt%) on Bejan number

4.12 Model validation

A 3- dimensional CFD model is developed to predict the outlet nanofluid temperature of the evacuated tube solar collector. The CFD result is validated with that obtained from experiments. The steady state simulation was carried out using the average values of measured data within the hourly time range of the experiment, 10 a.m. to 5:00 p.m. (MST) in order to utilize the availability of the sun in Malaysia for full day. The input parameter for the computational model was solar radiation (I), inlet nanofluid temperature (T_{in}) and mass flow rate. Simulation was carried out for predicting the outlet nanofluid temperature (T_{out}). Validation of the model was carried out by comparing the simulation results with the experimental values.

The CFD results for variations in outlet nanofluid temperature along the manifold for mass flow rate of 0.5 L/min are presented in Figure 4.20. The graph shows the differences outlet temperature between water and nanofluid according to the solar radiation from 10am to 5 pm.

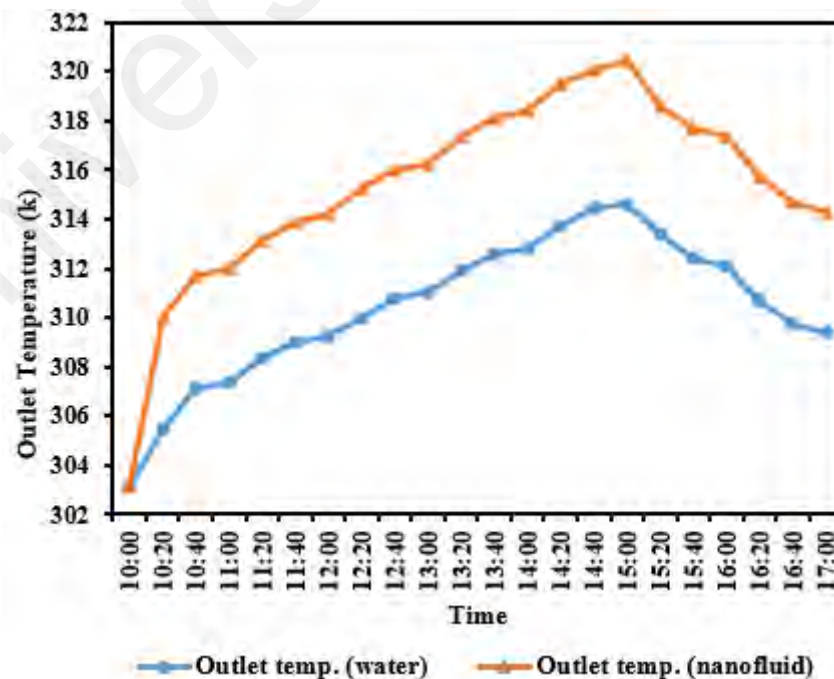
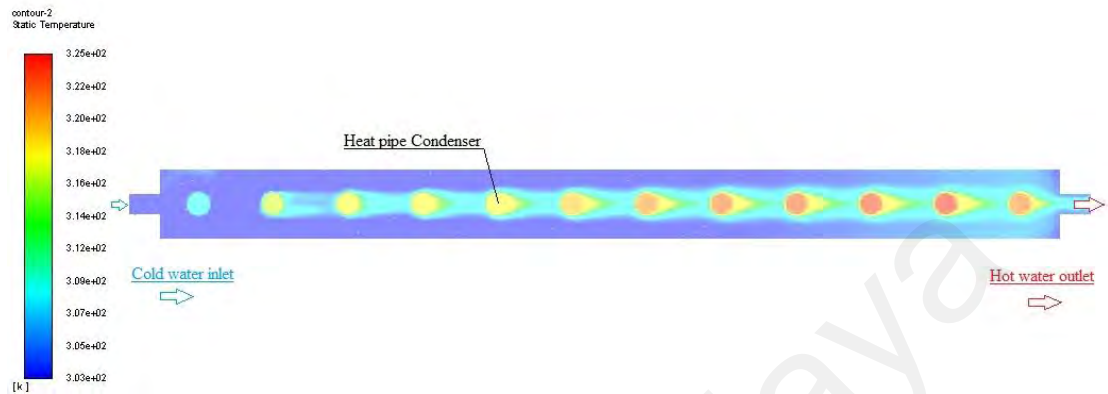
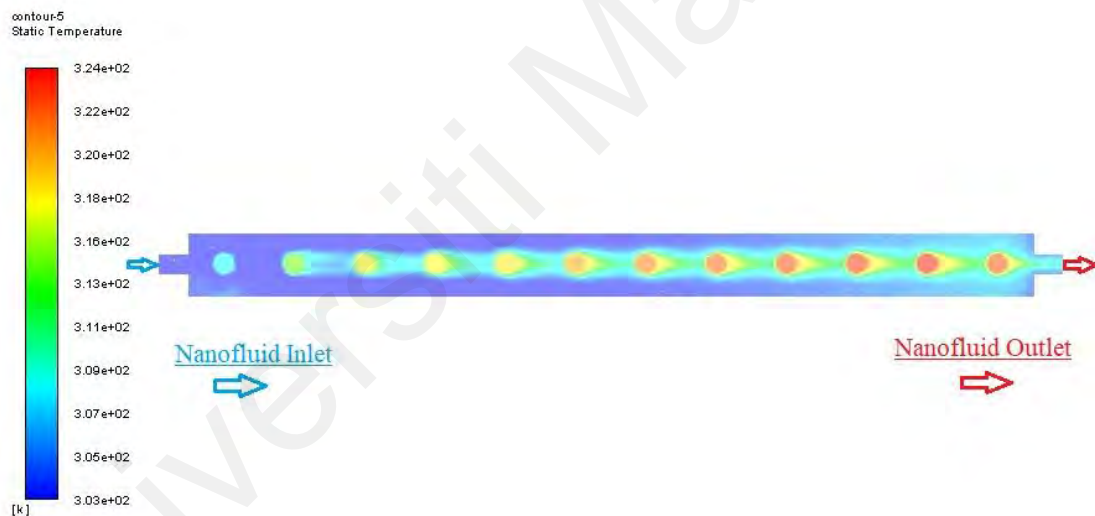


Figure 4.19:CFD result of outlet temperature for water and nanofluid.

Figure 4.20 indicates higher outlet water and nanofluid temperature at the outlet of pipe and lower portion of the manifold compared to the entrance and upper portion at 10:00 am.



a)

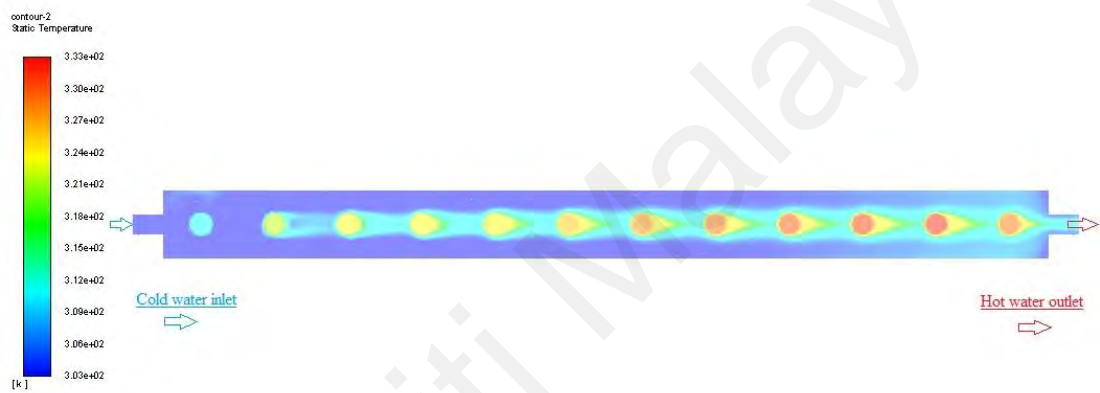


b)

Figure 4.20: Variation of a) water , b) nanofluid temperature along the manifold at 10 am.

This is expected since the inlet water absorbs heat from the head of heat pipe as it moves upward through the manifold. Since one side of the pipe in manifold is connected to heat pipes, the temperature distribution at one side of the pipe is higher compared to the other side. The heat transfer taking place is by a sequence of radiation, conduction

through the pipe thickness followed by convection inside the pipe. Since it takes more time for the heat flow to reach the center of the tube by convection, the nanofluid temperature at the center and top of the pipe inside manifold is lower than at the wall connected to heat pipes. Figure 4.21, Figure 4.22, Figure 4.23 show the Variation of static temperature for water and nanofluid temperature along the manifold at 11 am, 12pm and 1pm respectively .

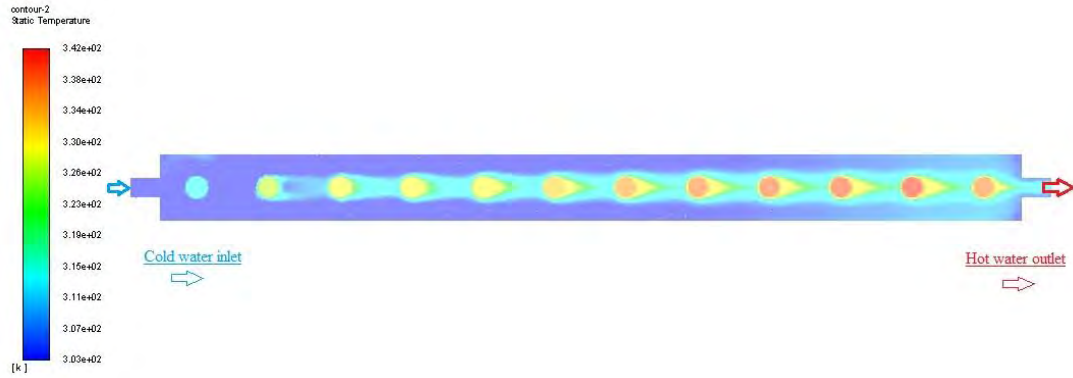


a)



b)

Figure 4.21: Variation of a)water , b) nanofluid temperature along the manifold at 11 am.

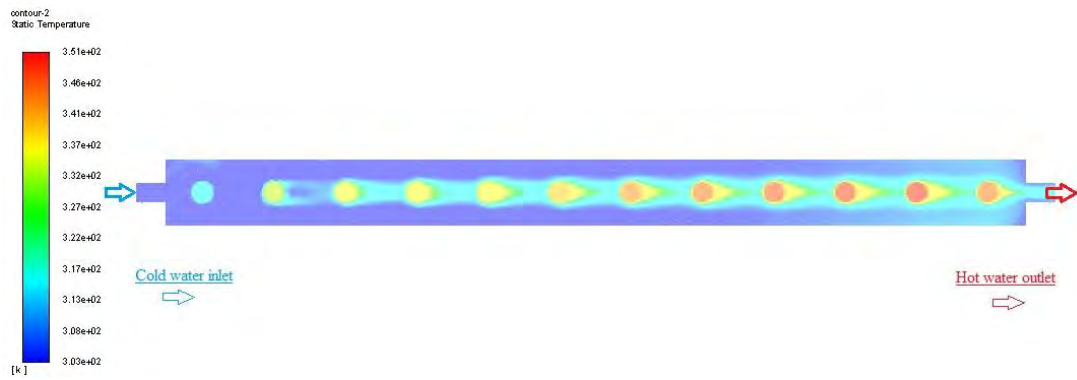


a)

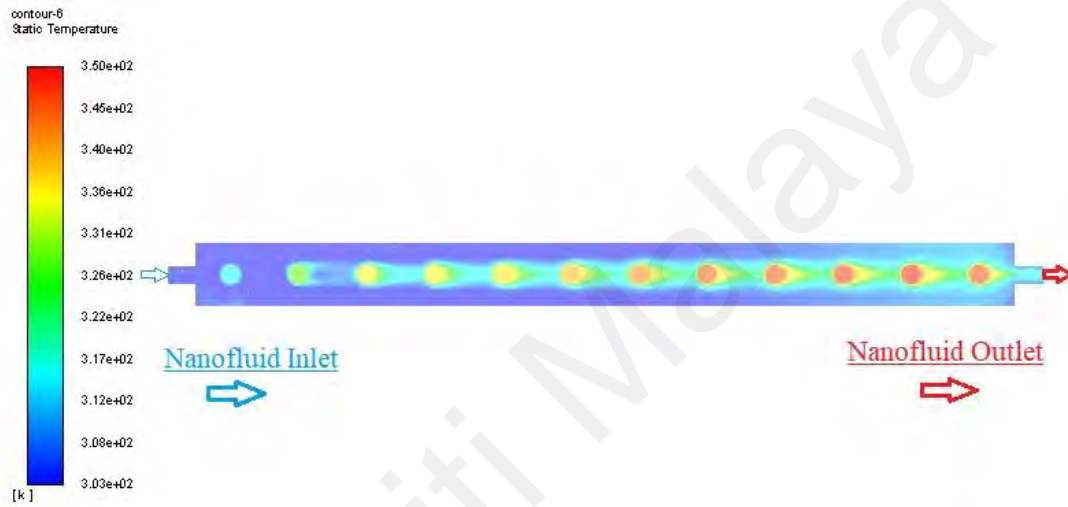


b)

Figure 4.22: Variation of a) water , b) nanofluid temperature along the manifold at 12 pm.



a)



b)

Figure 4.23: Variation of a) water , b) nanofluid temperature along the manifold at 1 pm.

4.12.1 Comparison of CFD predicted outlet nanofluid temperature with experimental data

Although the exact geometry of riser such as length and diameter intended of the computational domain, the head of heat pipes inside the manifold with details have been eliminated for simplification of simulation. Therefore, approximates CFD simulation may not describe the real conditions inside manifold due to the influence of head of heat pipes on flow distribution. So, the worse outcome of these assumptions and simplification in most simulation work could be that estimated error increase. Plots of experimental and

simulation results of outlet nanofluid temperatures for mass flow rate of 0.5 L/min is shown in Figure 4.24. According to the equation 3.28; the maximum relative error of 9.4% for outlet nanofluid temperature obtained for 0.1 wt% concentration with thermal conductivity 0,722 W/m.k , specific heat 3628 J/kg.K, density 994 and mass flow rate 0.5 L/min indicates good agreement.

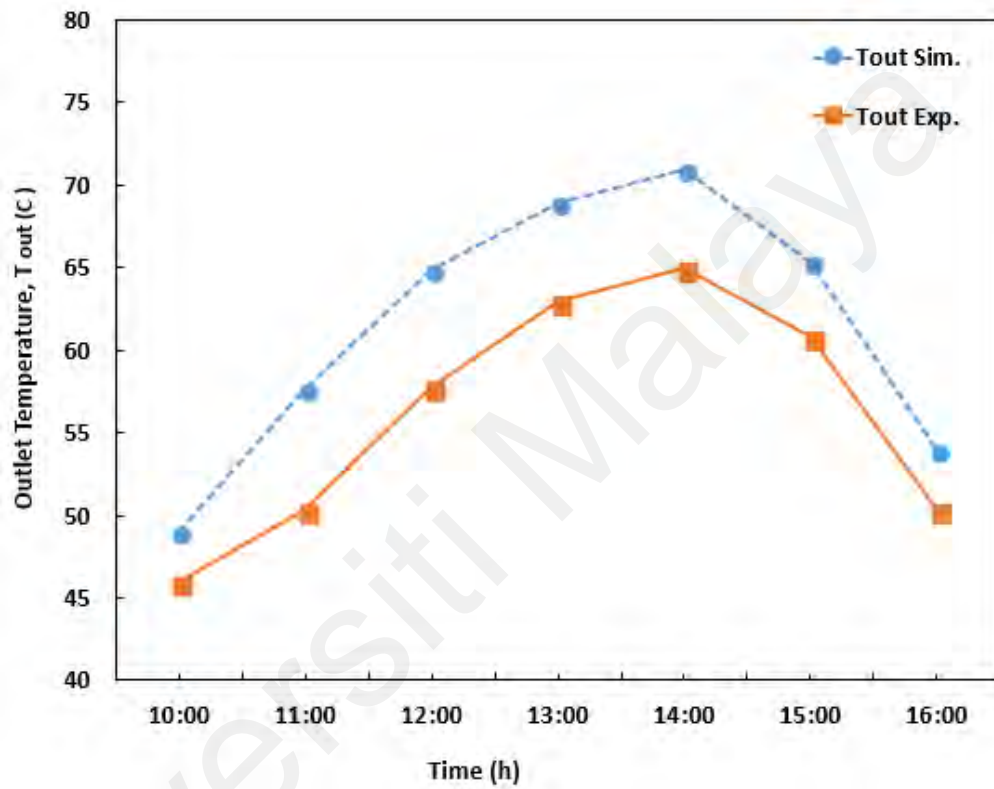


Figure 4.24: Variation of predicted and experimental outlet nanofluid temperature vs time for $\dot{m} = 0.5$ L/min

CHAPTER 5: CONCLUSION AND RECOMMENDATIONS

5.1 Conclusion

Prediction of the optimal viscosity and thermal conductivity of nanofluid is crucial for improvement of thermal management systems. In this study, Central Composite Design (CCD) with 2-level factorial designs were used to comprehend the effect of concentrations, temperature and specific surface area of GNP on thermal conductivity and viscosity of aqueous GNP nanofluid. The optimum results indicated that the best thermal conductivity value of GNP nanofluid occurred in higher concentration and it shows that viscosity of GNP nanofluids were decreased by temperature. The ANOVA results showed that there is no significant lack of fit in the design space. Moreover, the predicted data in comparison with experimental values prove that there is an excellent agreement between the mathematical model results and experimental data. Consequently, the mathematical model is found to be reliable and reasonably precise and can be used for prediction within the ambient of the factor's studies. In conclusion, new correlation based on empirical results with great accuracy were suggested to predict the viscosity and thermal conductivity of nanofluids contacting GNP. Then, Graphene nanoplatelets (GNP) nanofluids with different concentration (0.025, 0.05, 0.075 and 0.1 wt%) were introduced as a thermal efficiency improvement of evacuated tube solar collector (ETSC) in solar-water heater systems. The GNP nanofluids were prepared by two step method with ultrasonication probe, which was stable for more than three months.

The GNP nanofluids demonstrated high thermal conductivity with maximum enhancement of 27.6% with Newtonian fluid behavior. To investigate the thermal efficiency of ETSC system, three different volumetric flow rates were employed (0.5, 0.1, and 1.5 L/min). The results indicated significant enhancement on efficiency of the ETSC due to the excellent thermal and heat transfer properties of GNP nanofluids. The thermal efficiency of the system was enhanced up to 90.7% for 0.1 wt% of GNP nanofluid which

is 35.8% higher than DW at a flow rate of 1.5 L/min. Additionally, the maximum temperature difference of GNP nanofluids attained at a low volumetric flow rate of 0.5 L/min for the concentration of 0.1 wt%. The admirable heat-transfer property of GNP/distilled water nanofluid could enhance the working fluid efficiency in solar collector field and other applications in solar energy.

In addition, a theoretical study based on experimental data was presented to assess the second law of thermodynamics for system were exploited. The outcome reveals that applying of GNP nanofluid in setup, exergetic efficiency boosted by 20.5% compare to water at the same condition. In general, increase in entropy generation and pumping power losses is not desirable result but its impact is less noticeable compare to enhancement in thermal efficiency and exergetic. For 0.025 wt% particle concentration pumping power loss is 1.1% whereas for 0.1wt% concentration it has been 5.8%. The entropy number decrease with increasing the nanofluid concentration and flow rate which is desirable. Also, bejan number has been observed rises with adding nanoparticle to the base fluid.

Also, a CFD model of manifold in an evacuated tube solar collector is developed at steady state condition. The mass flow rate taken in manifold was 0.5 L/min. Comparison of the simulation results with the experimental data reveals that the model could predict the outlet nanofluid temperatures within a maximum relative error of 9.4%.

The development of this research work could afford energy producing industries and it could be a great option for non-metallic nanofluids in different thermal applications.

5.2 Challenges and future recommendations

From literature, an ETSC can be the best choice due to their excellent heat transfer capability. Though the production cost of an ETSC is getting lower, using nanofluids as working fluid is not yet cost effective due to the requirement of complicated and advanced equipment needed to prepare stable nanofluids as well as the high cost of nanoparticles. Moreover, stability of nanofluids is a major concern for the real-life applications of nanofluids. Therefore, ETSC system with GNP nanofluids is still a challenge from the economic and application point of views.

The overall observations from the experimental field tests of the ETSC system and the findings of the previous research reports indicates that the performance of this system depends on various parameters such as the weather condition which fluctuates widely in this region, the thermal properties of the nanofluid, the geometric design of the tank and evacuated tube type, supply water inlet temperature and flow rate. According to these parameters, several new topics could be suggested for further researches and investigations:

- One of the drawbacks of ETSC is that the collector tubes are very fragile and easy to be damaged. To overcome this drawback, research can be carried out on improving the structure of evacuated collector to make their body harder. For example, nanotechnology can be used to build a harder and powerful evacuated collector.
- Evacuated tubes are made of annealed glass which is much more fragile than tempered glass and the material mostly used is borosilicate glass. Experiments can be done on materials of glasses used in evacuated collector to have better efficiency.

- Grooved tubes which have spirally running grooves in inner surface can be used instead of usual tubes inside the collector to improve the efficiency. The heat transfer coefficient of grooved tube is assumed to be 2–3 times higher than plan tube with same specification.
- Solar collectors are basically of two types namely stationery and tracking, ETSCs are of stationary type. For stationary type solar collectors sun tracker can be used to track the maximum sunlight throughout the day. Though the cylindrical shape of the ETSCs helps to track the sun passively throughout the whole day but it is not able to absorb the maximum sunlight as the solar panel is positioned with a fixed angle. Solar tracker is able to orient the collector along the direction of the sunlight and ensures the absorption of maximum sunlight throughout the day by adjusting its orientation according to the sun. It is not essential to use a sun tracker but in different geographical conditions it can boost the collector energy
- To reach to the maximum efficiency of the system and minimize the effect of the design and environmental parameters an optimization study must be carried out on the effective design of the ETSC and the most appropriate thermal properties of the nanofluid.
- The mechanics of interaction of nanoparticle with base fluid, application of nanofluids in high and low temperature range and finding the ways for higher absorption ability should be explored by scientist in future research.
- This research carried out in a tropical climatic region. It is necessary to evaluate the characteristics and performance of the ETSC in other climatic conditions such as four seasons or cold weather regions.

- For industrial applications, a hybrid system can be developed to minimize the evacuated collector area and to improve the overall efficiency of the system by combining ETSCs with concentrating collector. To achieve high temperature, concentrating collectors use mirrors and lenses by concentrating sunlight of a large area onto a small area.

Universiti Malaya

REFERENCES

- Al-Ansary, H., & Zeitoun, O. (2011). Numerical study of conduction and convection heat losses from a half-insulated air-filled annulus of the receiver of a parabolic trough collector. *Solar Energy*, 85(11), 3036-3045.
- Al-Mashat, S. M. S., & Hasan, A. A. (2013). Evaluation of convective heat transfer and natural circulation in an evacuated tube solar collector. *Journal of Engineering*, 19(5), 613-628.
- Aladag, B., Halelfadl, S., Doner, N., Maré, T., Duret, S., & Estellé, P. (2012). Experimental investigations of the viscosity of nanofluids at low temperatures. *Applied Energy*, 97, 876-880.
- Altekar, M., Homon, C. A., Kashem, M. A., Mason, S. W., Nelson, R. M., Patnaude, L. A., . . . Taylor, P. B. (2006). Assay optimization: a statistical design of experiments approach. *JALA: Journal of the Association for Laboratory Automation*, 11(1), 33-41.
- Amrollahi, A., Hamidi, A., & Rashidi, A. (2008). The effects of temperature, volume fraction and vibration time on the thermo-physical properties of a carbon nanotube suspension (carbon nanofluid). *Nanotechnology*, 19(31), 315701.
- Assael, M., Chen, C.-F., Metaxa, I., & Wakeham, W. (2004). Thermal conductivity of suspensions of carbon nanotubes in water. *International Journal of Thermophysics*, 25(4), 971-985.
- Baby, T. T., & Ramaprabhu, S. (2011). Synthesis and nanofluid application of silver nanoparticles decorated graphene. *Journal of Materials Chemistry*, 21(26), 9702-9709.
- Badar, A. W., Buchholz, R., & Ziegler, F. (2012). Single and two-phase flow modeling and analysis of a coaxial vacuum tube solar collector. *Solar Energy*, 86(1), 175-189.
- Basavanna, S., & Shashishekar, K. (2013). CFD analysis of triangular absorber tube of a solar flat plate collector. *Int. J. Mech. Eng. & Rob. Res*, 2(1), 19-24.
- Bejan, A., & Kestin, J. (1983). Entropy generation through heat and fluid flow: American Society of Mechanical Engineers.
- Bianco, V., Marchitto, A., Scarpa, F., & Tagliafico, L. A. (2019). Numerical investigation on the forced laminar convection heat transfer of Al₂O₃-water nanofluid within a three-dimensional asymmetric heated channel. *International Journal of Numerical Methods for Heat & Fluid Flow*, 29(3), 1132-1152.
- Buschmann, M. H. (2013). Nanofluids in thermosyphons and heat pipes: Overview of recent experiments and modelling approaches. *International journal of thermal sciences*, 72, 1-17.
- Çağlar, A., & Yamalı, C. (2012). Performance analysis of a solar-assisted heat pump with an evacuated tubular collector for domestic heating. *Energy and buildings*, 54, 22-28.
- Cengel, Y. A., & Boles, M. A. (2002). Thermodynamics: an engineering approach. *Sea*, 1000, 8862.
- Chen, L., Xie, H., & Yu, W. (2012). Multi-walled carbon nanotube/silver nanoparticles used for thermal transportation. *Journal of Materials Science*, 47(14), 5590-5595.

- Choi, S. U. S., & Eastman, J. (1995). Enhancing thermal conductivity of fluids with nanoparticles (pp. 99-105): Argonne National Lab., IL (United States).
- Chougule, S. S., Pise, A., & Pardeshi, P. S. (2012). Studies of CNT-Nanofluid in Two Phase System. *International Journal of Global Technology Initiatives*, 1(1), F14-F20.
- Chougule, S. S., Pise, A. T., & Madane, P. A. (2012). *Performance of nanofluid-charged solar water heater by solar tracking system*. Paper presented at the IEEE-international conference on advances in engineering, science and management (ICAESM-2012).
- Colangelo, G., Favale, E., Miglietta, P., de Risi, A., Milanese, M., & Laforgia, D. (2015). Experimental test of an innovative high concentration nanofluid solar collector. *Applied Energy*, 154, 874-881.
- Das, S. K., Putra, N., Thiesen, P., & Roetzel, W. (2003). Temperature dependence of thermal conductivity enhancement for nanofluids. *Journal of heat transfer*, 125(4), 567-574.
- Davoudi, K. M., Nicola, L., & Vlassak, J. J. (2012). Dislocation climb in two-dimensional discrete dislocation dynamics. *Journal of Applied Physics*, 111(10), 103522.
- De Laquil III, P., Kearney, D., Geyer, M., & Diver, R. (1993). Solar-thermal electric technology. *Renewable energy: sources for fuels and electricity*, 213, 297.
- Ding, Y., Chen, H., Wang, L., Yang, C.-Y., He, Y., Yang, W., . . . Huo, R. (2007). Heat transfer intensification using nanofluids. *KONA Powder and Particle Journal*, 25, 23-38.
- Dongxiao, H., Zhaoguo, M., Daxiong, W., Canying, Z., & Haitao, Z. (2011). Thermal properties of carbon black aqueous nanofluids for solar absorption. *Nanoscale Research Letters*, 6, 457.
- Dović, D., & Andrassy, M. (2012). Numerically assisted analysis of flat and corrugated plate solar collectors thermal performances. *Solar Energy*, 86(9), 2416-2431.
- Duangthongsuk, W., & Wongwises, S. (2009). Measurement of temperature-dependent thermal conductivity and viscosity of TiO₂-water nanofluids. *Experimental thermal and fluid science*, 33(4), 706-714.
- Duangthongsuk, W., & Wongwises, S. (2010). An experimental study on the heat transfer performance and pressure drop of TiO₂-water nanofluids flowing under a turbulent flow regime. *International Journal of Heat and Mass Transfer*, 53(1-3), 334-344.
- Eastman, J. A., Choi, S., Li, S., Yu, W., & Thompson, L. (2001). Anomalously increased effective thermal conductivities of ethylene glycol-based nanofluids containing copper nanoparticles. *Applied physics letters*, 78(6), 718-720.
- Ekramian, E., Etemad, S. G., & Haghshenasfard, M. (2014). Numerical investigations of heat transfer performance of nanofluids in a flat plate solar collector. *Journal ISSN*, 1929, 1248.
- Elias, M., Mahbubul, I., Saidur, R., Sohel, M., Shahrul, I., Khaleduzzaman, S., & Sadeghipour, S. (2014). Experimental investigation on the thermo-physical properties of Al₂O₃ nanoparticles suspended in car radiator coolant. *International Communications in Heat and Mass Transfer*, 54, 48-53.
- Esfe, M. H., Rostamian, H., Shabani-samghabadi, A., & Arani, A. A. A. (2017). Application of three-level general factorial design approach for thermal

- conductivity of MgO/water nanofluids. *Applied Thermal Engineering*, 127, 1194-1199.
- Esfe, M. H., Saedodin, S., Akbari, M., Karimipour, A., Afrand, M., Wongwises, S., . . . Dahari, M. (2015). Experimental investigation and development of new correlations for thermal conductivity of CuO/EG–water nanofluid. *International Communications in Heat and Mass Transfer*, 65, 47-51.
- Esfe, M. H., Saedodin, S., Bahiraei, M., Toghraie, D., Mahian, O., & Wongwises, S. (2014). Thermal conductivity modeling of MgO/EG nanofluids using experimental data and artificial neural network. *Journal of Thermal Analysis and Calorimetry*, 118(1), 287-294.
- Esfe, M. H., Saedodin, S., Biglari, M., & Rostamian, H. (2015). Experimental investigation of thermal conductivity of CNTs-Al₂O₃/water: a statistical approach. *International Communications in Heat and Mass Transfer*, 69, 29-33.
- Esfe, M. H., Saedodin, S., Mahian, O., & Wongwises, S. (2014a). Efficiency of ferromagnetic nanoparticles suspended in ethylene glycol for applications in energy devices: effects of particle size, temperature, and concentration. *International Communications in Heat and Mass Transfer*, 58, 138-146.
- Esfe, M. H., Saedodin, S., Mahian, O., & Wongwises, S. (2014b). Heat transfer characteristics and pressure drop of COOH-functionalized DWCNTs/water nanofluid in turbulent flow at low concentrations. *International Journal of Heat and Mass Transfer*, 73, 186-194.
- Esfe, M. H., Saedodin, S., Mahian, O., & Wongwises, S. (2014c). Thermal conductivity of Al₂O₃/water nanofluids. *Journal of Thermal Analysis and Calorimetry*, 117(2), 675-681.
- Esfe, M. H., Saedodin, S., Sina, N., Afrand, M., & Rostami, S. (2015). Designing an artificial neural network to predict thermal conductivity and dynamic viscosity of ferromagnetic nanofluid. *International Communications in Heat and Mass Transfer*, 68, 50-57.
- Ettefaghi, E., Ghobadian, B., Rashidi, A., Najafi, G., Khoshtaghaza, M. H., & Pourhashem, S. (2017). Preparation and investigation of the heat transfer properties of a novel nanofluid based on graphene quantum dots. *Energy Conversion and Management*, 153, 215-223.
- Evangelisti, L., Vollaro, R. D. L., & Asdrubali, F. (2019). Latest advances on solar thermal collectors: A comprehensive review. *Renewable and Sustainable Energy Reviews*, 114, 109318.
- Fan, J., Shah, L. J., & Furbo, S. (2007). Flow distribution in a solar collector panel with horizontally inclined absorber strips. *Solar Energy*, 81(12), 1501-1511.
- Faramarz, S., Said, F., Hossein, A., & Amin, B. (2010). Exergetic optimization of a solar photovoltaic array. *Journal of Thermodynamics*, 2009.
- Foster, R., Ghassemi, M., & Cota, A. (2009). *Solar energy: renewable energy and the environment*: CRC Press.
- Fotukian, S., & Esfahany, M. N. (2010). Experimental study of turbulent convective heat transfer and pressure drop of dilute CuO/water nanofluid inside a circular tube. *International Communications in Heat and Mass Transfer*, 37(2), 214-219.
- Gadi, M. B. (2000). Design and simulation of a new energy-conscious system (CFD and solar simulation). *Applied Energy*, 65(1-4), 251-256.

- Ganguly, S., Sikdar, S., & Basu, S. (2009). Experimental investigation of the effective electrical conductivity of aluminum oxide nanofluids. *Powder Technology*, 196(3), 326-330.
- Gao, Y., Zhang, Q., Fan, R., Lin, X., & Yu, Y. (2013). Effects of thermal mass and flow rate on forced-circulation solar hot-water system: comparison of water-in-glass and U-pipe evacuated-tube solar collectors. *Solar Energy*, 98, 290-301.
- Garg, P., Alvarado, J. L., Marsh, C., Carlson, T. A., Kessler, D. A., & Annamalai, K. (2009). An experimental study on the effect of ultrasonication on viscosity and heat transfer performance of multi-wall carbon nanotube-based aqueous nanofluids. *International Journal of Heat and Mass Transfer*, 52(21-22), 5090-5101.
- Gertzos, K., Pnevmatikakis, S., & Caouris, Y. (2008). Experimental and numerical study of heat transfer phenomena, inside a flat-plate integrated collector storage solar water heater (ICSSWH), with indirect heat withdrawal. *Energy Conversion and Management*, 49(11), 3104-3115.
- Ghaderian, J., & Sidik, N. A. C. (2017). An experimental investigation on the effect of Al₂O₃/distilled water nanofluid on the energy efficiency of evacuated tube solar collector. *International Journal of Heat and Mass Transfer*, 108, 972-987.
- Ghaderian, J., Sidik, N. A. C., Kasaeian, A., Ghaderian, S., Okhovat, A., Pakzadeh, A., . . . Yahya, W. J. (2017). Performance of copper oxide/distilled water nanofluid in evacuated tube solar collector (ETSC) water heater with internal coil under thermosyphon system circulations. *Applied Thermal Engineering*, 121, 520-536.
- Ghadimi, A., Saidur, R., & Metselaar, H. (2011). A review of nanofluid stability properties and characterization in stationary conditions. *International Journal of Heat and Mass Transfer*, 54(17-18), 4051-4068.
- Ghafari, S., Aziz, H. A., Isa, M. H., & Zinatizadeh, A. A. (2009). Application of response surface methodology (RSM) to optimize coagulation–flocculation treatment of leachate using poly-aluminum chloride (PAC) and alum. *Journal of hazardous materials*, 163(2-3), 650-656.
- Gheshlaghi, R., Scharer, J., Moo-Young, M., & Douglas, P. (2008). Application of statistical design for the optimization of amino acid separation by reverse-phase HPLC. *Analytical biochemistry*, 383(1), 93-102.
- Goharshadi, E. K., & Berenji, A. R. (2006). A new equation of state for predicting the thermodynamic properties of liquid alkali metals. *Journal of nuclear materials*, 348(1), 40-44.
- Goharshadi, E. K., Ding, Y., Jorabchi, M. N., & Nancarrow, P. (2009). Ultrasound-assisted green synthesis of nanocrystalline ZnO in the ionic liquid [hmim][NTf₂]. *Ultrasonics sonochemistry*, 16(1), 120-123.
- Graphene: Synthesis, Properties, and Phenomena*. (2013). (C. N. R. Rao & A. K. Sood Eds.): Wiley-VCH Verlag GmbH & Co. KGaA.
- Grote, K. (2013). *The influence of multi-walled carbon nanotubes on single-phase heat transfer and pressure drop characteristics in the transitional flow regime of smooth tubes*. (Masters in Engineering), University of Pretoria.
- Hadadian, M., Samiee, S., Ahmadzadeh, H., & Goharshadi, E. K. (2013). Nanofluids for heat transfer enhancement—a review. *Physical chemistry research*, 1(1), 1-33.

- Haghighi, E. B., Saleemi, M., Nikkam, N., Khodabandeh, R., Toprak, M. S., Muhammed, M., & Palm, B. (2014). Accurate basis of comparison for convective heat transfer in nanofluids. *International Communications in Heat and Mass Transfer*, 52, 1-7.
- Hamilton, R. L., & Crosser, O. (1962). Thermal conductivity of heterogeneous two-component systems. *Industrial & Engineering Chemistry Fundamentals*, 1(3), 187-191.
- Han, D., Meng, Z., Wu, D., Zhang, C., & Zhu, H. (2011). Thermal properties of carbon black aqueous nanofluids for solar absorption. *Nanoscale Research Letters*, 6(1), 457.
- Hatami, M., Ganji, D., & Gorji-Bandpy, M. (2014). A review of different heat exchangers designs for increasing the diesel exhaust waste heat recovery. *Renewable and Sustainable Energy Reviews*, 37, 168-181.
- Hejazian, M., & Moraveji, M. K. (2013). A comparative analysis of single and two-phase models of turbulent convective heat transfer in a tube for TiO₂ nanofluid with CFD. *Numerical Heat Transfer, Part A: Applications*, 63(10), 795-806.
- Hussain, H. A., Jawad, Q., & Sultan, K. F. (2015). Experimental analysis on thermal efficiency of evacuated tube solar collector by using nanofluids. *Sol Energy*, 4, 19-28.
- Hwang, K. S., Jang, S. P., & Choi, S. U. (2009). Flow and convective heat transfer characteristics of water-based Al₂O₃ nanofluids in fully developed laminar flow regime. *International Journal of Heat and Mass Transfer*, 52(1-2), 193-199.
- Hwang, Y., Lee, J., Lee, C., Jung, Y., Cheong, S., Lee, C., . . . Jang, S. (2007). Stability and thermal conductivity characteristics of nanofluids. *Thermochimica Acta*, 455(1), 70-74.
- Iijima, S. (1991). Helical microtubules of graphitic carbon. *Nature*, 354(6348), 56-58.
- Iordanou, G. (2009). *Flat-plate solar collectors for water heating with improved heat transfer for application in climatic conditions of the Mediterranean region*. Durham University.
- Iranmanesh, S., Ong, H. C., Ang, B. C., Sadeghinezhad, E., Esmailzadeh, A., & Mehrali, M. (2017). Thermal performance enhancement of an evacuated tube solar collector using graphene nanoplatelets nanofluid. *Journal of Cleaner Production*, 162, 121-129.
- Ise, N., & Sogami, I. (2005). *Structure formation in solution: ionic polymers and colloidal particles*: Springer Science & Business Media.
- Jacobson, M. Z., & Delucchi, M. A. (2011). Providing all global energy with wind, water, and solar power, Part I: Technologies, energy resources, quantities and areas of infrastructure, and materials. *Energy Policy*, 39(3), 1154-1169.
- Jang, S. P., & Choi, S. U. (2004). Role of Brownian motion in the enhanced thermal conductivity of nanofluids. *Applied Physics Letters*, 84(21), 4316-4318.
- Jiang, B., Xia, D., Zhai, F., Zhang, R., & Liu, X. (2019). Theoretical heat conduction equation based on micro particle vibration fundamental. *International Journal of Thermal Sciences*, 140, 521-529.
- Kalogirou, S. A. (2004). Solar thermal collectors and applications. *Progress in Energy and Combustion Science*, 30(3), 231-295.

- Kalogirou, S. A. (2009). Artificial neural networks and genetic algorithms in energy applications in buildings. *Advances in Building Energy Research*, 3(1), 83-119.
- Kalogirou, S. A. (2013). *Solar energy engineering: processes and systems*: Academic Press.
- Kamyar, A., Saidur, R., & Hasanuzzaman, M. (2012). Application of computational fluid dynamics (CFD) for nanofluids. *International Journal of Heat and Mass Transfer*, 55(15-16), 4104-4115.
- Karanth, K. V., Manjunath, M., & Sharma, N. Y. (2011). *Numerical simulation of a solar flat plate collector using discrete transfer radiation model (DTRM)—a CFD approach*. Paper presented at the Proceedings of the world congress on engineering.
- Karthikeyan, N., Philip, J., & Raj, B. (2008). Effect of clustering on the thermal conductivity of nanofluids. *Materials Chemistry and Physics*, 109(1), 50-55.
- Kaya, H., & Arslan, K. (2019). Numerical investigation of efficiency and economic analysis of an evacuated U-tube solar collector with different nanofluids. *Heat and Mass Transfer*, 55(3), 581-593.
- Kazemi-Beydokhti, A., Namaghi, H. A., & Heris, S. Z. (2013). Identification of the key variables on thermal conductivity of CuO nanofluid by a fractional factorial design approach. *Numerical Heat Transfer, Part B: Fundamentals*, 64(6), 480-495.
- Kebllinski, P., Eastman, J. A., & Cahill, D. G. (2005). Nanofluids for thermal transport. *Materials Today*, 8(6), 36-44.
- Kebllinski, P., Phillpot, S., Choi, S., & Eastman, J. (2002). Mechanisms of heat flow in suspensions of nano-sized particles (nanofluids). *International Journal of Heat and Mass Transfer*, 45(4), 855-863.
- Khanafer, K., & Vafai, K. (2018). A review on the applications of nanofluids in solar energy field. *Renewable Energy*, 123, 398-406.
- Kim, Y., & Seo, T. (2007). Thermal performances comparisons of the glass evacuated tube solar collectors with shapes of absorber tube. *Renewable Energy*, 32(5), 772-795.
- Korayem, A., Tourani, N., Zakertabrizi, M., Sabziparvar, A., & Duan, W. (2017). A review of dispersion of nanoparticles in cementitious matrices: Nanoparticle geometry perspective. *Construction and Building Materials*, 153, 346-357.
- Kroto, H., & Heath, J. (1985). C60: Buckminsterfullerene. *Nature*, 3(18), 162-163.
- Larsen, S. F., Altamirano, M., & Hernández, A. (2012). Heat loss of a trapezoidal cavity absorber for a linear Fresnel reflecting solar concentrator. *Renewable Energy*, 39(1), 198-206.
- Lee, G.-J., & Rhee, C. K. (2014). Enhanced thermal conductivity of nanofluids containing graphene nanoplatelets prepared by ultrasound irradiation. *Journal of Materials Science*, 49(4), 1506-1511.
- Lee, K. J., Yoon, S. H., & Jang, J. (2007). Carbon nanofibers: a novel nanofiller for nanofluid applications. *Small*, 3(7), 1209-1213.
- Lee, S. W., Kim, K. M., & Bang, I. C. (2013). Study on flow boiling critical heat flux enhancement of graphene oxide/water nanofluid. *International Journal of Heat and Mass Transfer*, 65, 348-356.

- Lee, S. W., Park, S. D., Kang, S., Bang, I. C., & Kim, J. H. (2011). Investigation of viscosity and thermal conductivity of SiC nanofluids for heat transfer applications. *International Journal of Heat and Mass Transfer*, 54(1-3), 433-438.
- Lee, Y., Birgeneau, R., Kastner, M., Endoh, Y., Wakimoto, S., Yamada, K., . . . Shirane, G. (1999). Neutron-scattering study of spin-density wave order in the superconducting state of excess-oxygen-doped La₂CuO_{4+y}. *Physical Review B*, 60(5), 3643.
- Lenert, A., & Wang, E. N. (2012). Optimization of nanofluid volumetric receivers for solar thermal energy conversion. *Solar Energy*, 86(1), 253-265.
- Lepers, T., Davesne, D., Chiacchiera, S., & Urban, M. (2010). Numerical solution of the Boltzmann equation for the collective modes of trapped Fermi gases. *Physical Review A*, 82(2), 023609.
- Liu, Y., Wang, W., Gu, L., Wang, Y., Ying, Y., Mao, Y., . . . Peng, X. (2013). Flexible CuO nanosheets/reduced-graphene oxide composite paper: binder-free anode for high-performance lithium-ion batteries. *ACS applied materials & interfaces*, 5(19), 9850-9855.
- Liu, Z.-h., & Liao, L. (2008). Sorption and agglutination phenomenon of nanofluids on a plain heating surface during pool boiling. *International Journal of Heat and Mass Transfer*, 51(9-10), 2593-2602.
- Lu, L., Liu, Z.-H., & Xiao, H.-S. (2011). Thermal performance of an open thermosyphon using nanofluids for high-temperature evacuated tubular solar collectors: Part 1: Indoor experiment. *Solar Energy*, 85(2), 379-387.
- Lu, L. Q., & Wang, Y. (2011). Sheet-like and fusiform CuO nanostructures grown on graphene by rapid microwave heating for high Li-ion storage capacities. *Journal of Materials Chemistry*, 21(44), 17916-17921.
- Mahbubul, I., Saidur, R., & Amalina, M. (2012). Latest developments on the viscosity of nanofluids. *International Journal of Heat and Mass Transfer*, 55(4), 874-885.
- Mahendran, M., Ali, T. Z. S., Shahrani, A., & Bakar, R. (2013). The efficiency enhancement on the direct flow evacuated tube solar collector using water-based titanium oxide nanofluids. *Applied Mechanics and Materials*, 465, 308.
- Mahendran, M., Lee, G., Sharma, K., Shahrani, A., & Bakar, R. (2012a). Performance of evacuated tube solar collector using water-based titanium oxide nanofluid. *Journal of Mechanical Engineering and Sciences*, 3(unknown), 301-310.
- Mahendran, M., Lee, G., Sharma, K., Shahrani, A., & Bakar, R. (2012b). Performance of evacuated tube solar collector using water-based titanium oxide nanofluid. *Journal of Mechanical Engineering and Sciences*, 3, 301-310.
- Makinde, O., & Animasaun, I. (2016). Thermophoresis and Brownian motion effects on MHD bioconvection of nanofluid with nonlinear thermal radiation and quartic chemical reaction past an upper horizontal surface of a paraboloid of revolution. *Journal of Molecular Liquids*, 221, 733-743.
- Mangal, D., Lamba, D. K., Gupta, T., & Jhamb, K. (2010). Acknowledgement of evacuated tube solar water heater over flat plate solar water heater. *International Journal of Engineering (IJE)*, 4(4), 279.
- Manjunath, M., Karanth, V. K., & Sharma, Y. N. (2011). Three dimensional numerical analysis of conjugate heat transfer for enhancement of thermal performance using finned tubes in an economical unglazed solar flat plate collector.

- Manuel, O.-R. J., Omar, J.-S., Antonio, Z.-A. M., & Armando, E.-O. (2013). Analysis of flow and heat transfer in a flat solar collector with rectangular and cylindrical geometry using CFD. *Ingeniería, Investigación Y Tecnología*, 14(4), 553-561.
- Marquis, F., & Chibante, L. (2005). Improving the heat transfer of nanofluids and nanolubricants with carbon nanotubes. *Jom*, 57(12), 32-43.
- Martinopoulos, G., Missirlis, D., Tsilingiridis, G., Yakinthos, K., & Kyriakis, N. (2010). CFD modeling of a polymer solar collector. *Renewable Energy*, 35(7), 1499-1508.
- Mehrali, M., Latibari, S. T., Mehrali, M., Indra Mahlia, T. M., & Cornelis Metselaar, H. S. (2013). Preparation and properties of highly conductive palmitic acid/graphene oxide composites as thermal energy storage materials. *Energy*, 58, 628-634.
- Mehrali, M., Latibari, S. T., Mehrali, M., Mahlia, T. M. I., Metselaar, H. S. C., Naghavi, M. S., . . . Akhiani, A. R. (2013). Preparation and characterization of palmitic acid/graphene nanoplatelets composite with remarkable thermal conductivity as a novel shape-stabilized phase change material. *Applied Thermal Engineering*, 61(3), 633-640.
- Mehrali, M., Sadeghinezhad, E., Latibari, S. T., Kazi, S. N., Mehrali, M., Zubir, M. N. B. M., & Metselaar, H. S. C. (2014a). Investigation of thermal conductivity and rheological properties of nanofluids containing graphene nanoplatelets. *Nanoscale Research Letters*, 9(1), 15.
- Mehrali, M., Sadeghinezhad, E., Tahan Latibari, S., Kazi, S. N., Mehrali, M., Zubir, M. N. B. M., & Metselaar, H. S. C. (2014b). Investigation of thermal conductivity and rheological properties of nanofluids containing graphene nanoplatelets. *Nanoscale Research Letters*, 9(1), 1-12.
- Mehrali, M., Sadeghinezhad, E., Tahan Latibari, S., Mehrali, M., Togun, H., Zubir, M. N. M., . . . Metselaar, H. (2014). Preparation, characterization, viscosity, and thermal conductivity of nitrogen-doped graphene aqueous nanofluids. *Journal of Materials Science*, 49(20), 7156-7171.
- Mehrali, M., Seyed Shirazi, S. F., Baradaran, S., Mehrali, M., Metselaar, H. S. C., Kadri, N. A. B., & Osman, N. A. A. (2014). Facile synthesis of calcium silicate hydrate using sodium dodecyl sulfate as a surfactant assisted by ultrasonic irradiation. *Ultrasonics sonochemistry*, 21(2), 735-742.
- Meibodi, M. E., Vafaie-Sefti, M., Rashidi, A. M., Amrollahi, A., Tabasi, M., & Kalal, H. S. (2010). The role of different parameters on the stability and thermal conductivity of carbon nanotube/water nanofluids. *International Communications in Heat and Mass Transfer*, 37(3), 319-323.
- Mekhilef, S., Safari, A., Mustaffa, W., Saidur, R., Omar, R., & Younis, M. (2012). Solar energy in Malaysia: current state and prospects. *Renewable and Sustainable Energy Reviews*, 16(1), 386-396.
- Meyer, J. P., McKrell, T., & Grote, K. (2013). The influence of multi-walled carbon nanotubes on single-phase heat transfer and pressure drop characteristics in the transitional flow regime of smooth tubes. *International Journal of Heat and Mass Transfer*, 58(1-2), 597-609.
- Minea, A. A., & Luciu, R. S. (2012). Investigations on electrical conductivity of stabilized water based Al₂O₃ nanofluids. *Microfluidics and nanofluidics*, 13(6), 977-985.
- Mintsa, H. A., Roy, G., Nguyen, C. T., & Doucet, D. (2009). New temperature dependent thermal conductivity data for water-based nanofluids. *International journal of thermal sciences*, 48(2), 363-371.

- Moghaddam, M. B., Goharshadi, E. K., Entezari, M. H., & Nancarrow, P. (2013). Preparation, characterization, and rheological properties of graphene–glycerol nanofluids. *Chemical Engineering Journal*, 231, 365-372.
- Mondragon, R., Julia, J. E., Barba, A., & Jarque, J. C. (2012). Characterization of silica–water nanofluids dispersed with an ultrasound probe: A study of their physical properties and stability. *Powder Technology*, 224, 138-146.
- Morrison, G., Budihardjo, I., & Behnia, M. (2004). Water-in-glass evacuated tube solar water heaters. *Solar Energy*, 76(1-3), 135-140.
- Murshed, S., Leong, K., & Yang, C. (2005). Enhanced thermal conductivity of TiO₂–water based nanofluids. *International journal of thermal sciences*, 44(4), 367-373.
- Murshed, S. S., De Castro, C. N., Lourenço, M., Lopes, M., & Santos, F. (2011). A review of boiling and convective heat transfer with nanofluids. *Renewable and Sustainable Energy Reviews*, 15(5), 2342-2354.
- Naddaf, A., & Heris, S. Z. (2018). Experimental study on thermal conductivity and electrical conductivity of diesel oil-based nanofluids of graphene nanoplatelets and carbon nanotubes. *International Communications in Heat and Mass Transfer*, 95, 116-122.
- Nam, J. S., Kim, D. H., Chung, H., & Lee, S. W. (2015). Optimization of environmentally benign micro-drilling process with nanofluid minimum quantity lubrication using response surface methodology and genetic algorithm. *Journal of Cleaner Production*, 102, 428-436.
- Namburu, P., Kulkarni, D., Dandekar, A., & Das, D. (2007). Experimental investigation of viscosity and specific heat of silicon dioxide nanofluids. *Micro & Nano Letters*, 2(3), 67-71.
- Nanda, J., Maranville, C., Bollin, S. C., Sawall, D., Ohtani, H., Remillard, J. T., & Ginder, J. (2008). Thermal conductivity of single-wall carbon nanotube dispersions: role of interfacial effects. *The Journal of Physical Chemistry C*, 112(3), 654-658.
- Nasiri, A., Shariaty-Niasar, M., Rashidi, A. M., & Khodafarin, R. (2012). Effect of CNT structures on thermal conductivity and stability of nanofluid. *International Journal of Heat and Mass Transfer*, 55(5–6), 1529-1535.
- Nguyen, C. T., Roy, G., Gauthier, C., & Galanis, N. (2007). Heat transfer enhancement using Al₂O₃–water nanofluid for an electronic liquid cooling system. *Applied Thermal Engineering*, 27(8-9), 1501-1506.
- Nkwetta, D. N., Smyth, M., Zacharopoulos, A., & Hyde, T. (2013). Experimental field evaluation of novel concentrator augmented solar collectors for medium temperature applications. *Applied Thermal Engineering*, 51(1-2), 1282-1289.
- Nosrati, S., Jayakumar, N., & Hashim, M. (2011). Extraction performance of chromium (VI) with emulsion liquid membrane by Cyanex 923 as carrier using response surface methodology. *Desalination*, 266(1-3), 286-290.
- Novoselov, K. S., Geim, A. K., Morozov, S. V., Jiang, D., Zhang, Y., Dubonos, S. V., . . . Firsov, A. A. (2004). Electric field effect in atomically thin carbon films. *science*, 306(5696), 666-669.
- Onsekizoglu, P., Bahceci, K. S., & Acar, J. (2010). The use of factorial design for modeling membrane distillation. *Journal of Membrane Science*, 349(1), 225-230.

- Otanicar, T. P., Phelan, P. E., Prasher, R. S., Rosengarten, G., & Taylor, R. A. (2010). Nanofluid-based direct absorption solar collector. *Journal of renewable and sustainable energy*, 2(3), 033102.
- Özerinç, S., Kakaç, S., & Yazıcıoğlu, A. G. (2010). Enhanced thermal conductivity of nanofluids: a state-of-the-art review. *Microfluidics and nanofluidics*, 8(2), 145-170.
- Park, E. J., Lee, S. W., Bang, I. C., & Park, H. W. (2011). Optimal synthesis and characterization of Ag nanofluids by electrical explosion of wires in liquids. *Nanoscale Research Letters*, 6(1), 223.
- Pei, G., Li, G., Zhou, X., Ji, J., & Su, Y. (2012). Comparative experimental analysis of the thermal performance of evacuated tube solar water heater systems with and without a mini-compound parabolic concentrating (CPC) reflector ($C < 1$). *Energies*, 5(4), 911-924.
- Penn, R. L. (2017). Particle-Mediated Crystal Growth. *Handbook of Solid State Chemistry*, 155-178.
- Phuoc, T. X., & Massoudi, M. (2009). Experimental observations of the effects of shear rates and particle concentration on the viscosity of Fe₂O₃-deionized water nanofluids. *International journal of thermal sciences*, 48(7), 1294-1301.
- Pryazhnikov, M., Minakov, A., Rudyak, V. Y., & Guzei, D. (2017). Thermal conductivity measurements of nanofluids. *International Journal of Heat and Mass Transfer*, 104, 1275-1282.
- Qi, T. (2007). Thermal performance of the U-type evacuated glass tubular solar collector. *Build Energy Environ*, 3, 012.
- Ranakoti, G., Irtisha, S. D., Kosti, S., & Nemade, R. (2012). Heat transfer enhancement by nano fluids. *ME642-Convective Heat and Mass Transfer*.
- Reddy, V. S., Kaushik, S., & Tyagi, S. (2012). Exergetic analysis and performance evaluation of parabolic trough concentrating solar thermal power plant (PTCSTPP). *Energy*, 39(1), 258-273.
- Reynolds, D., Jance, M., Behnia, M., & Morrison, G. (2004). An experimental and computational study of the heat loss characteristics of a trapezoidal cavity absorber. *Solar Energy*, 76(1-3), 229-234.
- Romero, M., Buck, R., & Pacheco, J. E. (2002). An update on solar central receiver systems, projects, and technologies. *Journal of solar energy engineering*, 124(2), 98-108.
- Roslan, R., Saleh, H., & Hashim, I. (2011). Buoyancy-driven heat transfer in nanofluid-filled trapezoidal enclosure with variable thermal conductivity and viscosity. *Numerical Heat Transfer, Part A: Applications*, 60(10), 867-882.
- Sabiha, M., Saidur, R., Hassani, S., Said, Z., & Mekhilef, S. (2015). Energy performance of an evacuated tube solar collector using single walled carbon nanotubes nanofluids. *Energy Conversion and Management*, 105, 1377-1388.
- Sabiha, M., Saidur, R., Mekhilef, S., & Mahian, O. (2015). Progress and latest developments of evacuated tube solar collectors. *Renewable and Sustainable Energy Reviews*, 51, 1038-1054.
- Sadeghi, G., Safarzadeh, H., & Ameri, M. (2019). Experimental and numerical investigations on performance of evacuated tube solar collectors with parabolic

- concentrator, applying synthesized Cu₂O/distilled water nanofluid. *Energy for sustainable development*, 48, 88-106.
- Sadeghinezhad, E., Mehrali, M., Saidur, R., Mehrali, M., Latibari, S. T., Akhiani, A. R., & Metselaar, H. S. C. (2016). A comprehensive review on graphene nanofluids: recent research, development and applications. *Energy Conversion and Management*, 111, 466-487.
- Sadeghinezhad, E., Mehrali, M., Tahan Latibari, S., Mehrali, M., Kazi, S. N., Oon, S., & Metselaar, H. S. C. (2014). Experimental investigation of convective heat transfer using graphene nanoplatelet based nanofluids under turbulent flow conditions. *Industrial & Engineering Chemistry Research*, 53(31), 12455–12465.
- Sadri, R., Ahmadi, G., Togun, H., Dahari, M., Kazi, S. N., Sadeghinezhad, E., & Zubir, N. (2014). An experimental study on thermal conductivity and viscosity of nanofluids containing carbon nanotubes. *Nanoscale Research Letters*, 9(1), 151.
- Sarkar, J., Ghosh, P., & Adil, A. (2015). A review on hybrid nanofluids: recent research, development and applications. *Renewable and Sustainable Energy Reviews*, 43, 164-177.
- Selmi, M., Al-Khawaja, M. J., & Marafia, A. (2008). Validation of CFD simulation for flat plate solar energy collector. *Renewable Energy*, 33(3), 383-387.
- Selvakumar, P., Somasundaram, P., & Thangavel, P. (2014). Performance study on evacuated tube solar collector using therminol D-12 as heat transfer fluid coupled with parabolic trough. *Energy Conversion and Management*, 85, 505-510.
- Sen Gupta, S., Manoj Siva, V., Krishnan, S., Sreeprasad, T., Singh, P. K., Pradeep, T., & Das, S. K. (2011). Thermal conductivity enhancement of nanofluids containing graphene nanosheets. *Journal of Applied Physics*, 110(8), 084302-084302-084306.
- Shahrul, I., Mahbubul, I., Khaleduzzaman, S., Saidur, R., & Sabri, M. (2014). A comparative review on the specific heat of nanofluids for energy perspective. *Renewable and Sustainable Energy Reviews*, 38, 88-98.
- Shanbedi, M., Heris, S. Z., Baniadam, M., Amiri, A., & Maghrebi, M. (2012). Investigation of heat-transfer characterization of EDA-MWCNT/DI-water nanofluid in a two-phase closed thermosyphon. *Industrial & Engineering Chemistry Research*, 51(3), 1423-1428.
- Sharma, N., & Diaz, G. (2011). Performance model of a novel evacuated-tube solar collector based on minichannels. *Solar Energy*, 85(5), 881-890.
- Shin, D., & Banerjee, D. (2011). Enhancement of specific heat capacity of high-temperature silica-nanofluids synthesized in alkali chloride salt eutectics for solar thermal-energy storage applications. *International Journal of Heat and Mass Transfer*, 54(5-6), 1064-1070.
- Shirvan, K. M., Mamourian, M., Mirzakhani, S., & Ellahi, R. (2016). Two phase simulation and sensitivity analysis of effective parameters on combined heat transfer and pressure drop in a solar heat exchanger filled with nanofluid by RSM. *Journal of Molecular Liquids*, 220, 888-901.
- Singh, R. V., Kumar, S., Hasan, M., Khan, M. E., & Tiwari, G. (2013). Performance of a solar still integrated with evacuated tube collector in natural mode. *Desalination*, 318, 25-33.

- Sultana, T., Morrison, G. L., & Rosengarten, G. (2011). *A Numerical and Experimental Study of a Novel Roof Integrated Solar Micro-Concentrating Collector*. Paper presented at the Australian Solar Energy Society Annual Conference (AuSES), Sydney, Australia, Nov.
- Sun, Z., Pöller, S., Huang, X., Guschin, D., Taetz, C., Ebbinghaus, P., . . . Schuhmann, W. (2013). High-yield exfoliation of graphite in acrylate polymers: a stable few-layer graphene nanofluid with enhanced thermal conductivity. *Carbon*, *64*, 288–294.
- Sundar, L. S., & Sharma, K. (2007). Thermal Conductivity Enhancement of Metallic Oxide Nanoparticles in Distilled Water. *International Journal of Materials Science*, *2*(3).
- Suzuki, A. (1988). General theory of exergy-balance analysis and application to solar collectors. *Energy*, *13*(2), 153-160.
- Tagliafico, L. A., Scarpa, F., & De Rosa, M. (2014). Dynamic thermal models and CFD analysis for flat-plate thermal solar collectors—A review. *Renewable and Sustainable Energy Reviews*, *30*, 526-537.
- Tang, R., Li, Z., Zhong, H., & Lan, Q. (2006). Assessment of uncertainty in mean heat loss coefficient of all glass evacuated solar collector tube testing. *Energy Conversion and Management*, *47*(1), 60-67.
- Tang, R., Yang, Y., & Gao, W. (2011). Comparative studies on thermal performance of water-in-glass evacuated tube solar water heaters with different collector tilt-angles. *Solar Energy*, *85*(7), 1381-1389.
- Taylor, R. A., Phelan, P. E., Otanicar, T. P., Adrian, R., & Prasher, R. (2011). Nanofluid optical property characterization: towards efficient direct absorption solar collectors. *Nanoscale Research Letters*, *6*(1), 225.
- Togun, H., Safaei, M. R., Sadri, R., Kazi, S. N., Badarudin, A., Hooman, K., & Sadeghinezhad, E. (2014). Numerical simulation of laminar to turbulent nanofluid flow and heat transfer over a backward-facing step. *Applied Mathematics and Computation*, *239*, 153-170.
- Tong, Y., Kim, J., & Cho, H. (2015). Effects of thermal performance of enclosed-type evacuated U-tube solar collector with multi-walled carbon nanotube/water nanofluid. *Renewable Energy*, *83*, 463-473.
- Trisaksri, V., & Wongwises, S. (2007). Critical review of heat transfer characteristics of nanofluids. *Renewable and Sustainable Energy Reviews*, *11*(3), 512-523.
- Tyagi, H., Phelan, P., & Prasher, R. (2009). Predicted efficiency of a low-temperature nanofluid-based direct absorption solar collector. *Journal of solar energy engineering*, *131*(4), 041004.
- Tyagi, V., Kaushik, S., & Tyagi, S. (2012). Advancement in solar photovoltaic/thermal (PV/T) hybrid collector technology. *Renewable and Sustainable Energy Reviews*, *16*(3), 1383-1398.
- Venkatachalam, C., Mariam, S. G., & Anchala, A. C. (2019). Thermal and Economic Analysis Review on Flat Plate, Parabolic Trough and Evacuated Tube Solar Collectors for Process Heat Applications. *Journal of Applied Sciences*, *19*(1), 1-8.
- Verma, S. K., & Tiwari, A. K. (2015). Progress of nanofluid application in solar collectors: A review. *Energy Conversion and Management*, *100*, 324-346.

- Vestlund, J. (2012). *Gas-filled, flat plate solar collectors*. Chalmers University of Technology.
- Wang, B., Hao, J., & Li, H. (2013a). Remarkable improvements in the stability and thermal conductivity of graphite/ethylene glycol nanofluids caused by a graphene oxide percolation structure. *Dalton Transactions*.
- Wang, B., Hao, J., & Li, H. (2013b). Remarkable improvements in the stability and thermal conductivity of graphite/ethylene glycol nanofluids caused by a graphene oxide percolation structure. *Dalton Transactions*, 42(16), 5866-5873.
- Wang, X.-Q., & Mujumdar, A. S. (2007). Heat transfer characteristics of nanofluids: a review. *International journal of thermal sciences*, 46(1), 1-19.
- Wang, Z. (2010). Prospectives for China's solar thermal power technology development. *Energy*, 35(11), 4417-4420.
- Wen, D., & Ding, Y. (2004a). Effective thermal conductivity of aqueous suspensions of carbon nanotubes (carbon nanotube nanofluids). *Journal of Thermophysics and Heat Transfer*, 18(4), 481-485.
- Wen, D., & Ding, Y. (2004b). Experimental investigation into convective heat transfer of nanofluids at the entrance region under laminar flow conditions. *International Journal of Heat and Mass Transfer*, 47(24), 5181-5188.
- Williams, W., Buongiorno, J., & Hu, L.-W. (2008). Experimental investigation of turbulent convective heat transfer and pressure loss of alumina/water and zirconia/water nanoparticle colloids (nanofluids) in horizontal tubes. *Journal of heat transfer*, 130(4), 042412.
- Xiao, X., Miao, L., Xu, G., Lu, L., Su, Z., Wang, N., & Tanemura, S. (2011). A facile process to prepare copper oxide thin films as solar selective absorbers. *Applied Surface Science*, 257(24), 10729-10736.
- Xie, H., Wang, J., Xi, T., Liu, Y., Ai, F., & Wu, Q. (2002). Thermal conductivity enhancement of suspensions containing nanosized alumina particles. *Journal of Applied Physics*, 91(7), 4568-4572.
- Xu, L., Wang, Z., Yuan, G., Li, X., & Ruan, Y. (2012). A new dynamic test method for thermal performance of all-glass evacuated solar air collectors. *Solar Energy*, 86(5), 1222-1231.
- Xuan, Y., & Li, Q. (2003). Investigation on convective heat transfer and flow features of nanofluids. *Journal of heat transfer*, 125(1), 151-155.
- Yan, S., Tian, R., Hou, S., & Zhang, L. (2008). Analysis on unsteady state efficiency of glass evacuated solar collector with an inserted heat pipe. *Journal of Engineering Thermophysics*, 29(2), 323.
- Yang, J.-C., Li, F.-C., Cai, W.-H., Zhang, H.-N., & Yu, B. (2014). On the mechanism of convective heat transfer enhancement in a turbulent flow of nanofluid investigated by DNS and analyses of POD and FSP. *International Journal of Heat and Mass Transfer*, 78, 277-288.
- Yang, Y., Zhang, Z. G., Grulke, E. A., Anderson, W. B., & Wu, G. (2005). Heat transfer properties of nanoparticle-in-fluid dispersions (nanofluids) in laminar flow. *International Journal of Heat and Mass Transfer*, 48(6), 1107-1116.
- Yeganeh, M., Shahtahmasebi, N., Kompany, A., Goharshadi, E. K., Youssefi, A., & Šiller, L. (2010). Volume fraction and temperature variations of the effective

- thermal conductivity of nanodiamond fluids in deionized water. *International Journal of Heat and Mass Transfer*, 53(15–16), 3186-3192.
- Yousefi, H., Nishino, T., Faezipour, M., Ebrahimi, G., & Shakeri, A. (2011). Direct fabrication of all-cellulose nanocomposite from cellulose microfibers using ionic liquid-based nanowelding. *Biomacromolecules*, 12(11), 4080-4085.
- Yousefi, T., Veysi, F., Shojaeizadeh, E., & Zinadini, S. (2012). An experimental investigation on the effect of Al₂O₃-H₂O nanofluid on the efficiency of flat-plate solar collectors. *Renewable Energy*, 39(1), 293-298.
- Yu, W., Xie, H., Wang, X., & Wang, X. (2011). Significant thermal conductivity enhancement for nanofluids containing graphene nanosheets. *Physics Letters A*, 375(10), 1323-1328.
- Zamzamian, A., KeyanpourRad, M., KianiNeyestani, M., & Jamal-Abad, M. T. (2014). An experimental study on the effect of Cu-synthesized/EG nanofluid on the efficiency of flat-plate solar collectors. *Renewable Energy*, 71, 658-664.
- Zhao, X., Wang, Z., & Tang, Q. (2010). Theoretical investigation of the performance of a novel loop heat pipe solar water heating system for use in Beijing, China. *Applied Thermal Engineering*, 30(16), 2526-2536.
- Zheng, R., Gao, J., Wang, J., Feng, S.-P., Ohtani, H., Wang, J., & Chen, G. (2011). Thermal percolation in stable graphite suspensions. *Nano letters*, 12(1), 188-192.
- Zhi, C., Xu, Y., Bando, Y., & Golberg, D. (2011). Highly Thermo-conductive Fluid with Boron Nitride Nanofillers. *ACS nano*, 5(8), 6571-6577.
- Zubriski, S. E., & Dick, K. (2012). Measurement of the efficiency of evacuated tube solar collectors under various operating conditions. *Journal of Green Building*, 7(3), 114-130.

LIST OF PUBLICATIONS AND PAPERS PRESENTED

S. Iranmanesh, M. Mehrali, E. Sadeghinezhad, BC. Ang, HC. Ong, A. Esmailzadeh (2016). Evaluation of viscosity and thermal conductivity of graphene nanoplatelets nanofluids through a combined experimental–statistical approach using respond surface methodology method. *International Communications in Heat and Mass Transfer* 79 (2016) 74–80, (Q1, Impact Factor: 4.46)

S. Iranmanesh, M. Mehrali, E. Sadeghinezhad, BC. Ang, HC. Ong, A. Esmailzadeh (2017). Thermal performance enhancement of an evacuated tube solar collector using graphene nanoplatelets nanofluid. *Journal of cleaner production* 162 (2017) 121-129, (Q1, Impact Factor: 6.39)

Universiti Malaysia